Structural RNA conjugated with gold nanoparticles as a tool for gene expression regulation

Strukturalne RNA skoniugowane z nanocząstkami złota jako narzędzie do regulacji ekspresji genów

Anna Graczyk

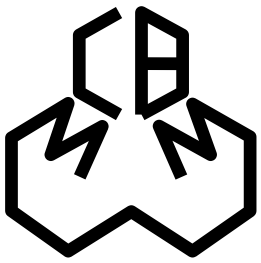

Supervisor Prof. Arkadiusz Chworos
Co-supervisor Dr Roza Pawlowska

Centre of Molecular and Macromolecular Studies,
Polish Academy of Sciences

PhD Thesis 2021

Acknowledgements

Science knows no country, because knowledge belongs to humanity, and is the torch which illuminates the world. Science is the highest personification of the nation because that nation will remain the first which carries the furthest the works of thought and intelligence.

Louis Pasteur

First and foremost, I would like to thank my supervisor Prof. Arkadiusz Chworos for the support and the time devoted to advance my scientific journey. I am also thankful for the research freedom that allowed me to stand on my feet and learn from my mistakes.

This thesis could never be completed without my co-supervisor – dr Roza Pawlowska. She is the reason why I kept on trying against the odds and has always been there for me as a mentor and a friend.

I am truly grateful for the wonderful friends who I met during my doctoral studies. They have always been around to share both, joyful and difficult moments.

Last but not the least, I would like to thank my parents for all the unconditional support and understanding.

Financial sources:

This research was supported by Funds for Young Researches for 2016, 2017, and 2018 under statutory funds of Centre of Molecular and Macromolecular Studies, Polish Academy of Sciences and the National Science Centre in Poland (NCN-2015/19/B/ST5/03087).

Achievements

Publications

1. **Graczyk A**, Pawlowska R, Jedrzejczyk D, Chworos A. Gold Nanoparticles in Conjunction with Nucleic Acids as a Modern Molecular System for Cellular Delivery. Molecules. 2020 Jan 3;25(1):204. doi: 10.3390/molecules25010204.
2. **Graczyk A**, Pawlowska R, Chworos A. Gold Nanoparticles as Carriers for Functional RNA Nanostructures. ACS Bioconjugate Chemistry 2021 32 (8), 1667-1674. doi: 10.1021/acs.bioconjchem.1c00211
3. Pawlowska R, Jedrzejczyk D, Janicka M, **Graczyk A**, Chworos A. Cytochrome c interaction with tRNA, the new properties of the known molecules. Acta Biochimica Polonica, S1, P7.35, 2014, 155 – post conference communication
4. **Graczyk A**, Jedrzejczyk D, Pawlowska R, Chworos A, The Complex of tRNA with Cytochrome C in Gel Studies. Collection Symposium Series, 2014, 14, 283-284 - post conference communication
5. **Graczyk A**, Pawlowska R, Chworos, A. Functional RNA-AuNP conjugates for gene expression regulation based on the GFP example. FEBS Open Bio, 11, P-01.2-21, 10.1002/2211-5463.13205 – post conference communication
6. Suwara J, Radzikowska-Cieciura E, Madaj R, **Graczyk A**, Pawlowska R. The influence of ectonucleotidases expression on ATP-dependent extracellular signalling. FEBS Open Bio, 11, P-08.2-38, 10.1002/2211-5463.13205 – post conference communication
7. Pawlowska R, Fastyn J, Suwara J, **Graczyk A**, Radzikowska-Cieciura E, Chworos A. Extracellular ATP enhances migration and invasion properties of human squamous carcinoma cells. Cell Bio Virtual – The American Society for Cell Biology (ASCB) and European Molecular Biology Organization (EMBO) Meeting - post conference communication

Conference Presentations

1. EMBO Workshop RNA: Structure meets function
   Poster: "RNA-Protein Interactions Studies - Theoretical and Experimental Methods"
   Jedrzejczyk D, Pawlowska R, Graczyk A and Chworos A
   Stockholm, Sweden, 1-4.07.2018
2. EMBO|EMBL Symposium: The Complex Life of RNA

Poster: „Spherical tecto-RNA (StRNA) - a fresh wave in the Spherical Nucleic Acids' science"
Graczyk A, Chworos A
Heidelberg, Germany, 3-6.10.2018

3. Gordon Research Seminar - RNA Nanotechnology
   Oral presentation: "Metal nanoparticles capped with structured RNA – the spherical incarnation of tectoRNA"
   Graczyk A – best speech award beneficent
   Ventura, CA, USA, 12-13.01.2019
4. Gordon Research Conference - RNA Nanotechnology
   Poster: "Metal nanoparticles capped with structured RNA – the spherical incarnation of tectoRNA"
   Graczyk A, Chworos A
   Ventura, CA, USA, 12-13.01.2019
5. The 45th FEBS Virtual Congress
   Poster: "Functional RNA-AuNP conjugates for gene expression regulation based on the GFP example"
   Graczyk A, Pawlowska R, Chworos A.
   Online conference, Ljubliana, 3-8.07.2021
6. The 45th FEBS Virtual Congress
   Poster: „The influence of ectonucleotidases expression on ATP-dependent extracellular signalling"
   Suwara J, Radzikowska-Cieciura E, Madaj R, Graczyk A, Pawlowska R
   Online conference, Ljubliana, 3-8.07.2021
7. XII Sesja Magistrantów i Doktorantów Łódzkiego Środowiska Chemików
   Oral presentation: „Gold nanoparticles as carriers for functional RNA nanostructures"
   Graczyk A (Main prize beneficent – for the best speech)
   Online conference, Łódź, Poland, 17.06.2021
8. 63. Zjazd Naukowy Polskiego Towarzystwa Chemicznego
   Poster: "The alpha-(di)thio and beta-gamma-phosphate modified ATP analogues - synthesis and hydrolytic stability"
   Radzikowska-Cieciura E, Fastyn J, Milczarek J, Graczyk A, Pawlowska R
   Online conference, Łódź, Poland, 13-17.09.2021
9. XIII Łódzkie Sympozjum Doktorantów Chemii
   Poster: „Nanocząstki złota jako nośniki dla regulatorowych RNA. Badania w modelu ludzkiego raka piersi MDA-MB-231"

Graczyk A, Pawlowska R, Chworos A
Łódź, 24.09.2021

10. 18th Biennial Congress of the Metastasis Research Society
    Poster: „Extracellular ATP increases migration of osteosarcoma MG-63 cells."
    Pawlowska R, Suwara J, Graczyk A, Fastyn J, Radzikowska-Cieciura E, Chworos A.
    Online conference, 15-17.11.2021
11. Cell Bio Virtual – The American Society for Cell Biology (ASCB) and European Molecular Biology Organization (EMBO) Meeting
    Poster: „Extracellular ATP enhances migration and invasion properties of human squamous carcinoma cells."
    Pawlowska R, Fastyn J, Suwara J, Graczyk A, Radzikowska-Cieciura E, Chworos A.
    Online conference, 1-10.12.2021

Abstract

Now, especially after the global emergence of the first mRNA vaccine against SARS-CoV-2, the importance of RNA research has never been more pronounced. Our understanding of the RNA has steadily deepened since the discovery and subsequent differentiation of the two types of nucleic acids, DNA and RNA. The ribonucleic acid (RNA) is particularly interesting due to its exceptional naturally occurring spatial properties responsible for multiplicity of RNA functions falling way beyond the Central Dogma of Molecular Biology. This quality of RNA led to development of the RNA architectonics, which relies on the RNA motifs used to create RNA nanostructures. As we were gaining the ability to determine and rationally design RNA structures, we also learned to replicate some of the natural processes. Consequently, the new RNA-based technologies that can be applied as therapeutics, sensors or diagnostic tools were introduced and all those can be gathered under the umbrella term of RNA nanotechnology. With the development of modern diagnostics, it has been found that an increasing number of diseases have a genetic cause that leads to impaired protein function. Such abnormalities in protein expression may cause disorders such as: cancers or Alzheimer's disease, likely caused by misfolded protein forming agglomerates, etc. The ability to regulate gene expression holds a promise to treat genetic malfunctions by suppression of defective gene with the RNA interference (RNAi). The use of RNA derived constructs is valuable and offers multiplicity of possible architectures that can be further utilized to design molecular device for a given target.

The purpose of presented thesis is to develop a structural RNA (tectoRNA) conjugate with spherical gold nanoparticle (AuNP). This approach combines two fields of nanotechnology and has a potential to create a uniform platform for a delivery of regulatory elements. Nanotechnology of nucleic acids has been studied since the basis or rational design of DNA was introduced. The use of RNA is of particular interest due to its established role in regulating gene expression through RNAi. The second area of nanotechnology implemented in this project is the nanotechnology of noble metals, specifically gold. Gold nanoparticles are known for their specific properties, which make them often used for bio-imaging, resonance scattering, energy transfer, biosensors and to study for instance cell endocytosis. Here, we developed a new generation of spherical nucleic acids in which AuNPs are conjugated to a structural RNA trimer carrying three regulatory sequences and a thiol linker. Similar approach was previously used to make spherical nucleic acids, where the AuNP was conjugated with regulatory siRNAs.

Introduction of the tectoRNA constructs into a spherical layout gives a chance to increase the local concentration of regulatory elements, implement proportional amounts of different regulatory sequences and finally improve regulatory effect of such molecules. It can therefore become a superior system for delivery of regulatory elements, that gives a solution for future drug design, where RNA-AuNP construct has a capacity to bring abundance of regulatory sequences to the cell.

Streszczenie

W dobie pandemii COVID-19, gdy szczepionki mRNA stają się nową normą, rola badań RNA wydaje się być nieoceniona. Od czasu odkrycia istnienia kwasów nukleinowych w latach 60-tych XIX wieku, a później ich rozdziału na DNA i RNA, nasze pojmowanie świata RNA nieustająco dojrzewa. Kwas rybonukleinowy (RNA) jest szczególnie interesujący, ze względu na jego naturalną zdolność do tworzenia struktur wyższego rzędu, a co za tym idzie, ma wiele funkcji znacznie wykraczających poza rolę matrycy w biosyntezie białek. Przestrzenna budowa i mnogość motywów strukturalnych występujących w RNA leżą u podstaw rozwoju architektoniki RNA, która pozwala na projektowanie i tworzenie nowych nanostruktur RNA w oparciu o naturalnie występujące motywy. Wraz z rozwojem tej dziedziny naukowcy nauczyli się odtwarzać i kontrolować naturalne procesy z udziałem RNA. Otwarło to drzwi dla nowych zastosowań RNA, np. w terapii, obrazowaniu, diagnostyce czy tworzeniu sensorów, czyli tak zwanej nanotechnologii RNA. Wraz z rozwojem diagnostyki medycznej, kolejne choroby okazały się mieć podłoże genetyczne wynikające z mutacji zaburzających funkcjonowanie białek. Takie mutacje prowadzą między innymi do powstania nowotworów czy choroby Alzheimera, mogącej wynikać np. z aglomeracji źle sfałdowanych białek. Regulacja ekspresji genów za pomocą interferencji RNA (RNAi) jest więc obiecującym sposobem leczenia takich przypadłości. Wykorzystanie racjonalnie projektowanych nanostruktur RNA i ich pochodnych otwiera wiele możliwości dla terapii celowanych.

Celem badań opisanych w niniejszej rozprawie było opracowanie koniugatu strukturalnego RNA (tectoRNA) i sferycznej nanocząstki złota (AuNP). Takie połączenie dwóch nanotechnologii, ma potencjał, aby stworzyć uniwersalną platformę dostarczania elementów regulatorowych do komórek. Nanotechnologia kwasów nukleinowych była tematem badań naukowych od czasu, gdy po raz pierwszy opisano racjonalne projektowanie struktur DNA. Jednakże zastosowanie struktur RNA jest szczególnie fascynujące przez wzgląd na jego strukturę przestrzenną i rolę w regulacji ekspresji genów za pomocą RNAi. Drugą nanotechnologią wykorzystaną w projekcie jest nanotechnologia metali szlachetnych, w tym przypadku złota. Nanocząstki złota cechują się szczególnymi właściwościami optycznymi, co znalazło zastosowanie w technikach obrazowania, oraz niską cytotoksycznością, co sprawia, że są one doskonałym narzędziem terapeutycznym. Analogiczne podejście do proponowanego w tej pracy

zastosowano, aby otrzymać sferyczne kwasy nukleinowe, gdzie nanocząstkę złota skoniugowano z regulatorowymi siRNA. Tutaj zaś przedstawiona jest nowa generacja sferycznych kwasów nukleinowych, zbudowanych na podstawie koniugatu AuNP i trimeru RNA wyposażonego w różne sekwencje regulatorowe oraz linker tiolowy umożliwiający koniugacje. Wykorzystanie tectoRNA w układzie sferycznym daje możliwość zwiększenia lokalnego stężenia sekwencji regulatorowych, wprowadzenia proporcjonalnych ilości różnych elementów regulatorowych i w rezultacie poprawy efektywności układu. Proponowany system ma więc szansę, aby stworzyć układ dostarczania elementów regulatorowych, który ma potencjał terapeutyczny, gdzie koniugat RNA-AuNP pozwala dostarczyć szereg elementów regulatorowych do komórek.

Table of Contents

Abbreviations

- DNA - deoxyribonucleic acid
- RNA - ribonucleic acid
- ds – double stranded
- ss – single stranded
- dA, dC, dG, T – DNA units, deoxyribonucleosides, adenosine, cytidine, guanosine, thymidine
- A, C, G, U – RNA units, ribonucleosides adenosine, cytidine, guanosine, uridine
- G1 – 1st generation
- RNA trimers G1: T1A1B1C1, T1A1B2C9
- RNA dimers examples G1: D1A1B1, D1B1C1, D1A1C1
- RNA monomers G1: G1A1, G1B1, G1C1, G1B2, G1C9
- siR1, siR2 etc. – 21nt ssRNA
- siR1-2 etc. – siRNA duplex composed of siR1 and siR2
- G3 – 3rd generation
- HS-siR1, HS-siR7 etc. – 21nt ssRNA with thiol linker
- HS-siR1-2 - siRNA duplex composed of HS-siR1 and siR2
- CoreA1, CoreA7, CoreA9 – 94nt RNA fragments that make up G3 RNA monomers, G3A1, G3A7 and G3A9, respectively
- RNA dimers examples G3: D3A1B1, D3A7B1, D3A9B1, D3A1C1, D3A7C1, D3A9C1
- RNA trimers G3: T3A1B1C1, T3A1B2C9, T3A7B1C1, T3A9B1C1
- 3WJ, 3wj-nRA – three-way junction motifs in RNA
- SARS-CoV-2 – Coronavirus SARS that caused a global pandemic started in 2019
- COVID-19 – a disease caused by SARS-CoV-2
- PAGE - polyacrylamide gel electrophoresis
- AuNPs - gold nanoparticles
- AgNPs – silver nanoparticles
- PtNPs – platinum nanoparticles
- k-turn – kink turn motif in RNA
- siRNA – small interfering RNA
- miRNA – micro-RNA
- piRNA - Piwi-interacting RNA
- mRNA – messenger RNA

- tRNA – transfer RNA
- rRNA – ribosomal RNA
- lncRNA – long noncoding RNA
- sncRNA – small noncoding RNA
- snoRNA - small nucleolar RNA
- RNAi – RNA interference
- FAM - fluorescein
- HPLC - High-performance liquid chromatography
- nt - nucleotide
- GFP – green florescent protein
- RFP – red fluorescent protein

Introduction

The aim of the thesis

The main objective of the following work is design, synthesis and application of a new generation of tectoRNA trimer conjugated with gold nanoparticle. In this approach the main role is played by the triangular RNA structure, which carries 3 regulatory sequences, one at each arm, to target a gene of interest. Such structure was proven to regulate the GFP gene expression in the model system and served as a fundament for the current project [1]. Here we demonstrate a new design based on a thiol modified tectoRNA trimer bound to spherical AuNP. The following studies show the step-by-step preparation and characterization of the new tectoRNA-AuNP conjugates to finally prove their functionality as potential mean for RNAi induction in cancer cells.

Ribonucleic acids – RNA

RNA in biology

RNA was proven to be a universal medium for bio-structural design and assembly. Nucleic acids and proteins are the fundamental biomolecules and key players in cellular processes. From a structural point of view, DNA, RNA and proteins are chain polymers that can further adapt three-dimensional (3D) shape (tertiary structure), stable and unique for each molecule. Relying on weaker interactions these biopolymers may also be assembled into multi-modular quaternary structures.

The DNA structure was determined by x-ray crystallography published in 1953 [2, 3], owing to work of Francis Crick, James Watson and Rosalind Franklin. Since then, plenty of attention has been given to studies of nucleic acids, their biological role in protein biosynthesis and genetic information management. However, those bio-elements have even more to offer than being at the front line of the Central Dogma of Molecular Biology. Although DNA and RNA are evolutionary related and share structural similarities, such as the sugar-phosphate backbone and four nitrogenous bases, they participate in different biological processes and may be found in different forms. DNA, made of 2'-deoxyribonucleotides (5' phosphates of dA, T, dC, dG), prevails in eukaryotic cells as a double stranded, B-form helix and functionally is mainly recognized as a genetic information carrier. RNA, on the

other hand, consists of ribonucleotides (5′ phosphates of A, U, G, C) and is usually found as single stranded chains, often folded into 3D shape (Figure 1).

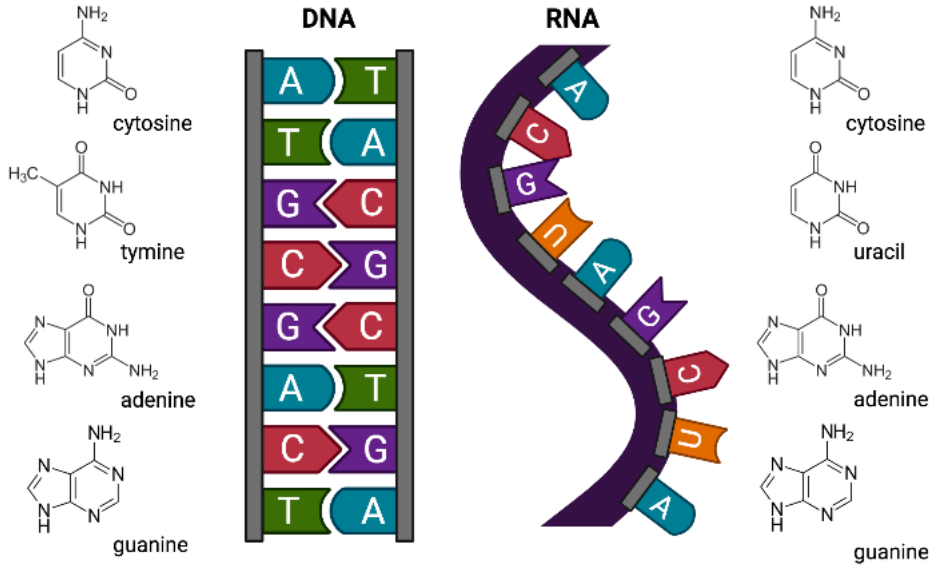

Figure 1. DNA and RNA structures (Created with BioRender.com)

RNA is primarily associated with its role in protein biosynthesis (tRNA, mRNA, rRNA) but also naturally exhibits number of functional and structural forms. The process of translation is a complex enzymatic procedure involving mRNA, ribosomes, transfer RNA molecules (tRNA) and protein factors (responsible for translation initiation, elongation and termination) [4, 5]. It is the most recognized biological process, laying at the foundation of the Central Dogma of Molecular Biology [6]. On the other hand, there is a group of noncoding RNAs which natural role is mostly related to regulatory actions in cell. Selected members of the RNA family are described below:

The messenger RNA (mRNA), in nature is synthesized in the process of transcription from the dsDNA matrix. It is a fundamental RNA molecule that serves as a template for protein biosynthesis. The development of sequencing techniques allowed better understanding of the human genome and revealed that only about 2% of human genome codes for protein [7]. Once transcribed, the pre-mRNA consists of exons and introns. In order to stabilize and prepare pre-mRNA for further processing, it is subjected to modifications, such as addition of a 5'-cap and polyadenylation of its 3′-end. The pre-mRNA is modified and spliced co-transcriptionally in nucleus to produce mRNA isoforms from selected exons. The consequent mature mRNA consists of: 1) Cap - N7-methylated guanosine at the 5′ end (5′ m7G, cap-0), connected to the mRNA chain by 5′ - 5′ triphosphate linkage.

In eukaryotes, the 2′-hydroxyl group of the two ribose sugars following 5′-cap may be methylated (cap-1, 2). This modification protects mRNA from exonucleolytic cleavage and is responsible for cap-dependent translation and serves as a recognition element for enzymes and protein factors involved in splicing, polyadenylation and transport; 2) 5′-untranslated region (5′UTR) is a nucleotide sequence, of a host-dependent length that is located downstream from 5′-cap. It can adopt 2° and 3° structure and is involved in translation initiation process [8]; 3) downstream from 5′UTR there is an initial AUG START codon, that allows for ribosome assembly and translation initiation; 4) at the 3′-end there is polyA tail that prevents mRNA from nucleolytic degradation and guides it from nucleus to ribosomes in cytoplasm; 5) the 3′-untranslated region (3′UTR) is a conserved sequence upstream from polyA which is involved in pre-mRNA processing, it's stabilization and translation regulation [9]; 6) upstream from 3′UTR there is a STOP codon, which serves as a translation termination signal; 7) the actual coding sequence, referred as the open reading frame (ORF), is located between the START and STOP codons (Figure 2) [10-12]. A mature mRNA can further be processed in cytoplasm or be translated to protein.

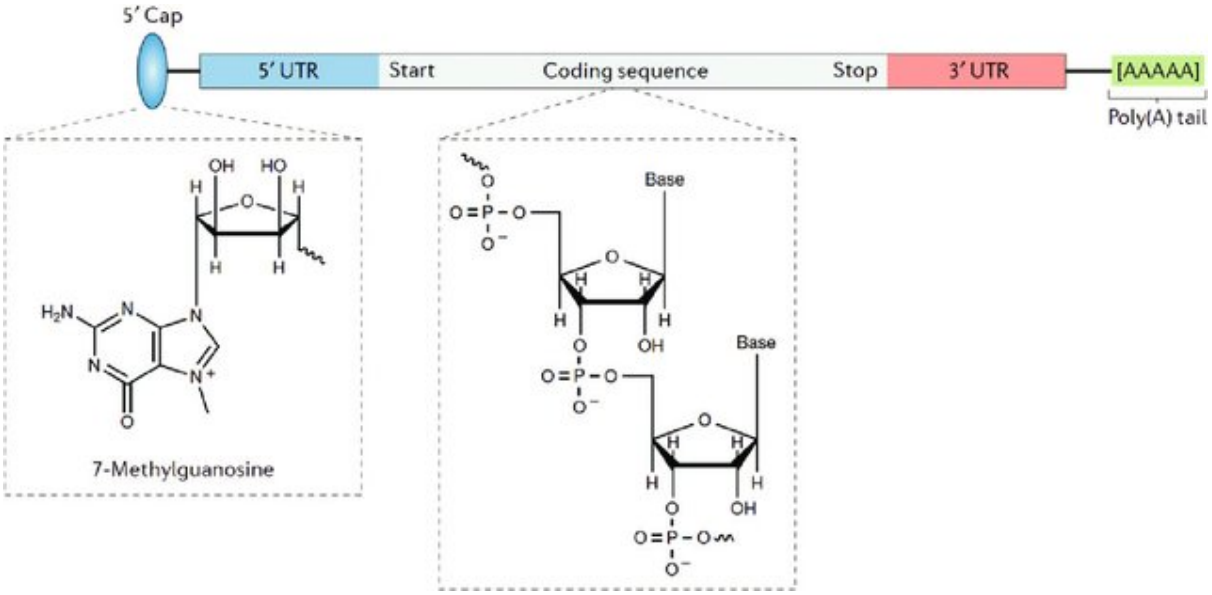

Figure 2. The mature mRNA structure model [13]

Transfer RNA (tRNA) is an adaptor that plays a key role in translating information encoded in mRNA into amino acid sequence to make a polypeptide chain of proteins [14, 15]. There is over 400 genes in human genome that encode for isoacceptor tRNAs (corresponding to the same amino acid) that are carriers for the 20 canonical amino acids (GtRNAdb database). tRNA has a highly conserved organization, with

cloverleaf secondary structure [16] that folds into tertiary L-shaped structure *via* coaxial stacking of helical and long-range interaction elements [17]. In the secondary structure representation of each tRNA a set of specific elements can be pointed out: acceptor stem, three stem–loops, D-loop, anticodon loop, TΨC loop and a variable loop (Figure 3). tRNA contains nucleoside modifications and non-canonical bases that are appended post transcriptionally, the most recognized are: dihydrouridine (D), found in the D-loop, inosine (I) often present in the 1st position of the anticodon, thymidine (T) and pseudouridine (Ψ), found in TΨC loop and methylated bases [18]. At the 3' end of the acceptor loop (74-76nt), in each tRNA exists conserved CCA sequence, which is added post transcriptionally by nucleotidyltransferases [19]. This is a key element in tRNA aminoacylation, where the amino acid is attached to the ribose of the last adenosine [20]. The structural properties alongside with specific nucleoside modifications in tRNA are necessary for ribosome attachment, codon recognition, enzyme accessibility and translation progress, which has been a subject of multiple studies [21, 22].

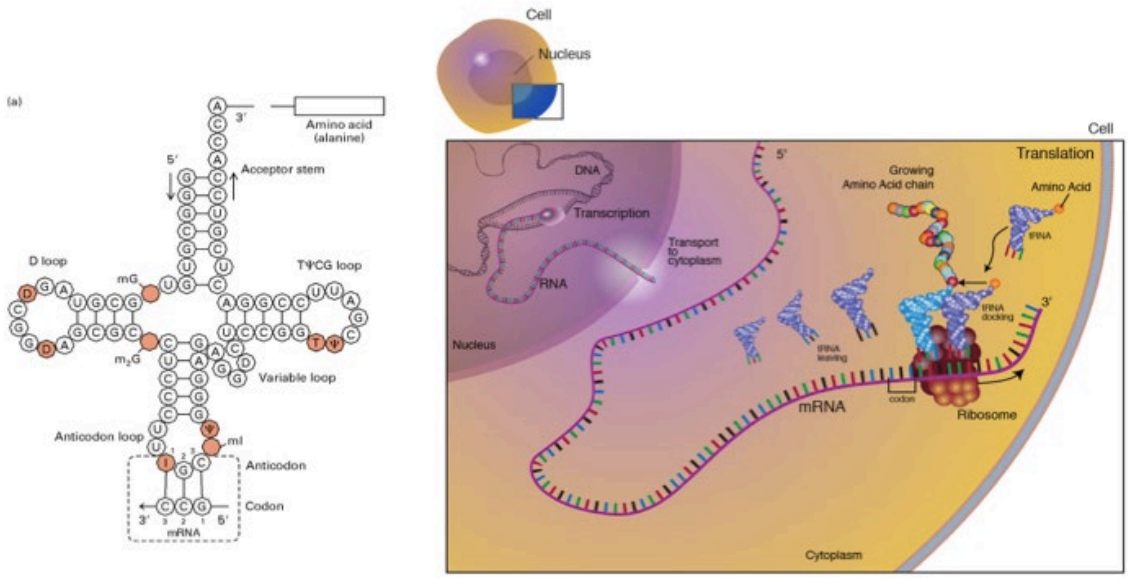

Figure 3. tRNA structure and biological role. The secondary clover leaf tRNA structure (left panel) [18]; the role of tRNA in protein biosynthesis (right panel) [23]

Ribosomal RNA (rRNA), although noncoding, accounts for about 80% of cellular RNAs [24]. It is strictly involved in the process of protein synthesis and together with a set of proteins forms ribosomes, the catalytic platform of translation. The ribosome is divided into two subunits, large and small, so are the rRNAs present in each of them [18]. Each rRNA has a unique tertiary structure with multiple stem

loop elements, similarly placed throughout different species. The rRNA is a fundamental machinery that is responsible for the whole translation process. In protein biosynthesis ribosomal RNA molecules form ribosome complex, recruit tRNAs and arrange them according to the mRNA matrix. They are responsible for catalytic peptide bond formation between upcoming aminoacyl-tRNAs and the forming polypeptide chain [25].

Beyond RNAs involved in the process of protein biosynthesis there exists a plethora of noncoding RNAs (ncRNAs), which are not translated into proteins, such as **small noncoding RNAs**: micro-RNA, short interfering RNA, piwi-interacting RNA and **long noncoding RNA**. The most studied purpose of these RNAs is gene expression regulation at the transcriptional and post transcriptional level, which is the main subject of the epigenetics or epitranscriptomics. However, the more we know about that group of RNA, the more biological processes they seem to part in.

A group of ncRNAs that act as antisense compounds is well recognized and important in the view of their biological function and therapeutic potential. **Micro RNA (miRNA)** was recognized after discovery of short regulatory RNA in *C. Elegans.* It binds to partially complementary mRNA fragments [26] and impacts its expression. The actual classification of miRNA as a group was termed in early 2000 when more examples of such regulatory elements were discovered [27-29]. miRNAs are abundant in cells and target multiple mRNAs. Typically, miRNAs are synthesized transcriptionally as pri-miRNAs, enzymatically cleaved in nucleus with assistance of RNase called Drosha [30], then as hairpin-like structures are transferred to the cytoplasm where, upon Dicer endonuclease cleavage, they mature into miRNA. However, alternative miRNA synthesis processes have been described [31] and are independent of Drosha or Dicer activity. Some miRNAs may serve as oncogenes or tumor suppressors, since changes in their abundance can be associated with cancer progression. Many studies focused on noninvasive cancer detection methods, based on miRNA markers [32-34]. From the therapeutic perspective it has also became interesting to either target miRNA molecules in order to block their function [35, 36] or to mimic the natural RNA interference process [37]. The RNA interference is widely studied therapeutic method, especially with utility of **small interfering RNAs (siRNA).** Similar to miRNA, siRNA is a product of Dicer cleavage of dsRNA and is known to be involved in RNAi silencing complex (RISC) that acts on mRNA to regulate its expression [38]. However, these two ncRNAs differ in their purpose and biogenesis. While miRNA is described mostly as host genome product, siRNA's origin is thought to be external, for example viral or transgenic [39].

Moreover, siRNAs are direct products of Dicer endonuclease acting in cytoplasm on fully complementary dsRNA fragments and miRNAs are strictly derived from nuclear hairpin precursors [38]. Contrary to miRNA, in most cases the gene expression regulation with siRNA occurs when its antisense strand, present in RISC, is fully complementary to mRNA and marks the cleavage site. The mRNA cleavage is catalyzed by the Argonaute protein after which the complex dissociates. Ideally, any mRNA can be targeted with a siRNA, which is promising from the therapeutic point of view, especially in treatment of thus far undruggable diseases. However, there still are concerns such as off-target effects and RNA serum stability that need to be addressed. The main players in the siRNA drug development are: siRNA modifications at the phosphate backbone, base or ribose moiety and selection of effective delivery agents, all to improve siRNA stability, limit off target effects and immune response [40-42]. As an effect of studies, the first siRNA based antisense therapy was developed and a first FDA approved drug was introduced to the market in 2018 [43]. The siRNA-based gene expression regulation is also the main theme of research presented in this thesis.

PIWI-interacting RNA (**piRNA**) is another representative of short RNA group, with length of 21–35nt [44]. These highly conserved small RNAs are predominantly single stranded, have a 2′-*O*-methyl modification at the 3′ termini and are found in most living organisms. In animals, piRNAs are accumulated in gonads rather than ubiquitously spread like other small RNAs, which emphasizes their crucial role in germline proliferation or spermatogenesis [45]. They may originate from long noncoding RNAs, mRNA or transposons but their biogenesis remains to be studied in more depth [46, 47]. Although piRNAs' biogenesis is not fully understood, it is certainly different from the siRNA or miRNA pathways [48] (Figure 4). Similarly, to siRNA/miRNA binding Ago proteins, the piRNA is strictly related to the PIWI protein family and forms silencing complex (piRISC) that allows to cleave the target RNA [49]. Except for the most studied regulatory role of piRNA, which was shown to impact transposons and be essential in developmental stage [49], they were shown to affect the chromatin structure by promoting the DNA methylation [50, 51]. This epigenetic regulatory role of piRNA in methylation of transposable elements is again important in fetal development but may also play a role in chromatin remodeling and histone modification that account for genetic plasticity [51]. Finally, piRNAs have been recently found to play a role in cancer development, as they part in gene expression regulation pre and post oncogenesis [52]. In addition, alterations

in piRNA levels between healthy and tumor cells were identified, which makes them an interesting biomarker for clinical diagnostics [53, 54].

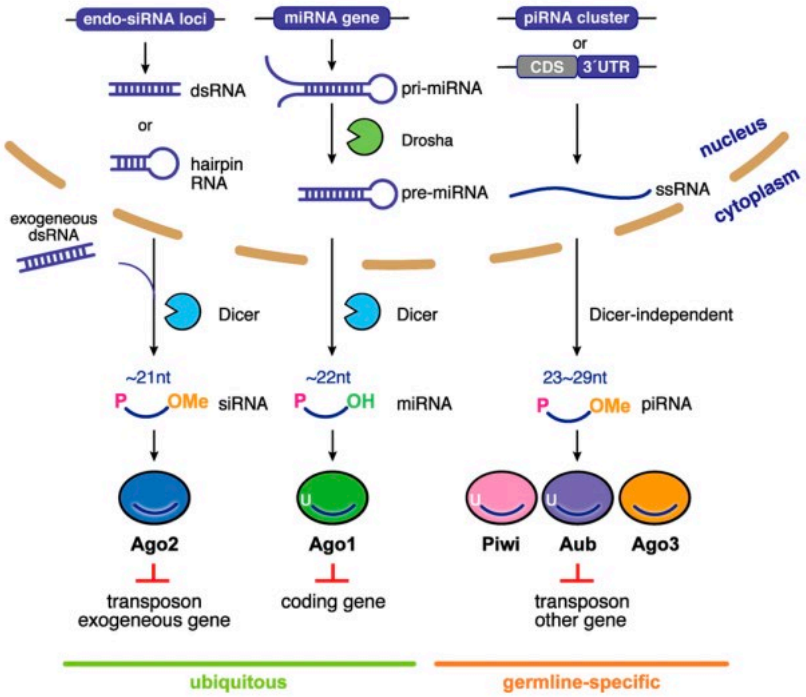

Figure 4. Small RNAs in the gene expression regulation [55]

The group of **long noncoding RNA (lncRNA)** combines all RNA transcripts that are longer than 200nt and are not templates for protein synthesis. Owing to the development of large-scale cDNA sequencing, it became possible to better understand the complexity and abundance of mammalian, and especially human transcriptome [56, 57]. In an extensive study from 2018, 270 044 lncRNA transcripts were identified in Human transcriptome, out of which 1867 lncRNAs were identified to have a scientifically validated biological function [58]. As a result of functional lncRNAs analysis, the 3762 different function and disease associations were recognized. Moreover, based on methylation profile, genome variation or miRNA interaction, 97 998 of the lncRNA were predicted to have a potential for disease studies. While the group of lncRNA comprises of variety of entities it is impossible to define one uniform set of features they share. Firstly, the lncRNAs may be synthesized in different ways (Figure 5). Most of the human lncRNAs are transcribed by RNA polymerase II or other RNA polymerases and, similarly to mRNA, are capped at the 5′ terminus and polyadenylated at the 3′ end [59]. These are mainly intergenic transcripts, derived from the fragments embedded within introns on the sense strand; antisense transcripts generated from the opposite strand of

protein coding genes [60]; or sense transcripts that are later stabilized upon RNase P cleavage [61]. Some of the lncRNAs are flanked with small nucleolar RNA (**snoRNA**), which is a conservative guide molecule naturally involved in post transcriptional modification of other RNAs such as rRNA or tRNA [62]. In some cases, the snoRNA is placed on both ends of the excised introns post splicing or at the 5′ terminus of the readthrough transcripts. Alternatively, the mRNA splicing may lead to formation of **circular RNA (circRNA, ciRNA)** from excised introns or back splicing of exons [63, 64]. lncRNAs also vary in terms of distribution in nucleus and cytoplasm and also within cells and tissues. At the moment lncRNAs are the most attractive due to their role in signaling pathways, chromatin function modulation and their impact on the gene expression at the transcriptional and post-transcriptional level. With the multiplicity of their biological functions, lncRNAs became interesting for both science and medicine, as biomarkers or therapeutic targets [59, 65].

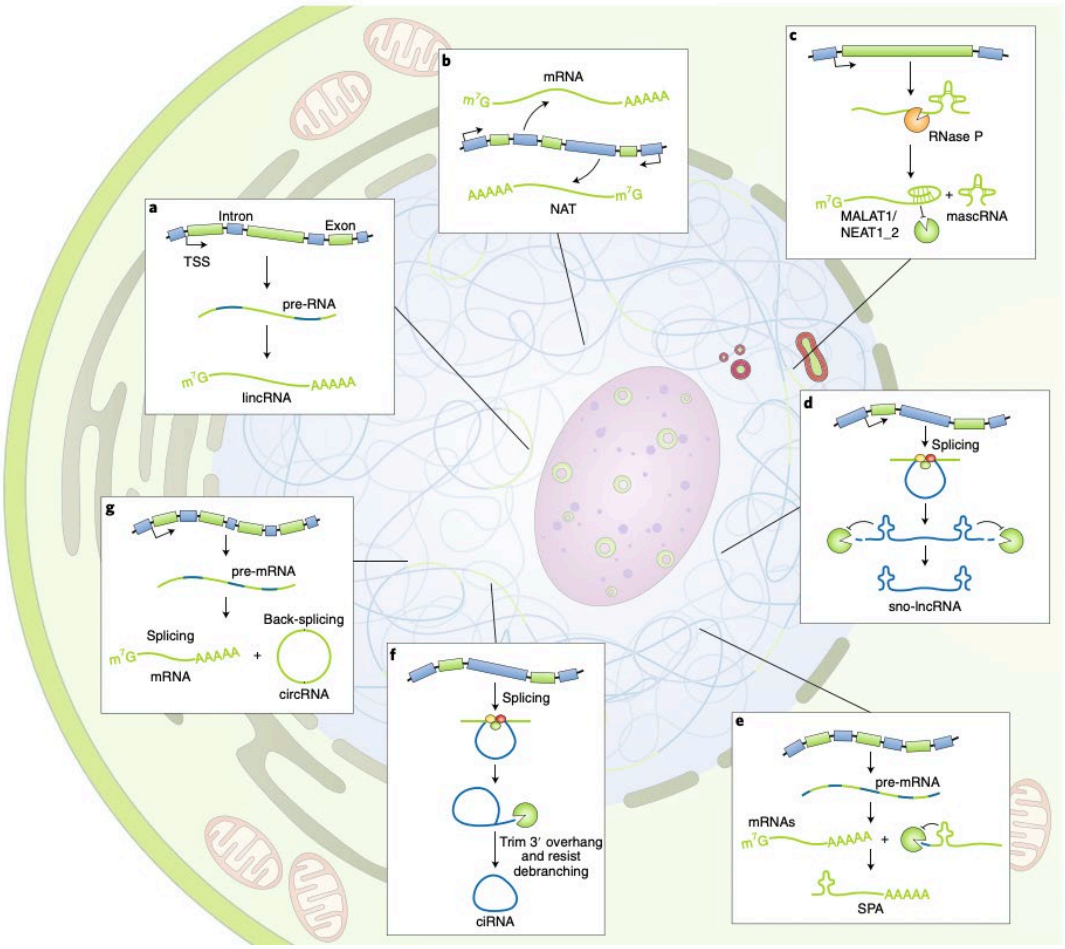

Figure 5. The origins of lncRNAs in mammalian cells [65]

Among noncoding RNAs there is a group of catalytic RNAs referred as **ribozymes** (ribonucleic acid enzymes) that are classified based on their enzymatic function

rather than size. First published in 1982, the ribozyme discovered in *Tetrahymena thermophila* rRNA intervening sequence, changed the way the RNA scientists perceived this molecule beyond being the genetic code [66]. About the same time, the catalytic activity was attributed to the RNA unit of ribonuclease P [67]. Only 7 years had passed since the self-splicing Group I intron ribozyme discovery till the Nobel Prize was awarded to Cech and Altman for their "discovery of catalytic properties of RNA". In nature ribozymes occur in variety of sizes and shapes and their common denominator is the catalytic function, which makes them important players in some biological processes. Besides the ribosomal RNA, that is to catalyze the peptide bond formation during the translation process (described above) [68], ribozymes can cleave or ligate the phosphodiester bonds which is crucial for mRNA splicing, processing, maturation and viral RNA replication [69]. Ribozymes owe their catalytic potential to the tertiary structure formation, which creates an optimal environment for the reaction. Often ribozymes are accompanied by metal ions that stabilize their structure and are directly involved in catalysis reaction [70]. This class of RNA may be divided into 2 categories of small and large ribozymes. The examples of small ribozymes are: **hammerhead**, the model ribozyme in scientific research, derived from plant viruses, which is a single folded RNA strand that can cleave itself and participates in rolling circle replication mechanism [71]; **hairpin**, similar to hammerhead ribozyme, discovered in tobacco virus, catalyzes self-cleavage and ligation in rolling-circle virus replication to produce RNA satellites [72]; hepatitis delta virus (**HDV) ribozyme**, essential for virus replication, catalyzes self-cleavage of rolling-circle replication products to single units [73]. The large ribozymes are for example: **group I and II introns**, that catalyze their own splicing in ribosomes and organelles [74], **RNase P**, involved in tRNA processing [67] and **ribosome** [75]. With the progress in the bioinformatics and synthetic biology it also became possible to take advantage of these catalytic RNAs, which has led to the artificial ribozyme development. With such toolbox in hand one can implement it for multiple purposes [76-78], such as gene expression regulation [79-81], in CRISPR applications [82, 83] but also for biosensing [84, 85].

Aptamers and **riboswitches** are another two elements of RNA family which function directly results from the special organization and 3D structure. RNA aptamers are RNA oligonucleotides that specifically bind to their target molecule, similar to the antibody-antigen pair [86]. Richness of target specific RNA aptamers was discovered and defined owing to the evolution of the SELEX technique (systematic evolution of ligands by exponential enrichment), first introduced in

early 1990 [87, 88]. Among molecules targeted with RNA aptamers, there are for example: thrombin [89], lysozyme [90], neomycin [91], prostate specific antigen (PSA) [92], dopamine [93] etc. The multiplicity of aptamer targets made them an exceptional tool for therapies and biosensing. There are also aptamer based sensors, or aptasensors, which precisely target selected molecule, for example: sensors for clinical screening [94], imaging [95, 96], detection of small molecules [97, 98] like neomycin [91] or theophylline [99], drugs [100] and many more [101, 102]. Aptamers are also an interesting therapeutic tool used not only for imaging and detection [102] but also for inhibition of the protein targets, for example circulating histones attributed to multiple organ dysfunction syndrome [103, 104]. Importantly, their target specificity was is advantageous for cell internalization. In such approach aptamers are conjugated with a drug of choice to facilitate delivery through selective interaction with target cells [105, 106].

The riboswitches, on the other hand, are unique due to their ability to rearrange structurally upon ligand binding [107, 108]. Naturally they play a key role in the feedback loop that regulates gene expression depending upon the presence of target molecule [109]. This distinctive feature of riboswitches draws attention of many scientists and studies have shown their applicability in the field of diagnostics, biosensing and therapy [110-112]. The rationally designed, synthetic riboswitches [113] usually have an aptamer-like element that captures the ligand of interest and triggers the structural rearrangement in the switching domain [114-117]. Such RNA devices are mostly applied for switchable gene expression regulation and fine tuning [118, 119] but also can be introduced into more complex devices such as ribozymes [120].

Taken all together, it is clear how important role RNA plays in nature as well as in research. The wide range of naturally occurring structural variants and functional richness made RNA an exciting target for studies.

Structural RNA

Any complex RNA structure may be demonstrated as a composition of different interactions (electrostatic forces, hydrogen bonds, stacking interactions) that are classified as primary (1°), secondary (2°) and tertiary (3°) structures.

The primary RNA structure is defined as a sequence of nucleotides, usually presented in 5′-3′ direction (Figure 6). Nucleotides are interconnected *via* phosphodiester bond formed between 3′-OH group of 1 nucleotide and 5′ phosphate of the following nucleotide. In nature RNA is produced during a transcription process accompanied by the enzymatic machinery composed of RNA polymerase and transcription factors that control the process [121]. For the chemical synthesis of RNA, the most common approach is currently based on phosphoramidite method using the solid-state matrix, which was first described for DNA production [122-124]. This method is effective to obtain long DNA fragments (over 100nt) and for incorporation of modified nucleotides [125]; it is however limited to synthesis of short RNA fragments due to lower coupling efficiency of the RNA phosphoramidite monomers. In order to obtain longer RNA strands (>50nt) the enzymatic method - run-off *in vitro* transcription is often utilized [126, 127]. This method is based on the transcription process and involves use of dsDNA templates, nucleoside triphosphates and RNA polymerase, which catalyzes the RNA chain polymerization. Currently, owing to the advances in the molecular biology, modifications of the RNA polymerase enzyme have been introduced to allow use of a broader range of nucleoside triphosphates, for example noncanonical bases or ones carrying modifications [128-130]. Although some reports of site-specific incorporation of modified RNA nucleotides have been presented [131, 132], the specificity and controllability of the polymerization process is still more difficult in enzymatic framework comparing to the solid-state synthesis. Instead, longer modified RNA strands may be obtained by ligation of modified and unmodified elements [133], crosslinking [134, 135], post-transcriptional modifications at the termini [136, 137] or 2′-OH of ribose [138-140]. Emerging field of click chemistry also offers a way of modifying nucleic acids. In the click preparation protocol, an unnatural nucleoside with click-reactive group is incorporated chemically or enzymatically into the sequence of interest, which may be further functionalized by a chemo-selective reaction between the labeled sequence and a modifier containing the cognate reactive group [141-145]. The RNA modification methodologies are however still in a great demand for improvement in terms of efficiency and stability of by-products and products [41].

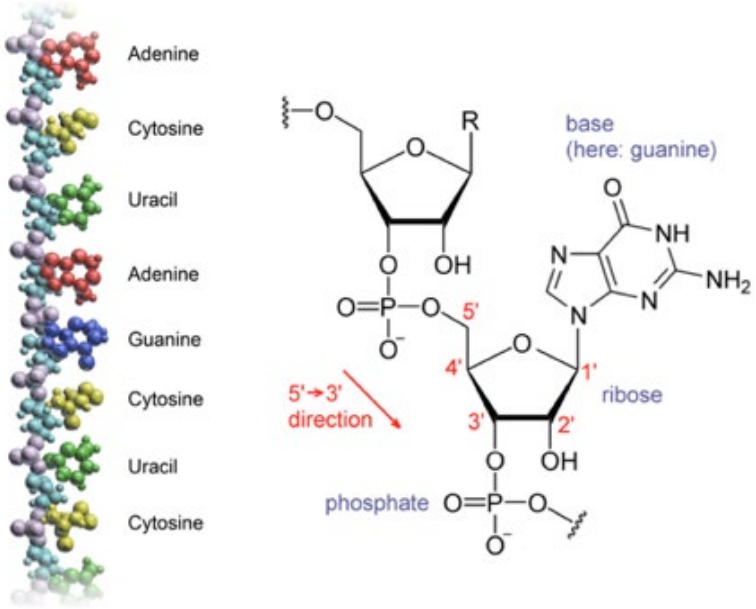

Figure 6. Primary RNA structure [146]

Formation of complementary Watson-Crick canonical base pairs gives raise to the secondary structure arrangement of the RNA into double stranded helix. RNA A-form helix, owing to the presence of 2'OH group on ribose forming the RNA backbone, is more thermodynamically stable than DNA B-form helix, structurally is more compact and stiffer, with a 2.9nm helical turn [147, 148]. The helical Watson-Crick segments in RNA are alternated with other 2° structural motifs like loops, bulges or multiway junctions/multihelix junctions. With development of bioinformatics tools, the secondary structure of RNA sequences can be predicted with a high degree of accuracy, based on energy minimization algorithms *via* software like mFold, RNAfold or RNAsoft [149-152].

Beyond the canonical Watson-Crick interaction, there is a library of possible 12 noncanonical base pairs that can be found within the same 2° helix or contribute 3° structure formation (Figure 7). The 12 noncanonical interactions were defined by Leontis and Westhof [153-156] and are often critical for specific RNA motifs formation, thus reflect on their specific function. The noncanonical interactions are defined based upon orientation of the two interacting bases, by specifying the interacting edges (Watson–Crick, Hoogsteen, or Sugar edge) and cis/trans orientation of the glycosidic bond (Figure 7). An example of a noncanonical base pairing can be found in the tRNA anticodon loop. A 5' anticodon base is referred as the wobble position and it allows for unusual base pairing, for example G-U, which broadens the tRNA codon specificity. Owing to that, one amino acid may be coded by several triplets [157]. A kink-turn (k-turn) is another example of a biological use of non-

canonical base pairing. It consists of a three-nucleotide bulge and a tandem trans sugar edge-Hoogsteen - G:A base pairs, which allows to form a sharp kink in the RNA duplex. Such motif was shown to be involved in protein binding to so called k-turn binding proteins [158].

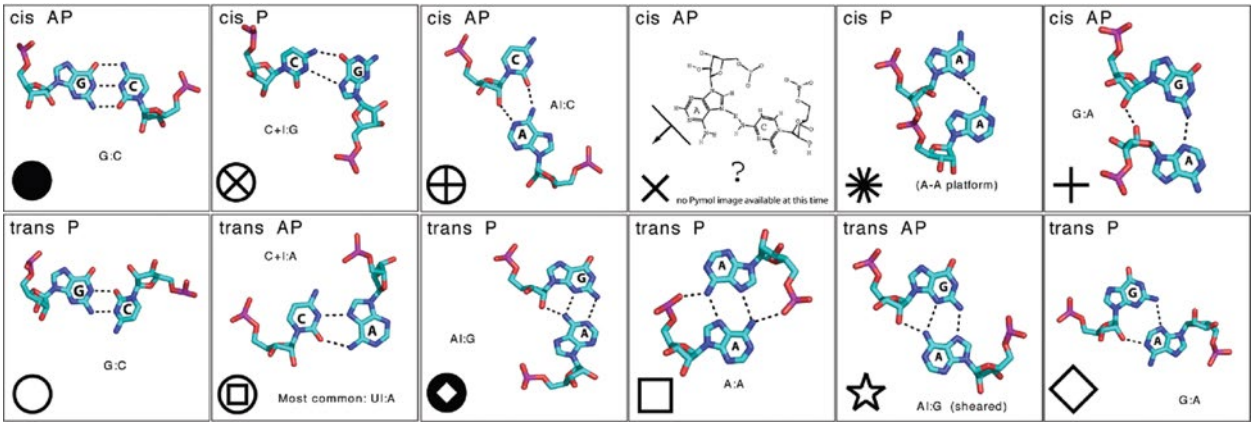

Figure 7. Non-canonical base pairs found in RNA adapted from [159]

RNA folds into 3D objects when the 2° structural segments interact. Such interactions are usually driven by Van der Walls forces, metal ion coordination, π-stacking of the aromatic rings but also hydrogen bonds formation between canonical and noncanonical base pairs at the single stranded regions, loops or bulges. The presence of divalent metal ions is necessary for proper 3° structure formation as they are often found in the noncanonical 3D arrangement in the interactions with phosphates and/or 2'-hydroxyl [160]. Similarly, to protein folding, in the stable 3D RNA structure specific RNA motifs may be distinguished and treated as modules of a greater unit. As the crystallographic and NMR RNA structures were deposited [161-163] and the field of bioinformatics greatly improved over the years, libraries of specific sequence signatures for RNA motifs were created (RNA FRABASE) [164, 165]. There exists an abundance of naturally occurring discrete sequences forming motifs like: RA-motif [166], multiway junction motifs [167], pseudoknots [168], kissing-loops [169], loop–receptor motifs [170], G-tetrads [171] and others [162]. With the structural knowledge and help of evolving computational tools it became possible to engineer new structures based on the naturally existing motifs extracted from larger RNA domains like P4-P6 domain of group I ribozyme, riboswitches or tRNA motif.

RNA nanotechnology

With the advancement in the fields of nanotechnology, computational prediction methods and structural nucleic acids, the possibility to create artificial, programmed, 3D nano-objects made of nucleic acids became possible. In early 1980 Ned Seeman [172] presented an idea of a 3D crystalline DNA material that could be assembled based on predicted base-pairing interactions. This idea was later confirmed experimentally [173] and the first synthetic branched DNA junction was obtained. Since this discovery, the DNA nanotechnology had been developing for almost two decades. In late 1990's an idea emerged to apply similar principles for RNA nanotechnology [174, 175]. Structural studies on nucleic acids have exposed the richness of stable structural motifs and modularity of RNA [126] that is different from DNA [176]. *De novo* DNA assembly is typically achieved by base pairing between short oligonucleotides which are shaped by introducing four-way junction motifs, derived from Holliday junction, to form structural DNA tiles [177]. In RNA framework, structural motifs may be 'extracted' from the original structure and utilized as building blocks to create a new RNA object (Figure 8) [159, 178-180]. This approach, based on RNA puzzles' assembly, called RNA architectonics, is essentially an extension of an RNA tectonics concept introduced by Westhof and Jaeger in 1996 [174, 175]. Currently, an inverse folding process is the most popular method for rational design of tectoRNAs [178]. It starts from the RNA motif database of resolved RNA structures (x-ray crystallography or NMR structures deposited in PDB). A set of defined motifs is extracted, organized to fit to the anticipated structure and linked with each other to complete the tectoRNA unit (Figure 8). The 3° model is converted to 2° diagram, where nucleotides, essential for motif's stability are conserved. Sequence modifications and extensions are possible in the linking elements (usually helixes) or loops to allow proper spacing or specific fragment insertion, it is however not recommended to extensively change the conserved structural fragments. Final 2° structures are then optimized computationally by free energy minimization algorithm [181, 182] to assure thermodynamic stability and reduce the potential alternative folds. A 1° sequence is derived from the 2° optimal model, synthesized and applied to experimental analysis with variety of methods staring from native PAGE electrophoresis, temperature gradient gel electrophoresis (TGGE), atomic force microscopy [1, 166, 183] or electron microscopy [127].

In the recent paper by Geary et al. one may see combination of all the above-mentioned methodology for design, assembly and visualization of a heart-shaped RNA nanoobjects [184].

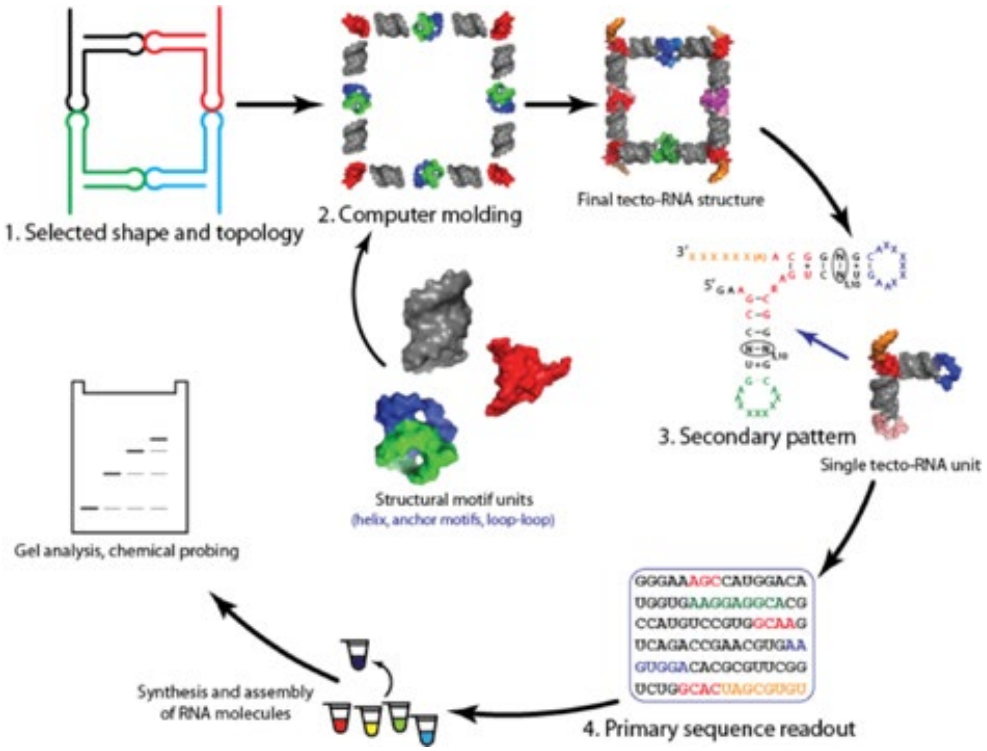

Figure 8. RNA rational design [159]

Another approach to form new RNA 3D objects is called RNA origami. Similar to the real origami art that allows to fold one sheet of paper into a 3D shape, the RNA origami, derived from DNA origami [185], allows to form a 3D object based on long single RNA strand. Similar to DNA nanotechnology, this approach introduces structural turns between helical elements with crossover motifs. However, while in DNA origami, the short structural staples play important role in holding the final 3D structure [186, 187], the RNA may be designed to self-assemble without additional support. This sophisticated method introduced by Geary et al [188] utilizes the above-mentioned rational design rules to model a final structure from single RNA strand but also is programmed in such a way that allows for co-transcriptional processing of the DNA template to the desired RNA structure. The DNA template is programmed such that the RNA polymerase moving along the template produces a set of stable hairpins that fold up and condense consecutively and allow for further long-range interaction and formation of a multidomain object [189]. The RNA origami was recently shown to be suitable for biomedical applications as it could

be programmed to be targeted by Dicer and release siRNAs [190] or equipped with thrombin binding aptamers to improve the anticoagulating effect of the aptamers [191, 192].

Regulatory and bioactive structural RNA

RNA plays an important role in cellular function. The most recognized is an mRNA that serves as a blue-print for the protein synthesis. However, non-coding RNAs are also largely represented among RNA family. The siRNA is one of the most recognized members of the non-coding RNA group. Together with miRNA, siRNA is responsible for gene expression regulation *via* the RNA interference (RNAi). In nature, this process was recognized to play a role in regulation of gene expression, especially in developmental stage, but also in resistance to viruses or transposons. External induction of this phenomenon was first described by Fire and Mello in late 90's, where the authors introduced exogenous dsRNA and observed its regulatory effect on reporter genes in *Caenorhabditis elegans* [193]. However, the role of siRNA in gene expression regulation was explained in 2001 by Elbashir et al. [194] Natural siRNAs are short (19-22nt) double stranded RNA fragments, which may be produced by cleavage of longer double stranded RNA by a nuclease Dicer [195]. This enzyme, belonging to the endoribonuclease group, recognizes dsRNA, longer than 21bp and cleaves ~20bp fragments leaving a two base 3'-overhang. It was shown that Dicer cleavage may occur for dsRNAs or hairpin RNA of different lengths, sequences, with sticky and blunt ends. Dicer preferably processes the dsRNA with 2nt 3' overhangs. However, the length of a cleavage product changes if the substrate's 3' overhang varies between 0 and 3nt. Similarly, the cleavage site shifts in the presence of unpaired bulges. That suggests that the enzyme 'counts' base paired nucleotides from the 3' overhang [196, 197]. In nature, the Dicer cleavage is followed by assembly and maturation of an RNA induced silencing complex (RISC), composed of guide siRNA strand and Argonaute proteins guiding the process of mRNA recognition and cleavage [198]. The mRNA cleavage is dependent on efficiency of siRNA recognition and binding. Thus, it became essential to understand rules governing this process, especially for the synthesis of externally delivered siRNAs. The extensive studies of siRNA silencing efficiency have finally led to establishment of the guidelines to follow while designing siRNAs and are currently referred as the Reynolds rules [199]. For example, these rules support the entry of desired siRNA strand (guide) to the RISC, as they favor weaker base

pairing (AU rich) at the 5′ of guide strand. Low internal stability as well as specific placement of A/U nucleotides in the siRNA (positions 3, 10, 19 of a passenger strand) are also essential in target recognition and cleavage, which is tied to the Argonaute protein (slicer) preference. The mRNA is cleaved at the 10th nucleotide from the 5′ end of guide RNA which is mediated by the PIWI domain of the Argonaute. Following mRNA cleavage, the RISC is released and mRNA is no longer functional. After that, the RISC can dissociate and its components may be recycled to form a silencing complex with another guide RNA. The released RISC can also be reused 'as is', with the same guide RNA, to target another copy of the same mRNA. The siRNA is recycled in all eukaryotes [200], but unlike simpler organisms where it stays effective through generations (e.g. C. elegans [193, 201]), RNAi effectivity in mammalian cells is much lower and lasts up to few days [202, 203]. Alongside the advancement in programmed RNAi and nanotechnology of delivery agents, the siRNAs emerged as potential therapeutics to be externally delivered to regulate unwanted gene expression [204, 205]. Another approach utilizing RNAi mechanism and siRNA fragments embedded into complex structural RNA was suggested [206, 207]. In this setup regulatory fragments are incorporated into or extend from the structurally defined motif to form tertiary structures such as dimers [208], trimers [1, 209], hexamers [210], cubes [180] or octahedrons [190]. Such RNA nanoparticles are advantageous due to the greater stability in cellular environment but most of all, the complex structure allows for simultaneous introduction of several siRNAs aiming for different targets or equipping the nanodevice in additional functionalities like aptamers [206, 207, 211], dyes [207, 211] or antibodies [212].

Triangular RNA molecules:

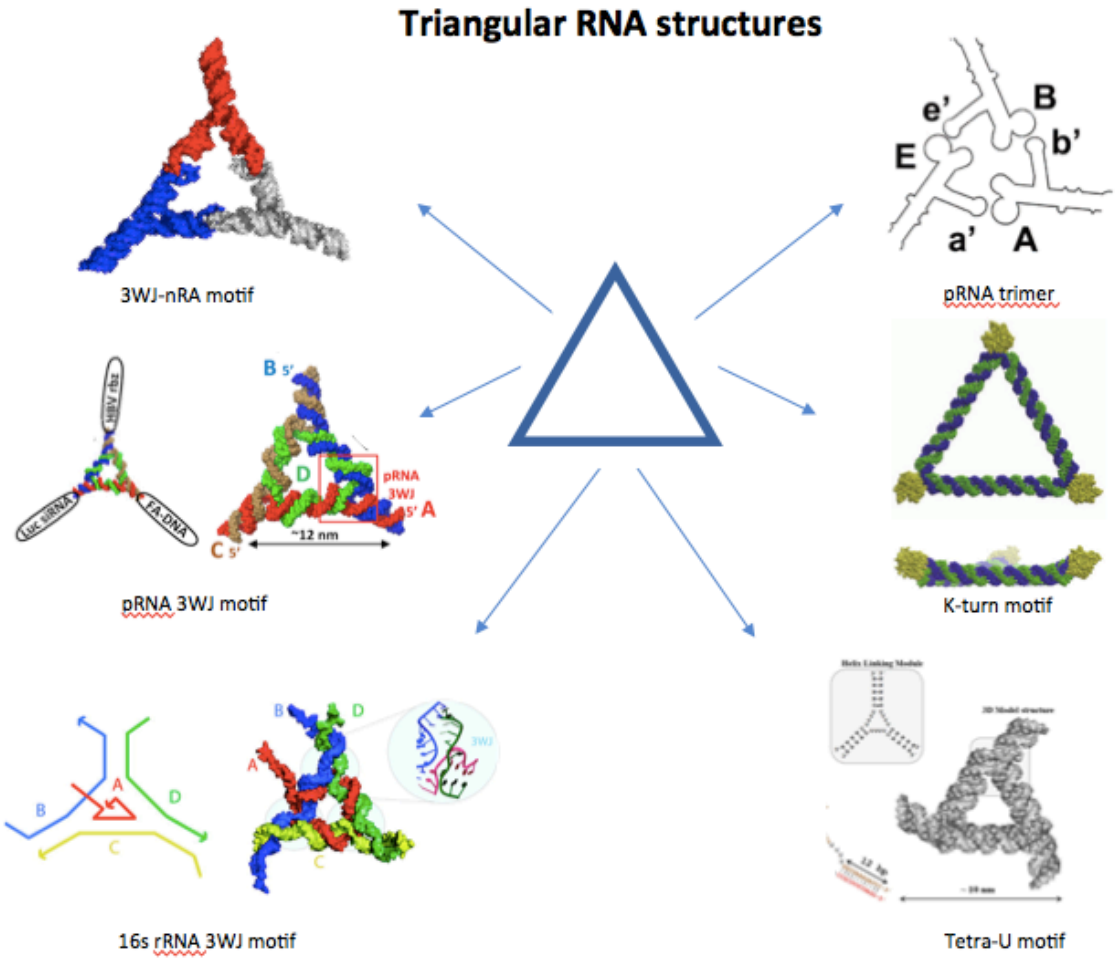

Figure 9. Triangular RNA structures. (3WJ-nRA motif [1], pRNA 3WJ motif [211], 16s rRNA 3WJ motif [213], pRNA trimer [209], K-turn motif [214], Tetra-U motif [215])

The first attempt to create triangular RNA structure with regulatory function was proposed in early 2000's [207], where the RNA trimer was made of the 3 monomers, each based on the pRNA motif (RNA from phi29 bacteriophage) [206, 216, 217]. The monomers were equipped with CD-4 glycoprotein binding aptamer, folate and siRNA fragment or fluorescently labeled siRNA. Such combination of functionalities allowed for target recognition, binding and simultaneous visualization of delivered constructs. Such structural RNAs were showed to be processed by Dicer [218] and were used against different cancer models, like nasopharyngeal carcinoma [218] or ovarian cancer [208]. In the ovarian tumor model, the pRNA based RNA dimer consisted of 2 siRNAs targeting against 2 genes simultaneously and a folate-receptor recognition tag [208]. This pRNA-based design was further developed and used to create boiling-resistant triangular RNA scaffolds [211]. The triangular module is a tetramer, based on three RNA fragments

forming 3WJ domains of phi29 pRNA with extended helixes and one RNA segment forming the triangle's scaffold (Figure 9). The angle between 2 of the helixes was approximately 60° and the helixes were equipped with specific sticky ends to allow binding between trimers and eventually form a hexamer or more complex 2D honeycomb-like arrays. The presented structure was successfully equipped with 3 fluorescent probes (MG and SPINACH RNA aptamers, Cy3-labeled DNA) for tracking of triangle formation. Later the same design, harboring ribozyme, anti-luciferase siRNA, and folate conjugated ssDNA was proven to maintain activity of each added functionalities. Likewise, an siRNA carrying RNA assembly based on DNA-derived DX tile motif, was used to form functional RNA lattices capable of RNAi induction [219]. Those examples have confirmed the uniformity of RNA structures and showed that multiple functionalities may be introduced to the single molecule.

The richness of the RNA world offers more than one way to form a desired shape, which was well demonstrated on the triangular platform. Previously mentioned kink turn [158] was utilized to form another equilateral triangle [220]. The K-turn in this design plays two key roles, it allows for specific, high affinity binding of the ribosomal protein L7Ae and formation of 60° angle upon its binding. By changing the number of K-turns introduced to the RNA structure one may impact the shape of the RNA-protein hybrid which was presented by the high-speed AFM technique [221]. To obtain a triangle, 2 RNA fragments carrying three (K-turn) motifs were designed. These motifs are separated by double helical segments upon assembly, and may be equipped with up to three L7Ae proteins in a concentration dependent manner. This RNA-protein complex was further modified by manipulating the length of the double helical fragments between apexes and modification of the protein itself [212]. In this approach the triangle was designed to regulate the cell surface receptor activity and, to achieve that, the apexes were equipped with the fusion protein consisting of L7Ae and two antibody-binding domains or fusion of L7Ae and N-terminally trimmed galectin. The modified galectin in nature leads to T-cell's glycoreceptors assembly and here was utilized as a tool for apoptosis induction. Authors showed that not only the triangle is able to successfully bind to the specific receptor on the cell surface but also, the triangle size variation allows to control apoptotic reaction. Based upon flow cytometry studies, authors suggested that the RNA structures form lattices on the surface of cells. As the triangle is larger the bound receptors are more spaced and it hinders apoptosis. Contrary, as the triangle diameter gets smaller, more of the constructs

attach to the surface bringing the receptors closer thus promoting apoptosis. This RNA-protein complex was finally modified by adding functional siRNA or fluorescently labeled RNA at the triangle sides to induce RNAi or visualize the construct in cells [221]. The presented construct was reported to specifically bind the target cells *via* affibody attached at the apexes and regulate the GFP gene expression. This K-turn triangle design was later studied to allow controllable attachment and steric positioning of the functional proteins [222], it was also modified to carry 3 different proteins by assembly of 3 protein-bound monomers *via* kissing loop motifs [214].

Another strategy undertaken to build an RNA triangle [213, 223], bases on the three-way junction (3WJ) motifs position at the corners. The first approach was based on the four RNA strands, where 3 strands form sides of the triangle and are held by the 4th internal core strand; [213]. The second approach consists of three monomers connected *via* specific kissing-loop interaction [223]. Each monomer was designed following the RNA architectonics and rational design approach [126, 159, 174, 178, 224] (Figure 10). It was based on the centrally placed 3WJ motif which allows to form a Y-shaped structure, with 3 double helical arms pointing out from the motif. One arm of a monomer carry the regulatory fragment at the ends, with 2nt 3'-overhang which facilitates Dicer cleavage. The 2 remaining arms are flanked with 6nt pairing loops, specific between monomers. The loop-ended arms are placed 60° from one another that allows formation of a nearly equilateral triangle upon trimer assembly. Previous study showed that the regulatory siRNA fragments incorporated into the structural RNA trimer were effectively released and induced RNAi [1]. The picture below presents the design and architecture of the trimer, referred in presented studies as a first generation (G1).

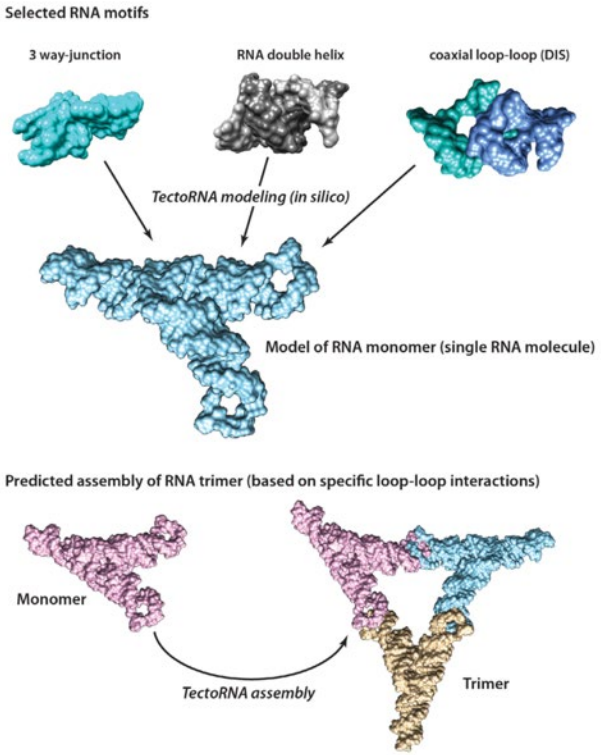

Figure 10. Structure of the triangular tectoRNA. From Jedrzejczyk, D. & Chworos, A. (2015) [223]

A tetra-U helix linking motif turned out to be a versatile platform for RNA structures assembly, allowing to fabricate corners of a triangle [215]. A triangle based on the tetra-U helix linking motif was built from four RNA strands, similarly to the beforementioned 3WJ triangle [213]. This structure had the 3 corners equipped with siRNAs targeted against GFP gene or red fluorescent dye for localization and was shown to enter the cells and regulate the gene expression. Authors also suggest that the tetra-U helix linking motif has potential to be used as a platform for assembly of squares, pentagons, hexagons and higher order polygons.

Square RNA structures:

In analogy to variety of methods used to form an RNA triangle, the nature of RNA and selection of motifs allow to build more complex structures such as squares [166, 225, 226], hexagons [179, 210], cuboids [180], octahedrons or 3D structures [190, 227] etc. In order to create a square structure, the motif of 90° angle is the most straightforward. It was achieved by incorporation of 4 right angle motifs (RA) to form corners of a square [166]. Each of the RA motifs were introduced to 4 separate monomers, with 2 helical arms equipped with specific loops to later assemble a tetramer in a square shape. The open end, sticking out from the RA motif, enabled functionalization leading to form a 2D lattices by binding between specific sticky

tail connectors. The controllability of square assembly and formation of lattices was further utilized to direct the AuNP deposition within the 2D scaffold [228]. Another type of assembly allowing to form an RNA square are based on the 3WJ or tRNA motifs [225] introduced to monomers, which associate *via* loop-loop interaction, same as in the triangle and the beforementioned tectosquare [166, 223]. The structure of the smallest square RNA construct (100 bases) was obtained by introduction of the IIa bulge domain from the internal ribosome entry site (IRES) of the hepatitis C virus (HCV) as a platform for 90^{o} angle formation. Here the monomers assembled based on complementarity [226]. Similar to the triangular framework, there is a square shaped RNA-protein complex [229]. This was built based on the RPL1 rRNA motif, which promotes formation of a ~90^{o} angle and specifically binds ribosomal protein RPL1 (from a thermophilic archaeon (*Methanocaldococcus jannaschii*), which is analogical to the L7Ae binding motif in the triangles. Such square RNA objects are also good candidates for siRNA functionalization.

RNA Polygons

An inverted loop-loop interaction originating from the RNAI/RNAII complex from *E. Coli* exhibits a characteristic 120^{o} bend at the helix junction, which was utilized in rational design of a nanoring RNA structure [179, 230]. By changing loop sequences, the 6 monomers can be designed to assemble specifically to form a final hexameric structure. The structure of monomers allows also for further modification or an extension at each monomer of the hexamer. This nanoring model was later assembled and analyzed experimentally [210] (Figure 11). In terms of siRNA incorporation, two main approaches may be undertaken: the siRNA sequence may be introduced into each monomer of the hexagon or protruded perpendicularly from each side, as extension of a monomer. Both nanoparticles' types can be processed by Dicer releasing functional siRNA fragments, showing a potential to become another siRNA carrier. Moreover, it was reported that those RNA constructs express increased thermal stability and in human serum. The co-transcriptional assembly of the nanoring structures carrying siRNA fragments was presented later [231]. An equimolar set of DNA templates was transcribed into tectoRNA elements with wild type T7 RNA polymerase in the presence of either classical nucleoside triphosphates or with UTP replaced by 2′ -fluorinated UTP. Such nanorings effectively hindered the GFP expression in the model system and, as expected, the fluorinated structure was more resistant to nucleolysis in blood

serum. Furthermore, the nanoring model was modified by hybridization with DNA or introduction of other functionalities, such as: RNA aptamers, fluorescent dyes, proteins [232]. The protruding dsRNA fragments in this design were attached to the nanoring *via* toehold interaction, which allowed to extend the range of possible functionalities and simplify modification. Structural RNA nanorings are effective tools for imaging (fluorescent dye localization), FRET imaging (fluorescently labeled R/DNA hybrids reassociation in the presence of cognate hybrids [233, 234], or gene silencing by attached siRNAs and aptamer directed delivery (EGFR specific aptamer).

With the development of RNA nanotechnology tools for therapeutic applications it became essential to explore the potential unintended immune activity and off target effects of such functional RNA structures [235]. The immune response of RNA, RNA/DNA and DNA polygons (triangles, tetragons, pentagons and hexagons) was investigated. It was determined that both RNA and RNA/DNA polygons stimulate release of IFN-β, suggesting that RNA presence is necessary to trigger interferon response. Polygons however, did not provoke the release of cytokines. The RNA/DNA polygon or RNA fiber aiming to deliver siRNA with simultaneous blockage of NF-k B and FRET signal induction were recently presented [236]. That structure was designed to regulate the target gene expression, visualize the RNA-DNA reassociation in cells (FRET) and perturb LPS-induced NF-kB translocation, hence regulate proinflammatory cytokine release. The nanotechnology of structures composed of RNA holds a great promise to play a role in targeted gene therapies, and with tunable immune response may offer some clinical possibilities [237].

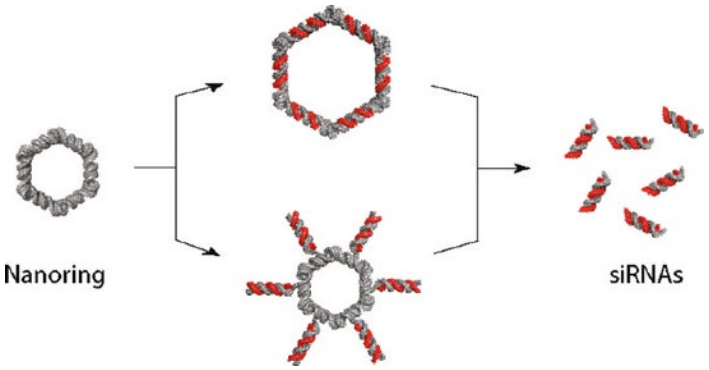

Figure 11. Example of functional RNA hexagon. Adapted from [238]

Other 3D RNA nanoparticles have also been utilized as multifunctional tools for biological applications. A cubical RNA particle build predominantly on the RNA double helix was presented in 2010 by Afonin et al [180]. Two models for the cube formation were designed, either hexameric or decameric, made of DNA, RNA or RNA/DNA, with dangling ends, where the corners were formed by 3 single strands [239]. The cubes were synthesized and analyzed by electrophoresis and CryoEM. Cubes are composed of short RNA fragments allowing for chemical synthesis as well as transcriptional synthesis with simultaneous assembly. The design allows for functionalization with siRNA, labels, aptamers etc. The RNA cubes were shown to regulate the gene expression in the model system and were further equipped with DNA toeholds with a view to generate siRNAs with fluorescent label at the dangling ends [240]. In this design a FRET signal is activated when the cognate hybrids re-associate in the presence of RNA/DNA duplex (co-transfection) carrying fluorescently labeled siRNA sense strand. Nanocubes composed of RNA (RNA/RNA, RNA/DNA) are able to provoke cytokine and interferon response in cells. The RNA/RNA constructs are processed by Dicer leading to RNAi which was not observed for DNA/RNA and RNA/DNA constructs, making the RNA interesting for potential clinical applications. The tunability and multifunctionality of the RNA structures was investigated in greater detail in the modified cube model without toeholds. The structures, called cubes and anti-cubes (reverse complement), expressed programmable shape-switching leading to activation of multiple functionalities such as RNAi, FRET, enzymatic activity or split-aptamer assembly [241]. The RNA cube was the most immunostimulatory among tested variants.

All previously described examples of RNA structures were mostly based on RNA architectonics, where RNA tiles could assemble into complex nanoobjects. There is however a developing technology of RNA origami that has also been used for gene expression regulation. Recently the RNA origami octahedron with RNAi functionality was presented [161]. Although formation of this construct does not change significantly the RNA stability, it was proven that a single RNA strand self-assembled into a 3D object, can make an RNAi inducer. Such elements are Dicer substrates and can regulate gene expression in the model system offering another approach for genetic therapy.

Metal nanoparticles in health sciences

The nanotechnology of metal nanoparticles has been evolving in parallel with the biotechnology, biomechanics, microfluidics and other fields of science. Metal nanoparticles (Me-NP) alone have interesting optical and biological properties, which were utilized in fields like pharmacy and cosmetics. Moreover, a wide panoply of metal nanoparticles has been functionalized with biomolecules, like ligands, drugs, antibodies, peptides, nucleic acids etc. to form specialized conjugates adaptable for therapeutic and diagnostic purposes (Figure 12). Among metal nanoparticles the nanoparticles of gold, silver and platinum are the most studied.

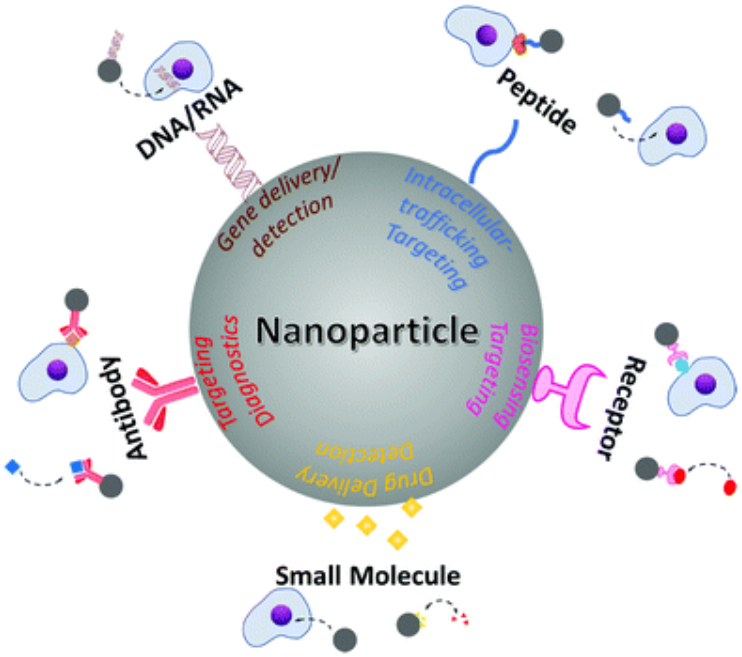

Figure 12. Biomedical applications of nanoparticles through conjugation with various active moieties including nucleic acids, peptides, receptors, antibodies, and small molecules. Taken with permission from Azharuddin, M., et al. [242]

Gold nanoparticles

Gold nanoparticles are known for their chemical inertness, enzymatic stability, neglectable cytotoxicity [243] and physicochemical characteristics [244, 245]. The advancement in chemical synthesis allows currently for efficient synthesis of AuNP and many unique shapes have been obtained and are available commercially, like for example spheres, nanorods or stars [246-248]. The fact that AuNP can be functionalized by ligand exchange, and their optical characteristics (surface plasmon of AuNPs and relatively large extinction coefficients) made them an

interesting component for studies in the fields of research, engineering and medicine [245]. Owing to the availability of AuNPs in various sizes and shapes, as well as, the ease of functionalization, AuNPs became recognized as good candidates for conjugation with biological ligands, such as: nucleic acids [249-251] peptides [252, 253], proteins [254, 255], enzymes [256-258], antibodies [259, 260], and chemotherapeutic agents [261, 262]. With the optical characteristics of AuNP and their biological stability, such conjugates can be used as biologically active-unit and are suitable for biological studies, imaging or drug delivery. The increased performance and stability of AuNP conjugates compared to the biologically active-unit alone has been previously proven for siRNA, peptides or drugs [263-266].

Gold nanoparticles have proven their utility in medical fields. For example, AuNPs were used in photothermal therapy [267, 268], where the optical properties are desired. Moreover, by functionalizing AuNP with target-specific moieties, one can imagine targeting selected cancer cells [269, 270]. The field of bioimaging has been benefitting from the optical properties of gold nanoparticles. In the laboratory scale AuNP are utilized in cellular studies to visualize cellular components or track nanoparticles to study their delivery, accumulation or metabolism [271, 272]. The AuNPs were also applied in the *in vivo* studies to aid mapping of lymph nodes [273] or vascular blood flow [274]. AuNPs are also used as a tool for cancer imaging and were reported to be a core element in detection probes for melanoma, prostate or carcinoma cancer cells, circulating breast cancer cells [275] and brain tumors [276].

The advancements made in this field allow to functionalize AuNP with diversity of cargos to be delivered to the target. Thiol compounds can form strong interaction with AuNP and were utilized to stabilize, immobilize AuNP or as an interface linking AuNP with other elements [277, 278]. A simple example of thiol functionalization of AuNP is a conjugate with a thio-glucose, which increases compound's stability, cell adsorption and biocompatibility. Such conjugates can be used for biosensing [279, 280], cancer therapy [281, 282], theragnostic tactics [283] and were recently characterized in depth [284]. It was shown that AuNP conjugated with selected antigens or immunostimulants are able to provoke immune response in cells [285, 286] or lead to production of specific antibodies [287]. Following such approach, AuNP may serve as a mean for delivery or as an adjuvant in modern vaccines. Interestingly, it is also possible to combine more than one type of cargo with AuNP and thus obtain the synergistic effect. For example a nanoparticle composed of: Au nanorods with proven photothermal activity, folic acid that enhances breast cancer specificity and a chemotherapeutic agent - Doxorubicin was shown to have

superior therapeutic power upon laser irradiation [288]. Similarly, a synergistic approach was undertaken to produce a potent anti-cancer popcorn-like nanostructures based on AuNP self-grown on the surface of extracellular vesicles encapsulated with Doxorubicin (EVdox) [289]. A variety of AuNPs applications have been demonstrated, such as: thermal therapy for cancer treatment [268, 270], melanoma diagnostics and targeted therapy [275], delivery of drugs, immunotherapeutic agents or nucleic acids [287, 290].

Platinum nanoparticles

Platinum is a well-recognized compound due to its industrial application, such as in catalysis or production of alloys used for example in automotive, jewelery, medicine or electronics. Besides that, it plays a key role in chemistry, biotechnology and nanomedicine. Platinum is used in chemistry as a catalyst for oxidation and reduction reactions and is widely exploited in catalytic converters but also in fuel cells or production of e.g. silicone, nitric acid and benzene [291]. However, in order to reduce the platinum exploitation and enhance its catalytic performance, much attention has been devoted to study of Pt nanomaterials to replace the standard Pt catalysts [292]. From the medical point of view, platinum nanoparticles (PtNPs) have been studied as a potential mean for cancer therapy, diagnostic screening, imaging and infection treatment. Platinum nanoparticles at 0 oxidation state are considered to be nontoxic (FDA note from 2018 [293]) and are stable in the cellular environment [294, 295].

PtNPs can be synthesized in the variety of sizes. Small (<3nm) PtNPs were reported to enter bacterial cells and cause bacterio-toxic effect while larger ones were bacteria-inactive which was attributed to their inability to enter bacterial cells [296]. At the same time, the zebrafish involved study has shown that, while being bacterio-toxic, the pectin stabilized PtNPs (2-5nm) were harmless to the host organism, thus cured bacterial infection without side effects [297].

Platinum nanoparticles may also be coated with fluorescent probes and utilized for imaging, as they can enter cells without cytotoxic effects [298]. Another attractive approach to produce highly fluorescent and stable probe for bioimaging is to evoke fluorescence from nanoparticles' clusters composed of mixed metal nanoparticles (Ag, Au, Pt, and Cu). Such nanoclusters were shown to be fluorescent *via* phase transfer and have capacity to be functionalized with desired ligands like peptides for further use in diagnostics [299]. Platinum nanoparticles were also utilized as

colorimetric probes [300] that were thus far applied in a numerous applications included detection of nucleic acids, antibiotics, proteins, viruses, bacteria, tumor markers and other bioactive components [301]. Platinum nanoparticles, like other metallic nanoparticles, are promising tools for therapy. It was presented that, contrary to the platinum derivatives, commonly used in cancer chemotherapy, the PtNPs exhibit much greater sensitization of biological sample when ionization is applied. The DNA damage during irradiation is increased upon PtNP attachment, which is desired in radiotherapy [302]. As PtNPs may be conjugated with selected ligand to aim a specific cellular target, they hold a promise to become tools for cancer therapeutics. For example, it was reported that cancer-specific PtNP modified with cysteines to target the HER2 receptor were not only successfully reaching the target breast cancer cells but also enhanced radiation sensitization [303].

Silver nanoparticles:

Considering metal nanoparticles for biomedical applications it is necessary to review silver nanoparticles (AgNPs). Silver is commonly known for its antimicrobial traits which made AgNPs an interesting component of medical coatings, cosmetics, fabrics and other materials. Owing to optical, catalytic and antibacterial properties of silver nanoparticles they have been widely applied for therapies, diagnostics but also play important role in dentistry and wound healing [304]. There are few methods used for generating AgNPs of different properties and functionalities, including eco-synthesis of AgNPs involving microorganisms and plants [305]. Granted their industrial utility and lower price compared to AuNP and PtNP, it should not be surprising that AgNPs still have a significant contribution to the overall number of nanoproducts produced.

Unlike gold and platinum, silver nanoparticles are not a common choice for drug delivery. It is mostly due to the uncertainties relating to AgNPs biocompatibility. However, AgNPs conjugates with anti-inflammatory agents were proven to be successful as anesthetics and exhibited improved performance compared to classical anti-inflammatory drugs [306, 307]. Different mechanisms have been attributed to the antibacterial potency of AgNPs, for example Ag ions and AgNPs may attach to the bacterial walls and membranes, damage intracellular elements or provoke oxidative stress [308, 309]. Amongst all studied applications, the most vivid seems to be potential use of AgNPs in the control of malaria [310].

Silver nanoparticles have a significant contribution to the cancer therapy. For example, they can successfully deliver anti-cancer drugs such as methotrexate, doxorubicin and alendronic acid with better effectivity than the drugs alone with minimized side effects [311, 312]; AgNPs can be co-delivered in micelles with anti-cancer drugs like curcumin and were showed to enhance the cytotoxic effect of the construct [313]; AgNPs carries were also used for antisense drug delivery with photo-activated release, which was used in CD54 gene expression regulation in cancer cells [314]. Such AgNP-derived anti-cancer modules were also shown to work combined with a magnetic field or photothermal therapies [315, 316] and as signal enhancers for the fluorescence and x-ray diagnostics [317].

Owing to their antibacterial properties AgNPs became of interest for the oral care application and silver has been used in the area of dentistry over the years [318, 319]. Silver nanoparticles have been studied as a potential additive to be exploited in the field of orthodontics and dentistry to make antibacterial resins and fillings [320]. Similarly, the process of wound healing might be improved in the presence of AgNPs [321]. Similarly, the AgNPs coated with polyphenols were shown to have antimicrobial [322], antiviral, immunostimulatory properties [323], as well as to promote wound healing in a size dependent manner [324, 325]. With that in mind, series of AgNP-infused nanomaterials to be applied in wound healing management have been described [326].

The qualities of metal nanoparticles, such as their antimicrobial properties, drug assisting and a great panoply of medical and diagnostic applications make them an exceptional mean instrumental for many fields. As they emerged as potential drug delivery agents, it became pressing to further explore this quality of metal nanoparticles as well as combinations of beforementioned features. In the view of challenges in polar nucleic acids delivery, the perspective of using metal nanoparticles (Au, Ag, Pt) seems very attractive.

RNA-metal nanoparticles interactions

Metal nanoparticles may be equipped with new features by conjugation with biological cargo, including RNA. RNA is well known for its biological properties such as enzymatic activity (ribozymes), aptamer function or directing the process of gene expression silencing (RNAi) [327].

A unique form of oligonucleotide-AuNP conjugate was introduced in 1996, where DNA rational assembly was used to create colloidal nanoparticle assembly [328].

This has given rise to a new stream of studies focusing on so called spherical nucleic acids (SNA), nanostructures that exhibit biological properties of nucleic acids and utility of nano-scale materials [329]. SNAs are designed on the foundation of linear nucleic acids that are attached to the nanoparticle's core. Such spherical nanostructure was proven to enter the cells and be processed without causing cytotoxic effect [330, 331]. The DNA-based SNA have allowed to explore the field and extend to the RNA-based SNA. Spherical ribonucleic acids (SRNA) were utilized for gene expression regulation, building platforms for biosensing, immunostimulation and diagnostics. Considering the current technology, allowing to rationally design and produce RNA of choice, it seems natural to choose RNA as one of the functional groups for conjugation with metal nanoparticles. Such conjugate for biological application must be biocompatible, easily deliverable and stable in the cellular environment. Many uses of RNA in conjugation with metal nanoparticles, especially gold, have been reported thus far, examples of which will be described in this section. Such nanostructures were shown to be able to cross the lipid bilayer and to retain their biological activity [332]. RNA – metal conjugates are usually formed based on the thiol bonds, noncovalent or electrostatic interactions. The thiol-gold bond is known to be the strongest among mentioned interactions and is most often utilized [332-338]. The thiolated RNA is attached to the AuNP by citrate replacement from the nanoparticle surface (Figure 13). The remaining, forms of RNA-nanoparticle hybridization relay mostly on electrostatic interactions between differently charged layers of RNA, nanoparticles and other polymer intermediates [228, 339-344].

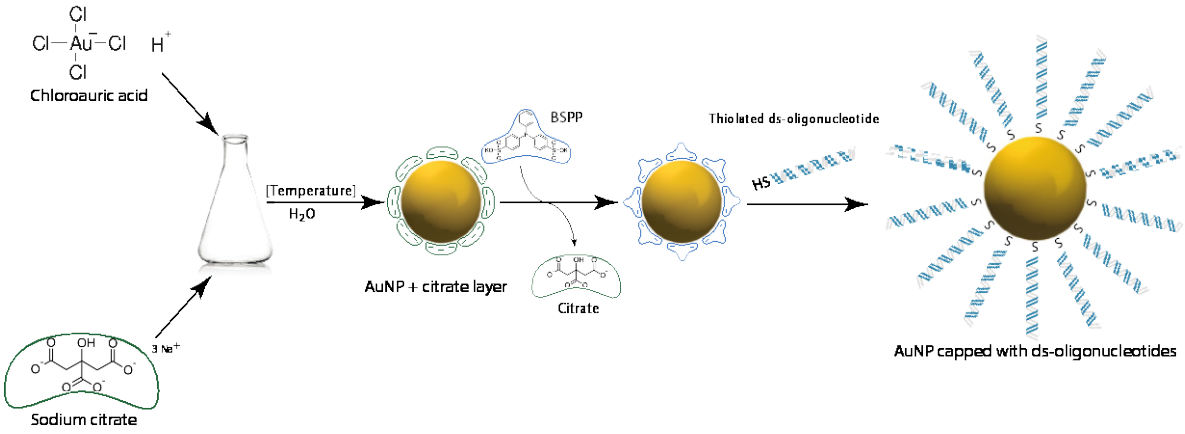

Figure 13. Schematic synthesis of thiol-linked spherical nucleic acids. Gold nanoparticles are synthesized from chloroauric acid in the presence of citrate; obtained AuNPs are treated with bis-(p-sulfonatophenyl)phenylphosphine (BSPP) to replace citrate ions prior to attachment of tiolated nucleic acids. Adapted from[345]

Although RNA-metal nanoparticle complexes are the most abundant in gene regulation approaches, there exist a niche utilizing SRNA for other purposes. One example of SNA utility is the immunotherapy. As nucleic acids bind to endosomal toll-like receptors (TLRs) it became possible to utilize their spherical forms to stimulate immune response, impede it in autoimmune disorders [346, 347] or use in cancer immunotherapy [338]. Inserting nucleic acids into the spherical system has broadened the chances to extend their basic functionalities by adding modules, such as: chemical and fluorescent tags, used for detection or quantification; metals to assist imaging; antibodies, peptides and aptamers, boosting targeted delivery.

The RNA world offers a wide panoply of functional elements, such as aptamers, ribozymes or riboswitches. Scientist learned to tune these functional RNAs, to apply them in biosensing and diagnostics. RNA aptamers are well recognized due to their specificity for a range of targets in cells (receptors, proteins, nucleic acids). Owing to development of the SELEX methodology it became feasible to select and produce desired, target-specific aptamers [348]. Such structures may be conjugated with AuNP, which gives a chance to target a particular element in cells and visualize them. This was applied for example to detect prostate-specific membrane antigen (PSMA) [349, 350]. Expanding the aptamer-bound SNA, by addition of drug (doxorubicin), lead to formation of a device able to recognize prostate cancer cells *via* aptamer interaction, visualize them in CT scans and finally destroy the cancer cells [351]. Another aptamer-based approach was used for Neomycin B detection [352]. Here the polyA was used as an anchor to attach RNA fragment. A fluorescent probe bearing RNA aptamer fragment was added and in the presence of Neomycin B the strands assembled, quenching fluorescence.

On the other hand, mRNA-derived structural RNA fragments, known as riboswitches can be affected upon interaction with small molecules, protein, RNA or ions [353]. Upon ligand interaction, a riboswitch changes its spatial shape, which was utilized in biosensing. Similar to regular RNAs, riboswitches can be conjugated with AuNP and that was applied to prepare sensing RNA arrays. In this setup selected riboswitches were immobilized on the AuNP surface and used for detection of secondary messengers, cobalt ions, theophylline [354] and flavin mononucleotide (FMN).

However, the gene expression regulation is the most studied utility of SRNA, since it has a potential to treat genetic diseases or tune protein expression [333]. Many approaches have been undertaken to achieve the RNAi. However, like other therapeutic approaches, this one also struggles with delivery methodology that

could bypass the cellular defense mechanisms. The use of spherical nanoparticles offers a chance to overcome this obstacles as they were previously reported to penetrate cells without external transfection agents nor they have caused cytotoxicity [332355]. The most robust RNA-AuNP conjugates are equipped with additional elements enhancing cell penetration. An example of such nanoparticle is an siRNA-AuNP hybrid supplemented with a poly-β-amino ester, allowing to screen the negative charge form RNA, facilitating cellular delivery [356]. Addition of a cell penetrating peptides has also allowed to greatly improve cellular penetration, which was proven in a cervical cancer model. The nanoparticle composed of RGD peptide, siRNA and AuNP core was proven effective *in vitro* (HeLa) and *in vivo*, as it penetrated the tumor and led to target gene regulation [357]. A tremendous success has been also presented with SNA activity in the central nervous system (CNS). Not only were they able to cross blood-brain-barrier but, most of all, they lead to RNAi and reduction of the tumor volume [335, 336, 358]. This was an important step for drug delivery to the CNS, knowing that therapies have long been struggling to overcome the tumor tissue barrier. Likewise, an important progress was made in the field of topical drug delivery (administered through the skin). The SNA composed of epidermal growth factor receptor (EGFR) - targeted siRNA and AuNP was applied as a potential treatment of skin conditions. Those nanoconjugates were shown to penetrate through mice' skin upon topical administration and regulated EGFR expression, thinning the epiderma [334].

By combining the fluorescence and regulatory functionalities it was possible to obtain a biomimetic probe [85, 341]. Scientists showed that this tool could simultaneously regulate the c-Myc oncogene expression and visualize the RISC's activity with the fluorescent probe complementary to the innate Ago-miRNA complex. This allowed to regulate the gene of interest and track the process in parallel.

Although the thiol-AuNP conjugation is the most commonly used, there exist a plethora of RNA-AuNP conjugates relaying on the noncovalent interactions (Figure 14). Mostly electrostatic interactions are utilized as an alternative for thiol conjugation as it does not require RNA modification and can be achieved by stacking differently charged layers [339]. Such nanoparticles were used for gene expression regulation and equipped with multiple modifications, showing their applicability in the field of bio-nanotechnology and therapeutics.

One of the routes leading to formation of this type of SNA is the use of dendronized components, with a cumulative positive charge being able to attract and hold

negatively charged siRNA fragments. Such nanoparticles were reported to regulate the gene expression without causing any toxic side effects [340, 342].

In the electrostatically held RNA-AuNP system there is also room for functional development. An example of such functionally complex structure is a siRNA-AuNP conjugate equipped with transferrin or folic acid, that support receptor mediated cell penetration. It was effectively delivered to the prostate cancer cell model and regulated the gene expression [343].

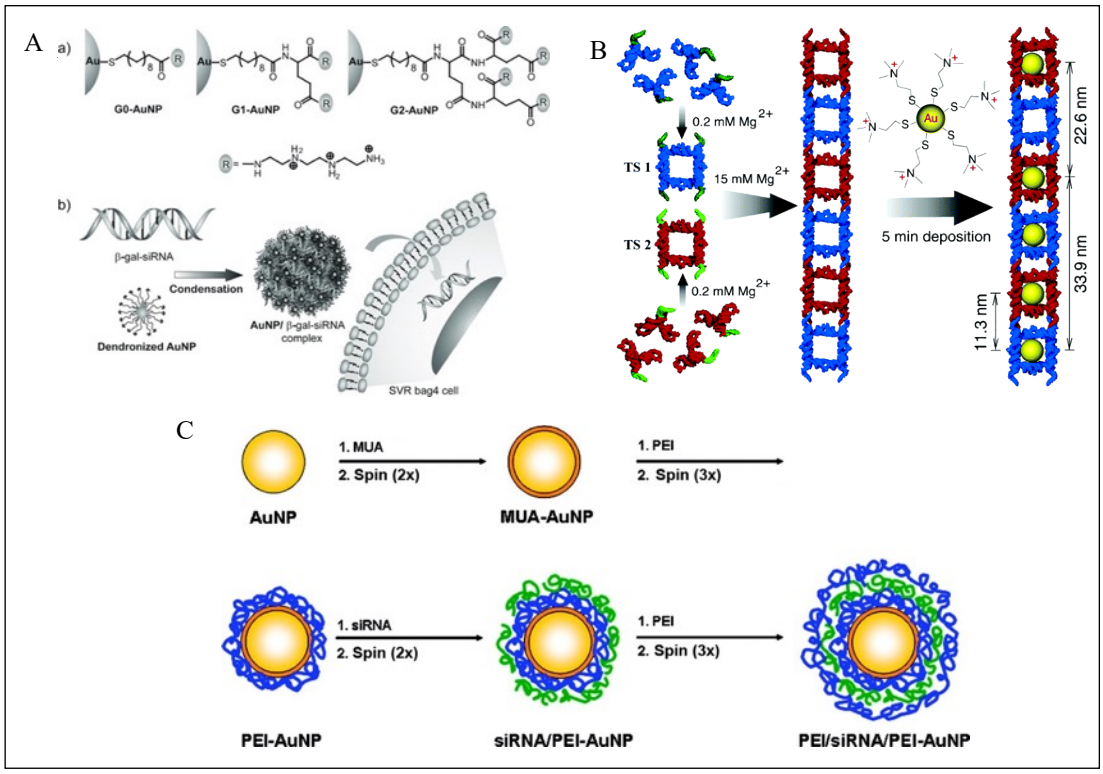

*Figure 14. Non-covalent RNA-AuNP interactions. (**A**) RNA entrapped within the dendronized polymer layer [340]. (**B**) Hierarchical supramolecular assembly of TS ladder decorated with cationic AuNPs [228]. (**C**) Layer by layer deposition of siRNA and poly(ethylene imine) (PEI) on the surface of AuNPs [339] (blue represents PEI, green represents siRNA). Taken with permission from: A [340], B [228], C [339]. Adapted from [345]*

An inverted tactic, displacing AuNPs from the nanoparticle's core was used as alternative RNA vector. This 3D nanoparticle was obtained by trapping AuNPs within dendrimeric network, that improved its stability. It served as a platform for RNA or DNA attachment and delivery showing Bcl-2 gene expression regulation in the model HeLa cells [344]. Interestingly this design enhanced the delivery system based on dendrimers alone, expressed lower cytotoxicity and was also proven effective in the glioblastoma model [359]. In the latter example, previously mentioned RGD peptide was introduced to the nanoparticle boosting cell penetration effect and thus improving regulatory performance.

Although much progress has been made since the first implementation of SNAs there is still room for improvement in terms of biocompatibility and functionality. The conjugation of before mentioned tectoRNA structures with nano-spheres has a potential to add another level of programmability to the SNA technology. Due to their composite structure, the tectoRNAs, by themselves, have already improved signaling capacity compared to regular siRNA. This hypothesis was confirmed in human cell lines, where single siRNAs or tectoRNAs were targeted to regulate the mRNA for green fluorescence protein (GFP) [1]. Driven by previous literature reports, it seems reasonable to combine both, metal nanoparticles and tectoRNA technologies to extend applicability of SNAs. One can imagine that metallic nano-sphere capped with structurally defined tectoRNAs (tectoRNA-MeNP) may expand applicability of the whole nanodevice, by enhancing its bioavailability, improving ability to penetrate cell membrane and increasing local concentration of regulatory element, and importantly, allowing for uniform delivery of a mixture of signaling elements. Such structures can further be explored in living cells as potential mean for gene therapy or be treated as building blocks to assemble macromolecular nanomaterials of various utilities.

Thus far, the most structurally advanced RNA form introduced into the SNA framework was before mentioned RNA aptamer. The structural properties of RNA have been shown to direct the formation of inorganic particles. For example, some natural RNA motifs may act as a catalyst for inorganic-particle formation, owing to their programmability and stable 3D structure. It was reported that palladium nanoparticles' formation can be driven by pyridyl modified structured RNAs [360]. According to the authors, the specific RNA fragments participate in organometallic compounds recognition and stabilize the metallic intermediates.

In this view, the structural RNA nanoparticles serve as a platform for spatial organization of metal nanoparticles, such as gold [361] or before mentioned palladium [360]. For example, the tectoRNA architecture was used as a scaffold for coordinated AuNP arrangement [361]. It is therefore within a reach to control metal nanoparticle layouts only by tuning RNA geometry, which is fundamental for modern nanodevices design. Among reviewed nanoparticles, gene expression regulation was only driven by the presence of siRNA. With the functional capacity of structural RNA world, it seems logical to look for solutions utilizing the best of both nanotechnologies of RNA and metal nanoparticles.

RNA nanotechnology in the COVID-19 era

Since the year 2020, all fields of life have been highly affected by the worldwide COVID-19 pandemic, caused by the severe acute respiratory syndrome coronavirus - SARS-CoV-2. The SARS-CoV-2 is a spherical, enveloped RNA virus, which means that its genetic material is composed of single-stranded, positive-sense RNA (+ssRNA) capped at a 5'-end and polyadenylated at the 3'-end. The envelope consists of 3 main proteins, namely: M protein, which is involved in viral assembly and budding; E protein, which is involved in morphogenesis, release and viral pathogenesis; and S protein which is responsible for cellular receptor recognition and cell invasion [362]. No cure has been reported thus far to manage the COVID-19 epidemics; however, a lot of efforts have been devoted to work on SARS-CoV-2 leading to better understanding of the disease, virulence and some potential drugs have been accepted to clinical trials. The heroic work of scientists and medics around the world have contributed tremendously to development of the first COVID-19 vaccine that was introduced in December 2020 by Pfizer–BioNTech. It was the first vaccine for this virus but was also a pioneer in the field of mRNA vaccines. The nanotechnology of RNA has emerged as a potential mean to produce drugs and antiviral vaccines that are able to compete with the classical therapeutics used in medicine.

Since the discovery of mRNA in early 1960 [363, 364] almost 40 years must have passed for the first oligonucleotide-based drug (Fomivirsen, now discontinued) to be approved by the US Food and Drug Administration (FDA), which marked the entrance of mRNA to the clinical research. However, the most significant steps in the field of RNA's clinical application have been made in the last decade, with the FDA approval of an RNAi drug against hereditary ATTR amyloidosis in 2018 (Patisiran) [365] and recent advances in clinical application of mRNA-based vaccines [366, 367].

In the light of worldwide COVID-19 pandemics, the mRNA vaccines became of interest, owing to the possibility of designing and producing them in a much shorter time and controlled way, compared to the classical peptide-derived vaccines. The major element of the mRNA vaccines is the messenger RNA, naturally lying at the interface between DNA and protein, which serves a matrix for protein biosynthesis in the translation process [366, 367]. To make a vaccine, an mRNA fragment is selected based on the viral genome. Such mRNA codes a viral protein, triggering an immune response, which is activated in the process of protein

translation in the host cells. This protein is later processed by the cell's metabolism (proteolytic vesicle, proteasome system) and may be taken up by the antigen presenting proteins belonging to the class I and II of a major histocompatibility complex (MHC I and MHC II). The antigen presented by the MHCs is recognized by the T-cells, which leads to induction of a cellular immune response. Part of the produced antigen may be released outside of a cell and then recognized by the B-cells, responsible for development of a humoral immunity. All those processes are interconnected with each other and are said to both, produce antibodies (B-cell activity) as well as provoke specific T-cell antiviral response [368, 369]. The mRNA vaccines are usually classified in one of the three main categories: 1) **non-replicating mRNA** vaccines, which are composed of mRNA fragment coding for the desired protein and are usually delivered within some carrier molecule; 2) **self-replicating mRNA** vaccines, that have a sequence containing a module responsible for replication of the mRNA (usually virus derived self-replication sequence) independent of the host; 3) ***in vitro* dendritic cell non-replicating mRNA** vaccines, which is the most advanced way of vaccine formation, where the host dendritic cells are extracted from blood, transfected with a specific mRNA, and finally returned to the patient - this method is however the least economic and thus least studied. With the outburst of COVID-19 epidemic, some mRNA vaccines were introduced to the clinical trials. Two of them, currently used worldwide, were proposed by the Moderna company and Pfizer–BioNTech (mRNA-1273 and BNT162b2, respectively). Another example of mRNA vaccine was presented under the commercial name - STARR™ Technology. This is a mRNA self-replicating vaccine encapsulated in a lipid-based carrier (LUNAR® by Arcturus therapeutics). The rapid progression of the vaccine field holds a great promise to compete with traditional vaccination methods and quicker reaction in the face of future epidemics [370].

In the field of post-infection treatment of COVID-19 the RNAi therapeutics seem to have a potential to create a robust line of targeted defense. The effectiveness of such method was already shown in cell studies to fight the infection with SARS-CoV virus, which caused the SARS epidemics in 2002-2004 [371]. In this study, a set of siRNAs, targeted against 3'-UTR or the coronavirus Spike protein's (S) gene, were designed and synthesized. A study in Vero-E6 cells infected with a virus showed that 100 pmoles of the best performing siRNA sequences were able to inhibit SARS-CoV replication in the cell line, 48h post-infection/transfection. Analogically, siRNA-based therapeutics were proposed in response to COVID-19 epidemics by

the cooperation of 2 American companies Alnylam and Vir. A set of siRNAs, targeting highly conserved regions of the SARS-CoV-2 genome, was synthesized and analyzed in the virus model (data wasn't shown). Companies claimed that the selected siRNAs reached 95% inhibition of virion production at a concentration below 1nM for SARS-CoV-2, but also is predicted to inhibit SARS-CoV virus from the previous outbreak. What is interesting about this particular drug is the proposed way of delivery by inhalation directly into the lungs of infected patients. Such application of active ingredient is especially attractive in a fight against pulmonary infections as it may shorten drug's way to the most affected regions [372]. Several siRNAs targeting conserved regions of SARS-CoV-2 genome were screened recently and tested *in vivo* [373]. The selected siRNAs or their mixes were delivered intravenously in lipid carriers and both showed to hinder viral expression, thus impeding the development of COVID-19 disease. The use of mixed siRNA fragments can minimize the likelihood of adaptive viral resistance. In order to get a highly functional drug it must be efficiently taken up by cells and stable in serum for extended period of time. RNA stability is often assured by RNA backbone of nucleobase modifications. An example of such is replacement of uridines with N1-methyl-pseudouridines in mRNA SARS-CoV-2 vaccines (Pfizer-BioNTech and Moderna). This was proven to boost vaccine effectiveness by stabilizing the structure and reducing immunogenity of mRNA [374] [375]. As for the delivery systems, their major role is to promote cellular uptake, protect the cargo and release upon delivery. Thus far, RNA oligonucleotides have been either conjugated [376] with different agents such as antibodies [377], peptides [378, 379], aptamers [380, 381], nanoparticles [382, 383], lipids [384, 385] or carbohydrates [386]; encapsulated in lipid nanoparticles [387, 388] or exosomes [389, 390] and in nucleic acid origami structures [391, 392]. The most recent clinical success of mRNA vaccines shows that the lipid nanoparticles are currently at the frontline of RNA drug delivery and are currently seen as a safe and effective delivery vehicle [388]. The topic of therapeutic oligonucleotides delivery and modification has been extensively studied and there exist a plethora of reports dedicated to it [393-395].

Results and discussion

The aim of this project is to design, synthesize, assemble and investigate AuNPs functionalized with rationally designed, structured RNA trimer. AuNPs serve as vehicle for delivery of functionalized RNA to living cells. The delivery system based on metal nanoparticles has already been proven to perform well for multiple cargos like DNA, RNA or small molecules [396, 330]. Spherical nucleic acids (SNA) represent a group of nucleic acids introduced into the spherical shape to obtain different functionalities. Such nanostructures were used to deliver nucleic acids to cells for therapeutic applications, immunostimulation, diagnostics and imaging or to regulate gene expression. The first such assembly of nucleic acid on the surface of nanoparticle was presented in 1996 by Mirkin's group [328], where short thiolated ssDNA were attached to the AuNP and used to form greater assemblies of colloidal gold. Similarly short RNAs were attached to the AuNPs *via* terminal thiol-metal interaction [330, 332, 396]. Such spherical architecture makes the siRNA accessible for enzymatic machineries which is crucial for biological activity of the compound.

The structural RNA trimer, developed based on the 3wj-nRA motif [1], is composed of three monomers, each bearing regulatory sequence, identical to siRNA targeted against the CopGFP gene that can be expressed in a model cellular system. Such trimers can be processed by endonuclease Dicer resulting in siRNA release that can lead to RNAi response. To develop an RNA trimer with a gene regulation functionality, a set of siRNAs was selected and tested in a model human breast cancer cell line MDA-MB-231, stably expressing GFP. The siRNAs that most effectively silenced the GFP expression were later implemented into monomers and a structural trimer. This is referred as a first generation (G1) trimer. The concept presented here, referred as a third-generation monomers (G3), is a modification of short RNA fragment with a thiol group at the 5' terminus, which after hybridization with a complement RNA fragment allows attachment of the structural RNA to the surface of AuNP. The newly developed RNA/AuNP was optimized, characterized and investigated in the model cell line to show its regulatory activity.

Design of RNA trimer with thiol functionality (third generation)

This project utilizes a set of structural RNA trimers, bearing three regulatory sequences (siRNA) and a thiol linker to allow attachment to the gold nanoparticle. The structural RNAs with a thiol will further be called a third generation (G3) which was designed on a foundation of previously described first generation (G1) trimer [1] (Figure 15).

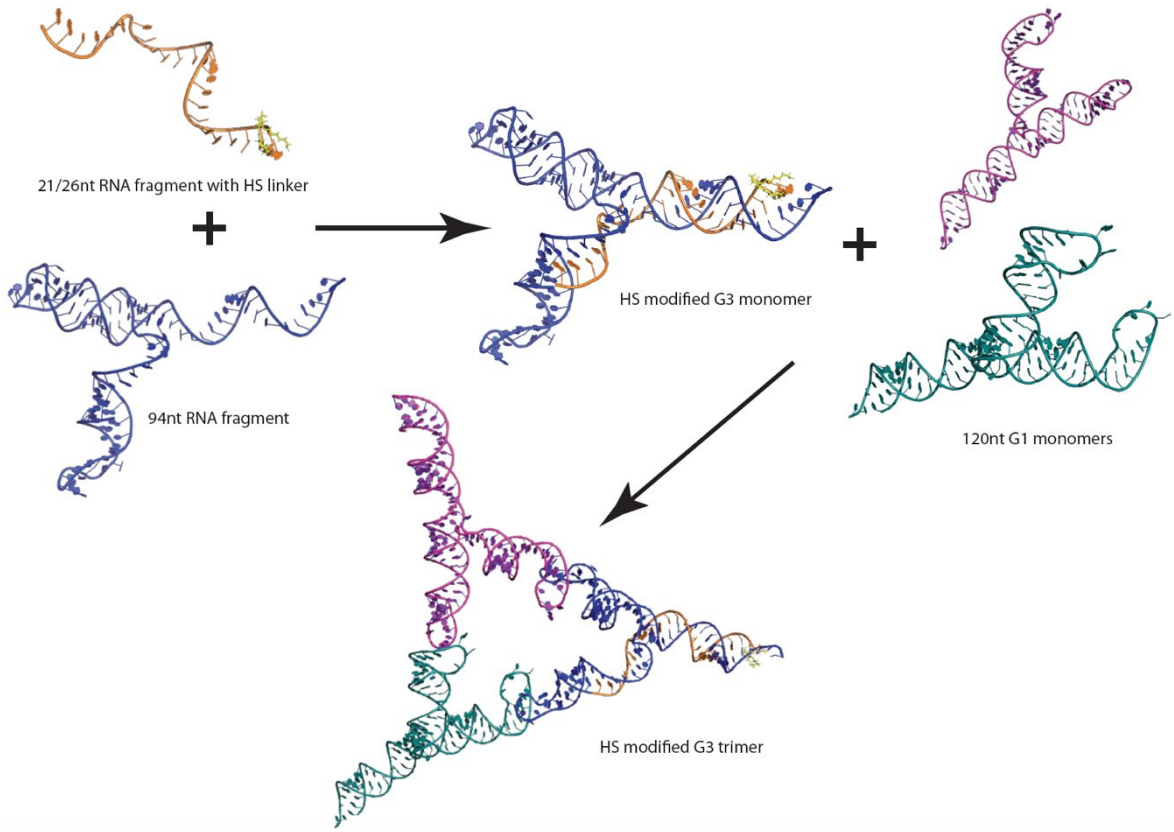

Figure 15. Third generation RNA trimer design

The regulatory sequences that are introduced into the trimer are based on previously selected and tested siRNA, that were proven to regulate the CopGFP gene expressed by the model cell line (MDA-MB-231 GFP/RFP) [1]. The siRNAs were designed following the Birmingham et. al (2007) protocol and validated in accordance with the Reynolds rules [199] to score a minimum of 4 points. Here we use selected siRNAs as a control for RNAi experiments in the GFP model and further for functionalization of metal nanoparticles.

In order to facilitate functionalization of a long RNA sequences the G3 trimer was designed. One of the G1 monomers (described in detail in the literature section), which is a single 120nt RNA strand, was redesigned by 'removing' a short RNA fragment (26nt) from the 5' end. The remaining 94nt long RNA fragment is still capable of forming partial 3WJ motif with 2 loops responsible for interactions with other monomers. This RNA fragment (94nt) is synthesized transcriptionally, in the similar fashion to G1 monomers. The remaining short RNA, in this project 21 or 26nt, is complementary to the 3' end of the monomer. Such oligonucleotides can be synthesized chemically by the phosphoramidite method that can facilitate required modifications, for instance thiol linker at the 5' end may be introduced synthetically. Having the two building blocks of the G3 monomer (Figure 16), one may associate them utilizing complementarity base pairing to form a new 5'-modified monomer. In this project two sets of a short fragments were used: 1) the 21nt RNA fragment with a gap at the 3WJ motif and 2) 26nt RNA fragment which allows to retrieve a 3WJ motif in the monomer. These 2 types of short RNA fragments were designed in order to test whether partial 3WJ motif is sufficient to form a stable trimer, while potentially simplifying Dicer treatment, since only one of two strands need to be cleaved. The scheme below juxtaposes a G1 monomer structure and 2 variants of a G3 monomer.

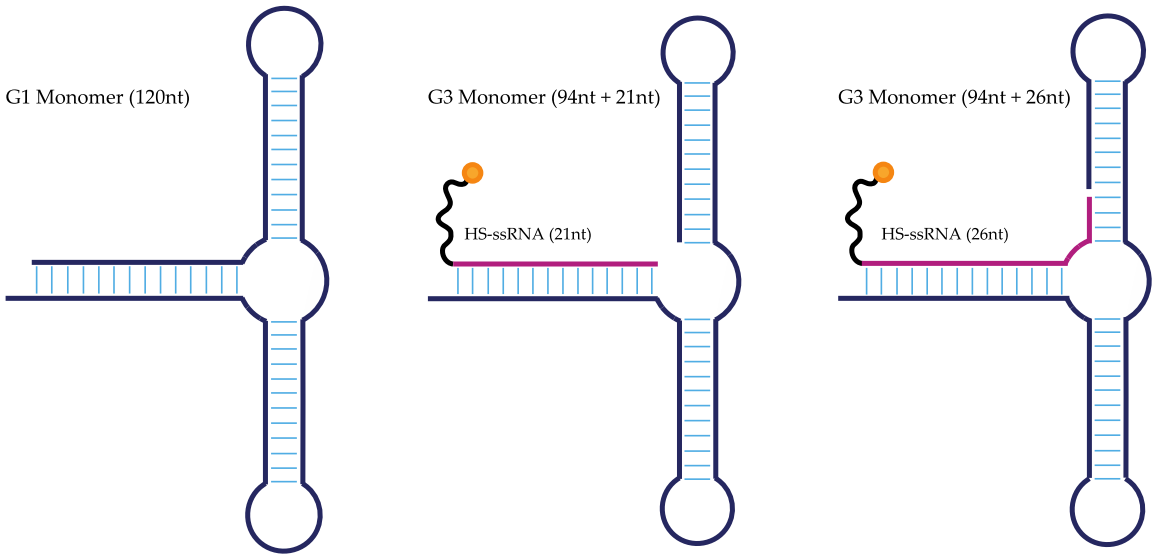

Figure 16. Comparison of schematic representations of 3 monomers G1, and two G3 variants.

siRNA synthesis and association

Short RNA fragments (21 and 26nt) used in this project were produced by chemical solid-phase synthesis from phosphoramidites in-house at the Centre of Molecular and Macromolecular Studies, Polish Academy of Sciences or purchased from Future Synthesis. Oligonucleotides were purified by HPLC, dried and resuspended in 1xTE buffer for storage. The size and purity of short chemically synthesized RNA fragments were checked during the HPLC purification step and later with mass spectrometry.

Selected siRNAs were associated by thermal renaturation and analyzed by the polyacrylamide gel electrophoresis (PAGE), in nondenaturing conditions, to visualize duplex formation (Figure 17). The naming system of siRNAs corresponds to a single strand number (e.g., siR1 and siR2 make siR1-2) and the CopGFP gene with the siRNA sequence targets. Detailed description and sequences of the investigated siRNA may be found in the appendix. The picture below shows formation of duplexes from 2 synthetic RNA strands (21nt long each). As expected, siRNAs, whose one strand is modified with thiol linker (HS-siR1-2) or fluorescein (FAM-siR5-6) migrate somewhat slower compared to the identical siRNA without the modification. The siCop6 duplex seems to be the least stable in the experimental condition and was not used for further experiments.

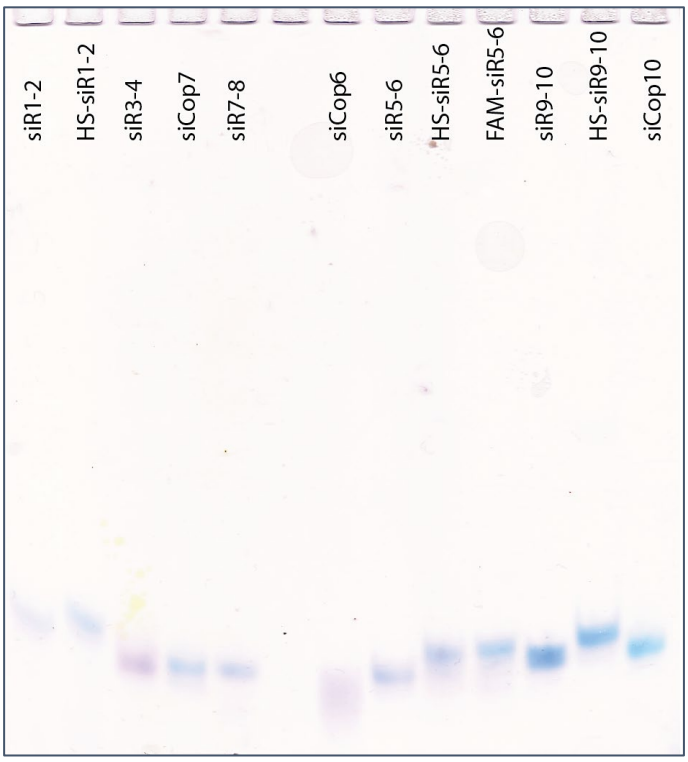

Figure 17. siRNAs duplexes visualized on the 10% native PAGE, stains-all

Because the efficiency of chemical RNA synthesis is length dependent, and reasonable for up to 70-80nt, longer RNA fragments (94 and 120nt), are produced enzymatically by *in vitro* transcription on the dsDNA templates.

DNA matrix amplification

A set of single stranded DNA templates and DNA primers were designed and synthesized in house or commercially (Genomed). The DNA templates were designed appropriately for PCR amplification and contained the sequence encoding the core elements of a monomer, namely 3wj-nRA motif sequence, helical arms, and specific coaxial loops. Primers were designed to modify the template by adding the T7 promoter sequence and appropriate sense/antisense pair to introduce siRNA sequence at the open end of a monomer. The detailed sequences of the DNA templates and primers may be found in the appendix**.**

The PCR protocol for G3 monomers was optimized, because different polymerases were chosen to be used for amplification based on the PCR optimization. Each template was amplified following the 2-step protocol with 5 cycles performed in the lower annealing temperature to ensure forward primer to attach and make copies of the double stranded DNA; this was followed by 30 elongation cycles in the optimal temperature calculated as an average melting temperature of both primers. Properly performed PCR yielded dsDNA product, longer than the DNA template by the length of T7 promoter sequence - 18nt [397] and flanking variable fragments, that are added by the primers in order to introduce regulatory sequences. The PCR products were purified with the QIAquick PCR Purification Kit (Qiagen) and evaluated on the 1.5% agarose gel (Figure 18) in the presence of EtBr. The cleaned PCR products were all used for *in vitro* transcription with T7 RNA polymerase.

Figure 18. A PCR product after purification. Agarose gel analysis for dsDNA templates for the G3 RNA synthesis (G3A1, G3A7, G3A9).

In vitro transcription

The *in vitro* transcription with the T7 RNA polymerase was run to produce RNA on the previously prepared dsDNA (PCR products). Proper introduction of the T7 promoter sequence to the PCR product plays the key role in the transcription protocol. It is a signaling fragment allowing for initiation of the transcription process with the T7 RNA polymerase. This fragment is not transcribed allowing for separation of DNA template and RNA product on the gel. Utilizing the size difference, the transcription progress can be analyzed with the agarose gel electrophoresis, before purification (picture not shown). If the RNA product was visible on the agarose gel, the enzymatic transcription process was stopped and RNA products were purified by extraction from denaturing polyacrylamide gel. Purified RNA fragments were stored in 1xTE buffer and the concentration of the samples was measured on the NanoDrop (ThermoScientific).

RNA length and purity analysis

In order to verify the purity and length of transcriptionally produced RNAs the denaturing PAGE was prepared (Figure 19).

Figure 19 The 1st and 3rd generation of RNA after transcription, 10% Urea PAGE, Stains-all

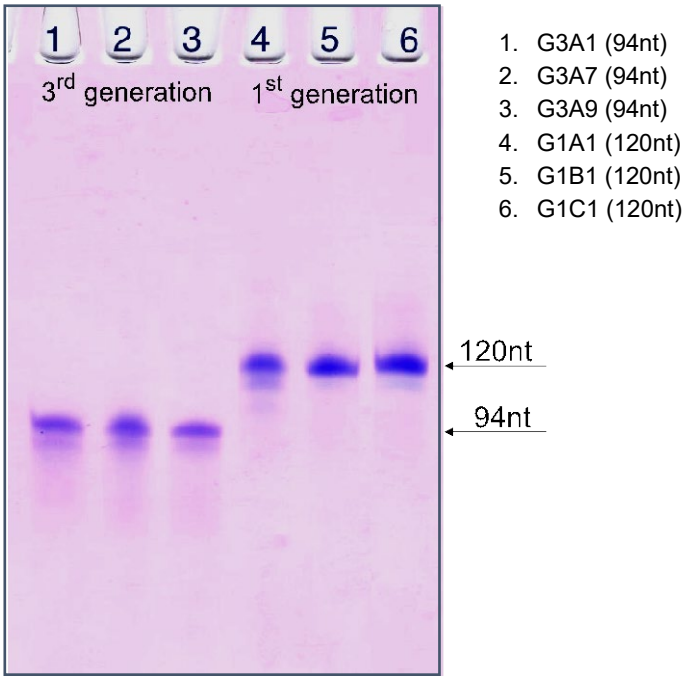

Monomers of G1 and G3 generations were shown to migrate at expected level and their purity was sufficient for the further experiments. The G1 RNA monomers (120nt) were produced following the previously optimized protocol and thus could be used as size markers for the G3 monomers.

RNA trimer association

In order to develop the most suitable protocol for the G3 trimer association, two factors were investigated: magnesium ions concentration and association protocol (stepwise association *vs.* one-pot association protocol). The presence of divalent magnesium ions is crucial for the formation of the structural motifs and noncovalent, long-distance loop-loop interactions.

Trimer was associated from using G1 monomers: G1B1, G1C1 and CoreA7 with HS-RNA-7 for G3 monomer association. Several Mg^{2+} concentrations were tested: 0.2mM, 1mM and 2mM of $MgCl_2$. These experiments were done either in one-pot protocol or stepwise, where monomers were associated separately and then pulled together to associate the trimer. Associated mixture was analyzed using the 1.5% agarose gel (EtBr) in 0.5xTE buffer with 0.2mM Mg^{2+}.

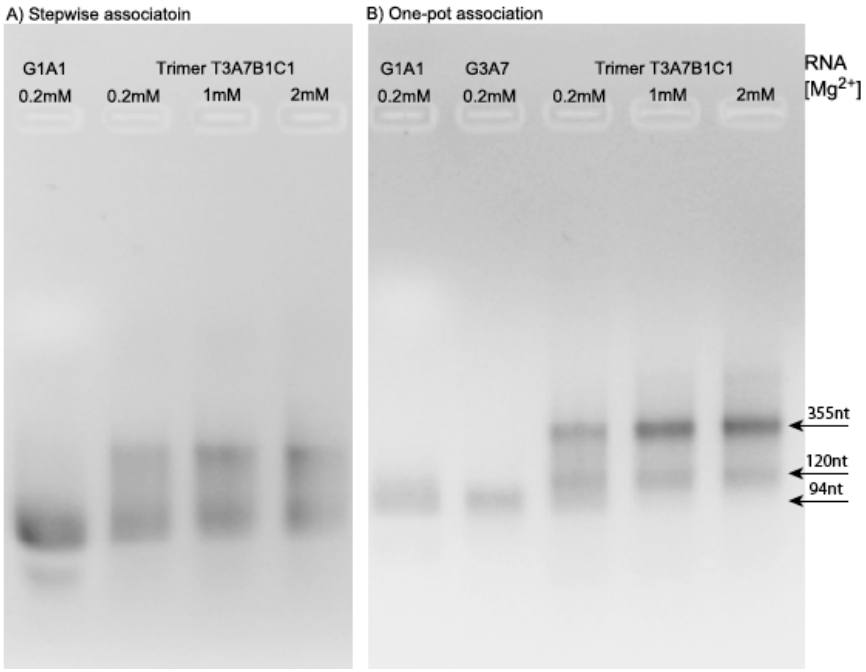

Figure 20. RNA monomer and trimer analysis in stepwise and one-pot association protocols, RNA samples in amount of 30poml in the presence of 0.2mM, 1mM or 2mM Mg^{2+} (1.5% agarose gel, TB 0.5X, 0.2mM Mg^{2+}, EtBr, UV light),

Looking at gel migration analysis (Figure 20) it is clear, that stepwise protocol was not as efficient as one-pot association protocol for G3 trimer assembly. Stepwise assembly is time consuming and also yields in significantly less of the trimer, regardless of the magnesium ions concentration. When it comes to the yield of added $MgCl_2$, the 1mM magnesium seems to result in the optimal trimer formation based on the agarose gel experiments.

An agarose gel electrophoresis was performed for analysis of dimer and trimer formation after assembly following the one step protocol with 1mM $MgCl_2$. The constructs were analyzed with the 1.5% agarose gel electrophoresis in 0.5xTE buffer

in the presence of EtBr. The gel image is presented below (Figure 21). Both, dimers and trimers were shown to be formed and their migration patterns differ. All tested structures (siRNA, monomer, dimer and trimer) can be easily distinguished on the agarose gel.

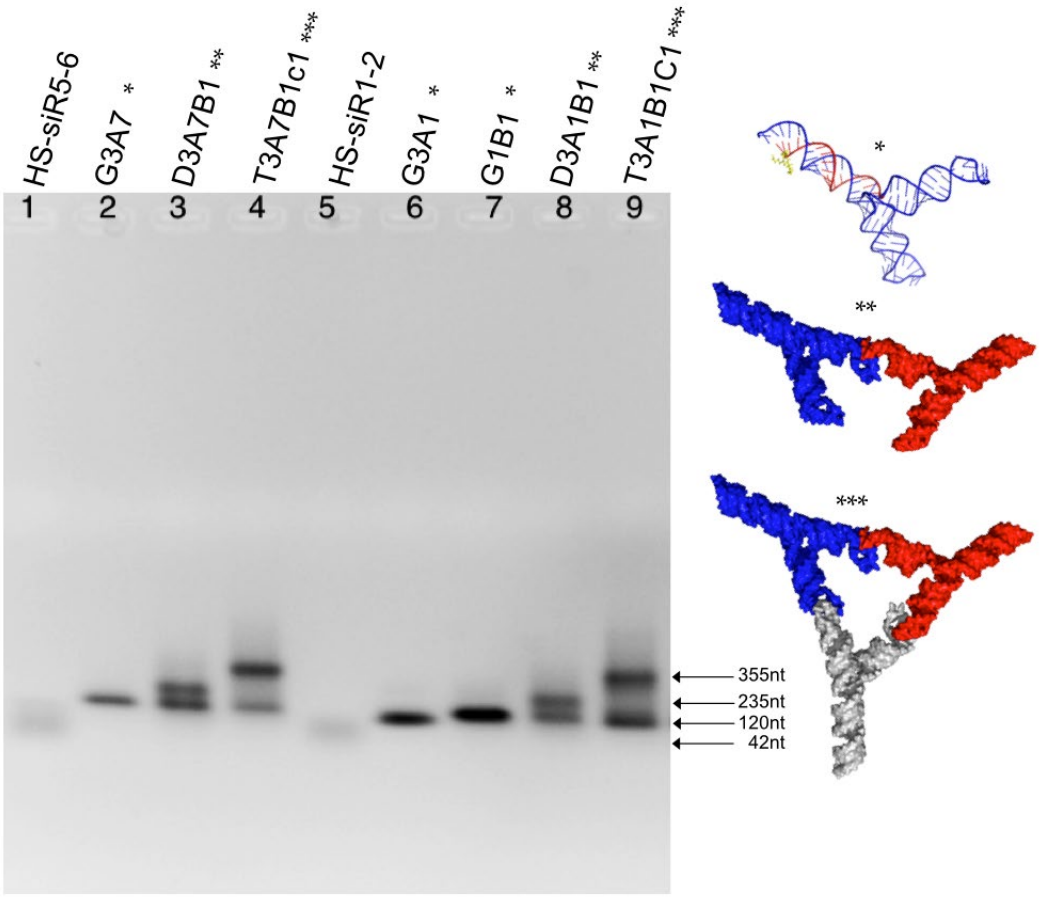

Figure 21. The association of dimers and trimers at the native 1.5% agarose gel (EtBr, UV light)

Similar experiment was performed with nondenaturing PAGE, where the association of G1 monomers and G3 monomers was studied. Based upon previous experiment the one-pot protocol was used to associate 3 different G3 trimers. The G1 trimer was used as a reference. Additionally, a set of 6 possible dimers, that can be potentially formed between a G3 and G1 monomers during association, was included to the analysis: D3A1B1, D3A7B1, D3A9B1, D3A1C1, D3A7C1, D3A9C1. The D1B1C1 dimer was used as a reference.

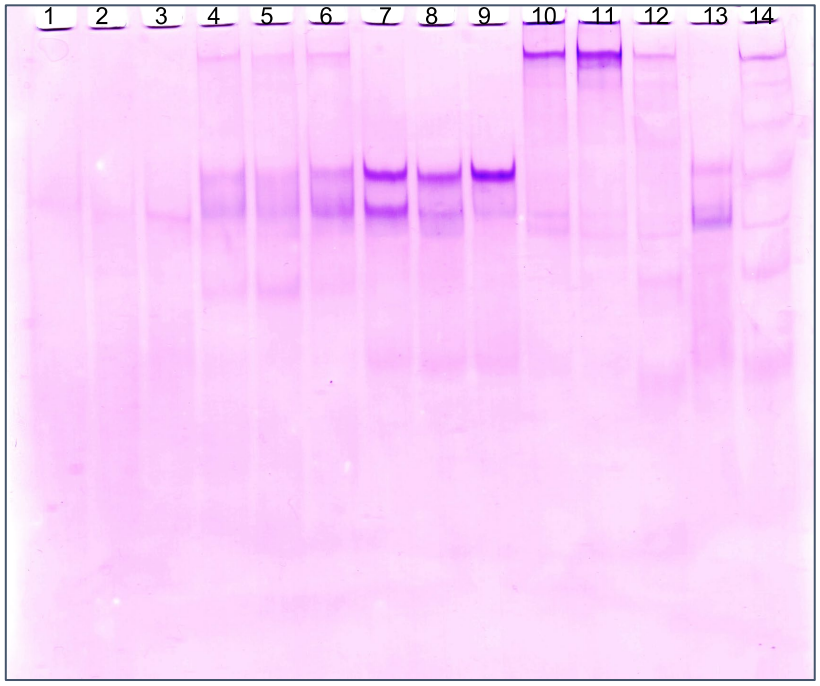

Order of samples on the gels:
G3 Monomers:
1. G3A1
2. G3A7
3. G3A9

G3 Dimers:
4. D3A1B1
5. D3A7B1
6. D3A9B1
7. D3A1C1
8. D3A7C1
9. D3A9C1

G3 Trimers:
10. T3A1B1C1
11. T3A7B1C1
12. T3A9B1C1

G1 Controls:
13. D1B1C1
14. T1A1B1C1

Figure 22. The association study in the presence of 0.2mM Mg2+ (10% native PAGE, 200V, 7h, 4^{0}C, stains-all)

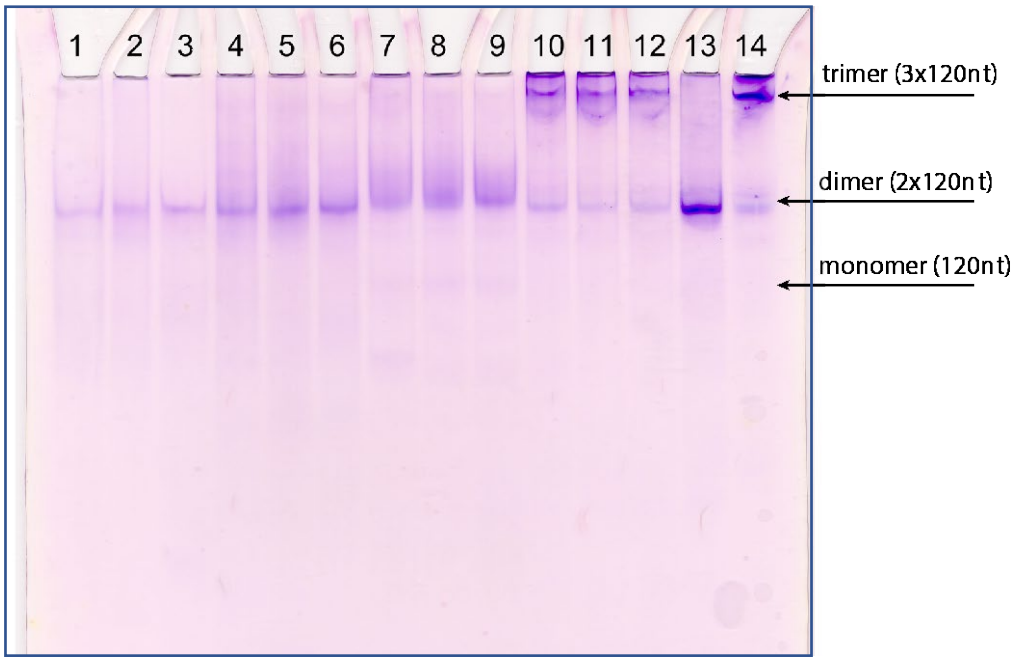

Figure 23. The association study in the presence of 1mM Mg^{2+} (10% native PAGE, 300V, 7h, 4^{0}C, stains-all)

Monomers, dimers and trimers were associated by one step protocol in the presence of 0.2mM or 1mM magnesium and analyzed with the 10% native PAGE (Figures 22-23). In the gel experiments each RNA sample consisted of the same final amount of RNA. It turned out that the addition of 0.2mM Mg^{2+} is sufficient for the trimer formation. In the presence of 1mM magnesium ions monomers are not visible and the smears are less visible. Monomers may difficult

to visualize due to formation of homodimers (likely *via* S-S bond) and cannot be distinguished from heterodimers. In the same time, T3 trimer formation is not significantly improved in the higher Mg^{2+} concentration and for this reason, 0.2mM $MgCl_2$ was used in the further associations.

Endonucleolytic digestion of structural RNA with Dicer

Delivery of regulatory siRNA is essential to externally induce RNAi process in cells. Larger structures, such as trimers, may also be utilized for gene expression regulation, however these have to be cleaved in order to produce functional siRNA. Dicer is an RNAse III endonuclease that is responsible for cleavage of long dsRNA into 21-23nt fragments, leading to formation of miRNA or siRNA in cells. This study aimed to confirm that new generation of trimer can be processed by Dicer. Selected RNA constructs were used for enzymatic reaction in the presence of Dicer and results were analyzed with bioanalyzer (Figure 24).

Figure 24. Bioanalysis result presenting Dicer processing of tectoRNA constructs. Dicer treated samples in lines 2, 4 and 6 are about 20nt shorter than the untreated RNA in lines 1, 3 and 5. RNA sizes estimated based on the 4nt internal control (green).

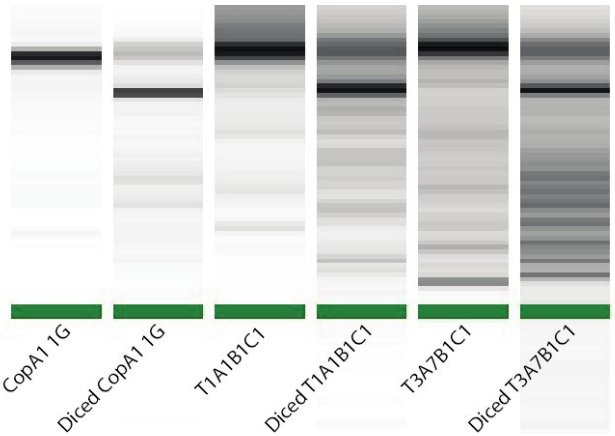

Untreated RNA constructs were used as controls in this study. Trimers are not visible due to denaturing experimental conditions and the short siRNAs (~21nt) are not observed in the electropherogram generated with the used device setup. The upper bands, in lines 1, 3 and 5, correspond to 120nt full-length monomer. In lines 2, 3 and 5, corresponding to the diced RNA samples, the 120nt upper band disappears while ~20nt shorter band becomes well visible.

This result complies with the fact that Dicer usually generates ~21nt fragments from longer dsRNAs [398] proving that the new generation trimer is a good candidate for RNAi studies in cells.

In vitro studies in eukaryotic cell lines

The following section is devoted to cellular studies of the proposed regulatory RNA nanoparticle. Initially a set of cytotoxicity experiments was performed in order to select the most suitable metal nanoparticle for conjugation with RNA structures. To do this, the spherical nanoparticles, namely: gold, platinum and silver, of different sizes were added to the cells and their cytotoxicity was tested with the colorimetric method. This experiment was carried in 3 cancerous human cell lines and one primary cell line as a reference. The selected nanoparticle was then used to optimize the process of conjugation with previously described regulatory RNAs. Having obtained the optimal conjugation protocol, the newly prepared regulatory nanoparticles were characterized by dynamic light scattering, transmission electron microscopy and finally their cytotoxicity was analyzed in the model cell line. Knowing that the RNA trimers are processed by endonuclease Dicer *in vitro,* one could expect that it may be also processed by Dicer in cells. Therefore, as the main purpose of this project was to produce regulatory nanoparticles, the final and the most important step was to investigate whether the conjugate induces RNAi and leads to regulation of a selected gene. This was done in the model cell line MDA-MB-231 with a stable expression of a reporter gene – CopGFP using fluorescence methods to observe the gene expression regulation indicated by GFP signal reduction and transmission electron microscopy to observe cell penetration by the RNA-AuNP conjugates. Four cell lines were used in the project, including 3 adherent cell lines and one suspension cell line.

MDA-MB-231 GFP/RFP – adherent cell line

The human breast cancer cell line MDA-MB-231 and MDA-MB-231 GFP/RFP were isolated from M. D. Anderson Cancer Center, where the fluorescence carrying one was a lentivirus modified line, stably expressing GFP and RFP (puromycin resistance). It is the main model used in this project and the CopGFP gene is the reporter gene targeted with all investigated regulatory sequences.

Fibroblasts – adherent cell line

Fibroblasts (CLTH) cell line are human dermal foreskin fibroblasts, the only primary cell line used in this project. It is the most abundant cell type in connective tissue, responsible for extracellular matrix formation and collagen synthesis.

Fibroblasts are therefore essential structural elements and base for many tissues. Those cells were used for cytotoxicity studies as a healthy, noncancerous reference.

MCF-7 – adherent cell line

The human breast cancer cell line MCF-7 was established in Michigan Cancer Foundation-7 (name referring to the institute where the cell line was established). These cells are less invasive compared to MDA-MB-231 breast cancer cells. MCF-7 cells were used as an alternative breast cancer cell line for cytotoxicity studies.

Molt-4 – suspension cell line

The T-lymphoblast cell line Molt-4, derived from leukemic cells of a patient with acute lymphoblastic leukemia. This are suspension cells growing singularly. Molt-4 cells were used as the only suspension cancerous cell line model for cytotoxicity studies.

The MTT assay is a typical protocol used for assessment of compounds' cytotoxicity. This assay allows for a colorimetric analysis of cells' metabolic activity, more precisely, the activity of NAD(P)H-dependent oxidoreductase enzyme, which is highly active in heathy, metabolically active cells. The activity of this enzyme can be colorimetrically measured due to its ability to reduce a yellow tetrazolium dye - MTT (3-(4,5-dimethylthiazol-2-yl)-2,5-diphenyltetrazolium bromide) to purple, insoluble formazan. This way, the cells' condition and metabolic activity may be monitored by comparing the treated cells to the control (untreated cells). The absorbance for this assay is measured at 570 nm with 650nm reference [399]. MTT test has been used for the metal nanoparticles cytotoxicity analysis.

Selection of noble metal nanoparticles for cellular studies

In order to establish the optimal conditions for the cellular delivery experiments cytotoxicity of selected noble metals' nanoparticles was tested.

For the cytotoxicity studies spherical nanoparticles of 3 noble metals were selected, namely: gold nanoparticles (AuNPs: 10, 50 and 100nm), silver nanoparticles (AgNPs 100nm) and platinum nanoparticles (PtNPs 50nm). Cytotoxicity of selected nanoparticles was tested with the MTT assay in cancer cell lines: MDA-MB-231 GFP/RFP, Molt-4, MCF-7, and in human fibroblasts.

In these experiments, cells were plated in the transparent 96-well plates at the 7000 cells/well, 24h before addition of nanoparticles. Nanoparticles were added in concentration range from 0.5µg/mL to 50µg/mL per well and incubated for 48h at 37°C with 5% CO_2 prior to the MTT assay.

Gold nanoparticles cytotoxicity

Cytotoxicity of gold nanoparticles was tested with the MTT assay in cancer cell lines: MDA-MB-231 GFP/RFP, Molt-4, MCF-7, and in human fibroblasts. The graphs below represent impact of AuNPs (diameters: 10nm, 50nm and 100nm) on the cell viability, 48h after treatment.

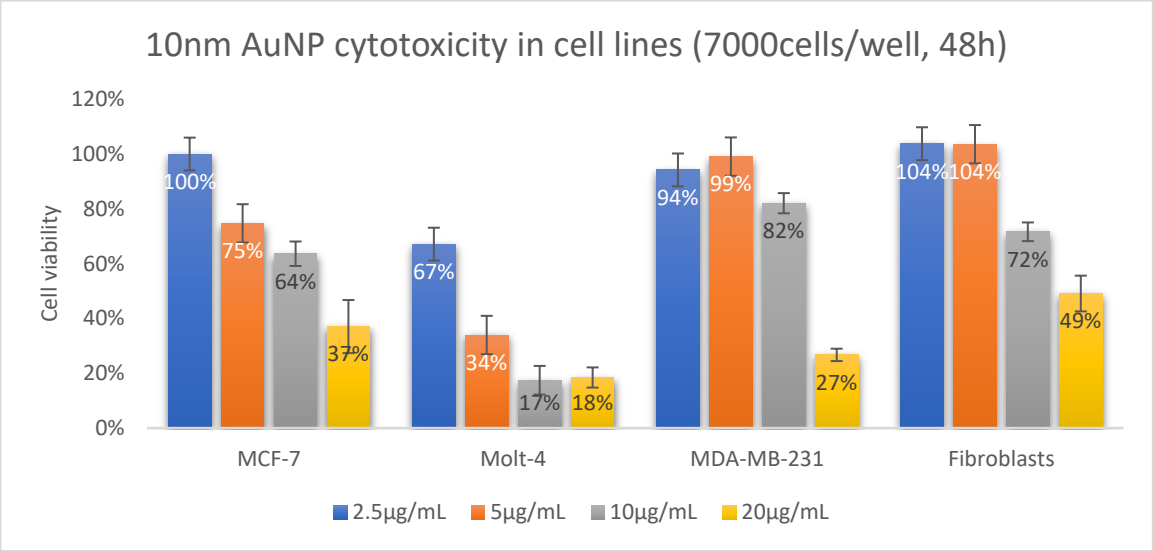

Figure 25. Selection of gold nanoparticles for cellular studies. Four cell types (cancer cell lines: MDA-MB-231, MCF-7, Molt-4, as well as in human fibroblast) were treated with 10nm AuNP and tested by MTT assay, 48h after treatment.

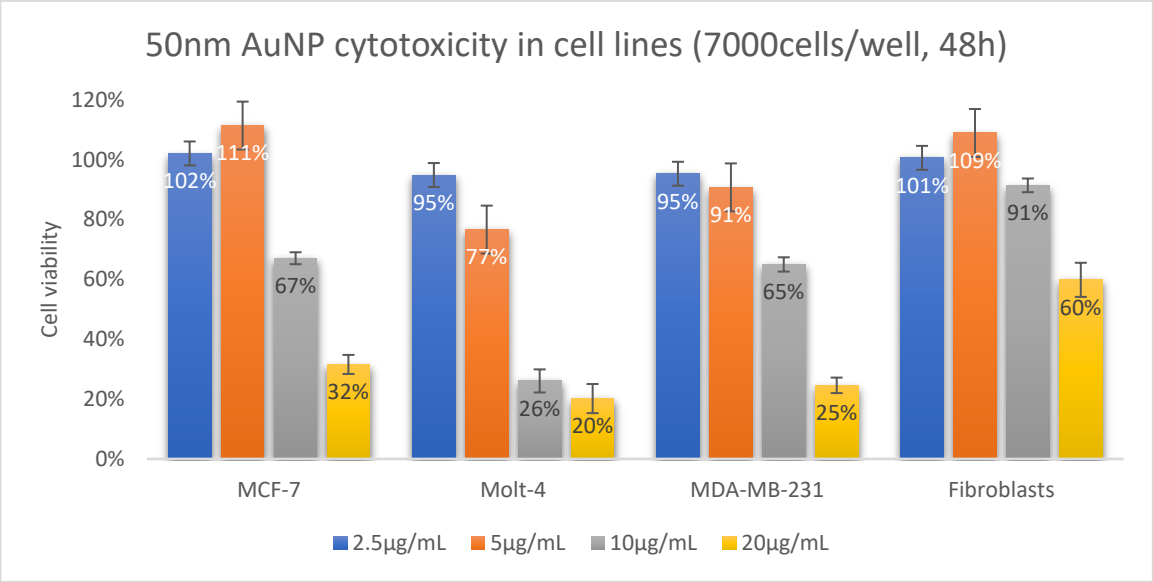

Figure 26. Selection of gold nanoparticles for cellular studies. Four cell types (cancer cell lines: MDA-MB-231, MCF-7, Molt-4, as well as in human fibroblast) were treated with 50nm AuNP and tested by MTT assay, 48h after treatment.

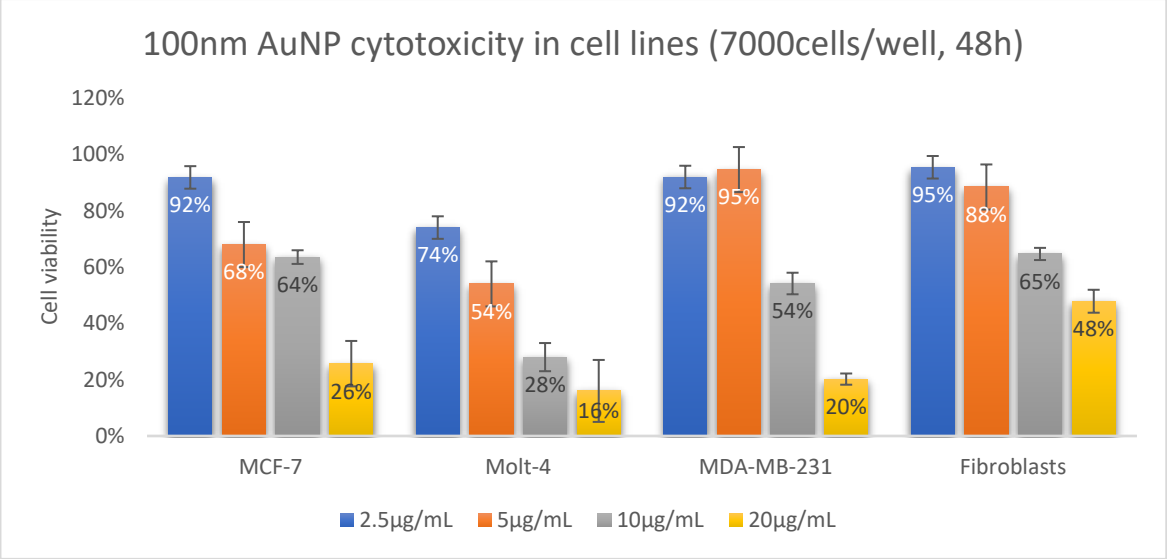

Figure 27. Selection of gold nanoparticles for cellular studies. Four cell types (cancer cell lines: MDA-MB-231, MCF-7, Molt-4, as well as in human fibroblast) were treated with 100nm AuNP and tested by MTT assay, 48h after treatment.

The suspension cell line – Molt-4 – was the most sensitive to gold nanoparticles compared to adhesive cell lines. In this type of cells, the 10nm AuNPs was not toxic at 2.5µg/mL while 50nm and 100nm AuNP at 5µg/mL. Fibroblasts, on the other hand, seem to be the most resistant to the AuNP presence, with 50nm being the least toxic size of AuNPs (20µg/mL is nontoxic while for 10 and 100nm 10µg/mL is a safe concentration). MDA-MB-231 and MCF-7 cells exhibited the same reaction to the presence of AuNPs, with 10µg/mL being the maximum nontoxic concentration. In MDA-MB-231 cells the bigger nanoparticles are more toxic while in the case of MCF-7 cells the cytotoxicity of all 3 nanoparticle diameters is similar.

Silver nanoparticles cytotoxicity

Cytotoxicity of 100nm silver nanoparticles was tested with the MTT assay in cancer cell lines: MDA-MB-231 GFP/RFP, Molt-4, MCF-7, and in human fibroblasts.
The graph (Figure 28) represents 100nm AgNPs impact on the cell viability, 48h after treatment.

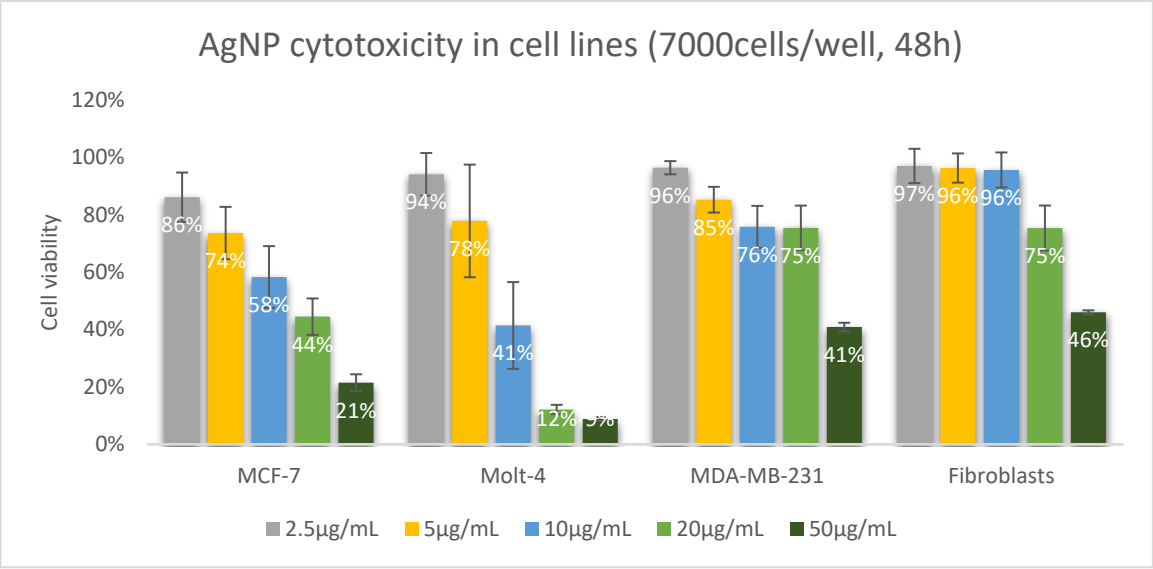

Figure 28. The 4 cell lines (cancer cell lines: MDA-MB-231, MCF-7, Molt-4, as well as in human fibroblast) were treated with 100nm AgNP and tested by MTT assay, 48h after treatment

According to the MTT, all adherent cells maintain at least 50% viability in the presence of at least 10µg/mL silver nanoparticles. For MDA-MB-231 and fibroblasts the 50µg/mL od AgNPs caused cytotoxic effect of more than 50%, which makes those cells unaffected. When it comes to the suspension cell line – Molt-4 the silver nanoparticles at concentration of 5µg/mL were not toxic, suggesting greater sensitivity of this cells to AgNPs.

Platinum nanoparticles cytotoxicity

Cytotoxicity of 50nm platinum nanoparticles was also tested with the MTT assay in cancer cell lines: MDA-MB-231 GFP/RFP, Molt-4, MCF-7, and in human fibroblasts. The graph (Figure 29) represents 50nm PtNPs impact on the cell viability, 48h after treatment.

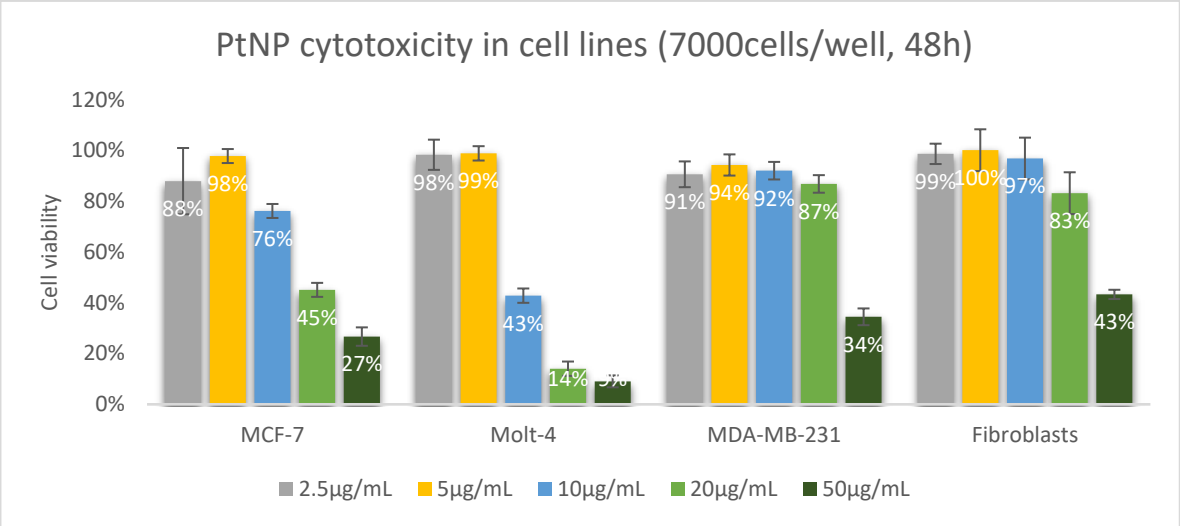

Figure 29. The 4 cell lines (cancer cell lines: MDA-MB-231, MCF-7, Molt-4, as well as in human fibroblast) were treated with 50nm PtNP and tested by MTT assay, 48h after treatment

According to the MTT studies all adherent cells maintain at least 50% viability in the presence of at least 10µg/mL platinum nanoparticles. For MDA-MB-231 and fibroblast up to 20µg/mL of PtNPs was not toxic. Similar to the result from AgNPs cytotoxicity studies, the MCF-7 cell line seems to be the most sensitive (the steepest toxicity trend) out of adherent cell lines tested. When it comes to the suspension cell line – Molt-4, the platinum nanoparticles at concentration of 5µg/mL were not toxic, suggesting greater sensitivity of this cell line to the presence of PtNPs.

Selection of the optimal nanoparticle for further investigation

In summary, all tested nanoparticles are suitable to be used for cellular experiments. The model cell line for the RNAi studies is MDA-MB-231 stably expressing genes of green and red fluorescence proteins (GFP and RFP) for which 10µg/mL of any AuNP and 20µg/mL of AgNPs and PtNPs are nontoxic. The most studied model for nucleic acids delivery is AuNP, therefore the smallest tested 10nm AuNPs has been selected for the further experiments also because it was the least toxic in MDA-MB-231 cells.

To make sure that nanoparticles at low concentrations are also safe for the model cell line, additional MTT assay was performed, for the 0.5, 1 and 2.5µg/mL AuNP and the result is presented (Figure 30).

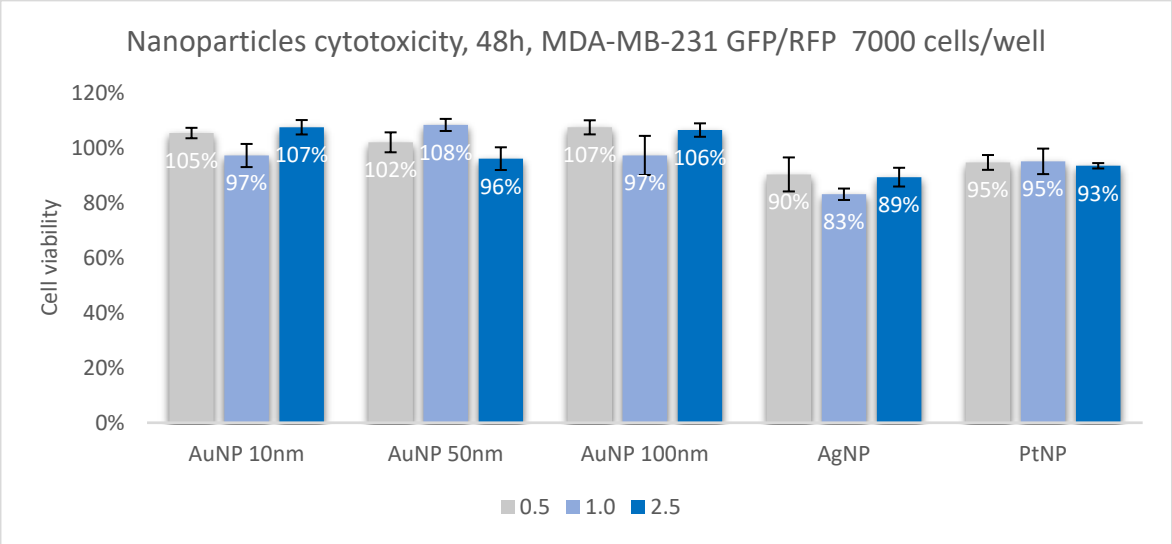

Figure 30. Cytotoxicity of low concertation nanoparticles in MDA-MB-231 (N=10)

The result confirmed expected linearity in nanoparticles' toxicity and none of the tested conditions was toxic to the model cell line.

Conjugation of RNA (siRNA and structural RNA) with AuNPs

In this project a conjugate composed of gold nanoparticle core and RNA fragments were studied. At first, as a control, a set of siRNA-AuNPs, was obtained following the literature protocol [332]. This is the standard approach used in spherical nucleic acid, based on siRNA conjugation preparation, however modified to accommodate conjugation with structural RNAs. Based on the optimized protocol, an RNA trimer was conjugated with AuNP. The final structure consists of 10nm AuNP and the G3 trimers (T3), that have a thiol linker introduced with the short, complementary, synthetic RNA.

siRNA capped gold nanoparticles

AuNP titration with siRNA

To obtain the siRNA-capped gold nanoparticles a set of 3 HS-siRNA (HS-siR1-2, HS-siR5-6, HS-siR9-10) was associated and then hybridized with AuNP. The process of SNA hybridization was done by progressive increase of the salt concentration [332] (Figure 31).

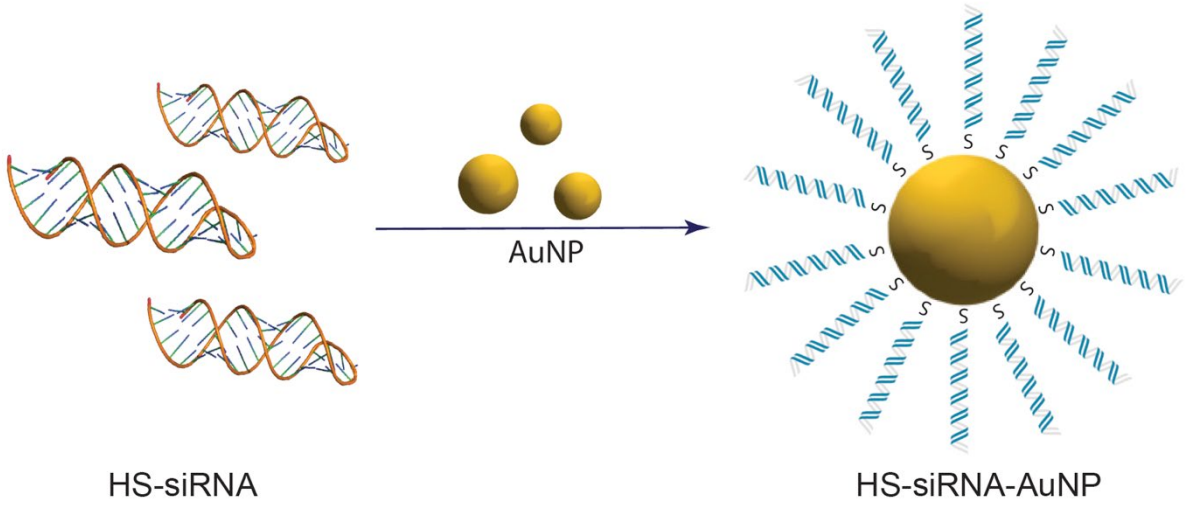

Figure 31. General scheme presenting the composition and assembly of spherical nucleic acid from HS-siRNA and AuNP. The salt ageing protocol was used here [332].

At first, AuNP was titrated with increasing amounts of the HS-siR5-6 in order to select the optimal siRNA-AuNP ratio for the experiments. To do that, different ratio of HS-siRNA: 5, 10, 20, 30, 40 and 50pmoles were prepared and hybridized with the equivalent of 1pmol of AuNP. An agarose gel electrophoresis was run to evaluate the siRNA-AuNP formation (Figure 32), with the 40pmol HS-siR5-6 being used as a reference (left line). The gel was visualized in the natural light (panel A) to observe the migration of hybridized RNA-AuNP complex. The AuNP alone does not enter into gel, so the only visible red band, correspond to the AuNPs, linked to RNA. The same gel was also visualized under the UV to observe the ethidium bromide signal, corresponding to dsRNA (panel B).

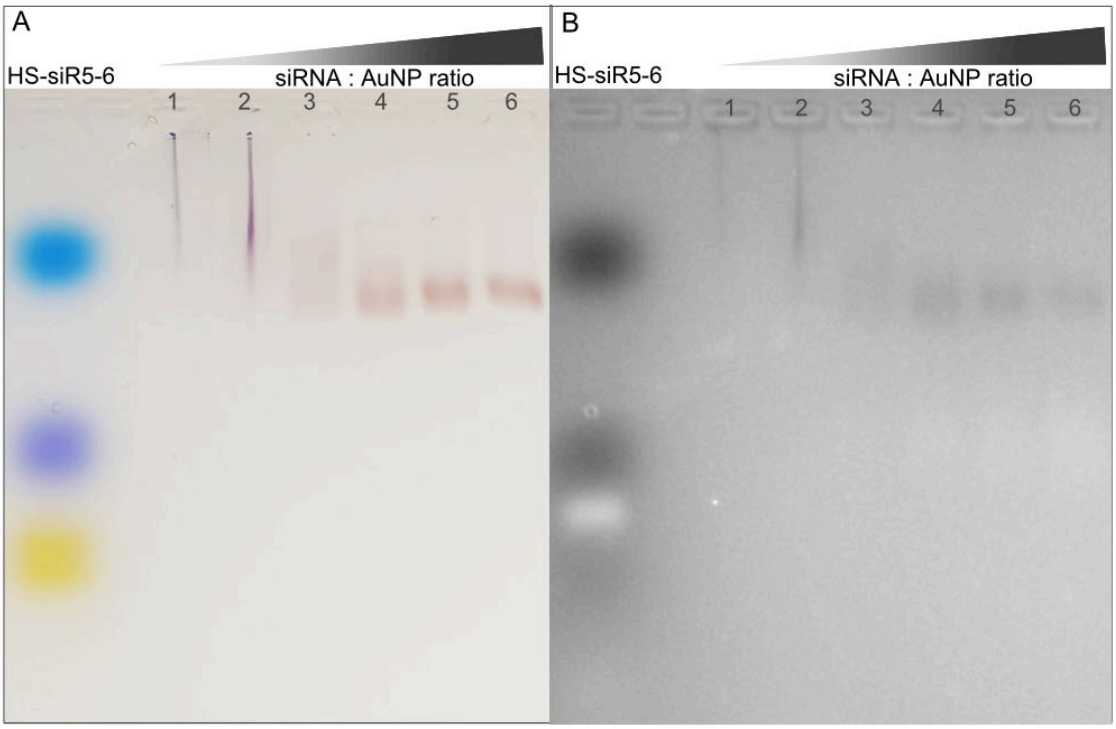

Figure 32. AuNPs titration with siRNA (1.5% agarose gel, A - natural light, B - UV light (EtBr), samples order: 0-control, 1-6 are samples with siRNA:AuNP ratio being 5:1, 10:1, 20:1, 30:1, 40:1 and 50:1 respectively)

It can be inferred from the gel that 5 and 10pmoles of siRNA is not sufficient to provide a full coverage of 1pmol AuNP, which is visible in line 1 and 2. These samples precipitate and do not migrate properly in the gel. In lines 3 to 6 the smear is not visible and the red band becomes more evident as the siRNA concentration increases. This shows that saturation of nanoparticle with siRNA allows to form more uniform complexes and the negative charge is cumulated enough to allow migration. A strong, red band from complexes is visible, such as in lines 5 and 6 (40:1 and 50:1 siRNA:AuNP ratio).

It can be therefore concluded that the 40pmol siRNA is sufficient to saturate 1pmol of 10nm gold nanoparticles and such ratio was chosen for the further studies.

Selected siRNA hybridization with AuNP

In this study the three selected HS-siRNAs were associated and hybridized with AuNP utilizing previously selected conditions. The formation of complexes was evaluated with the 1.5% agarose gel (Figure 33).

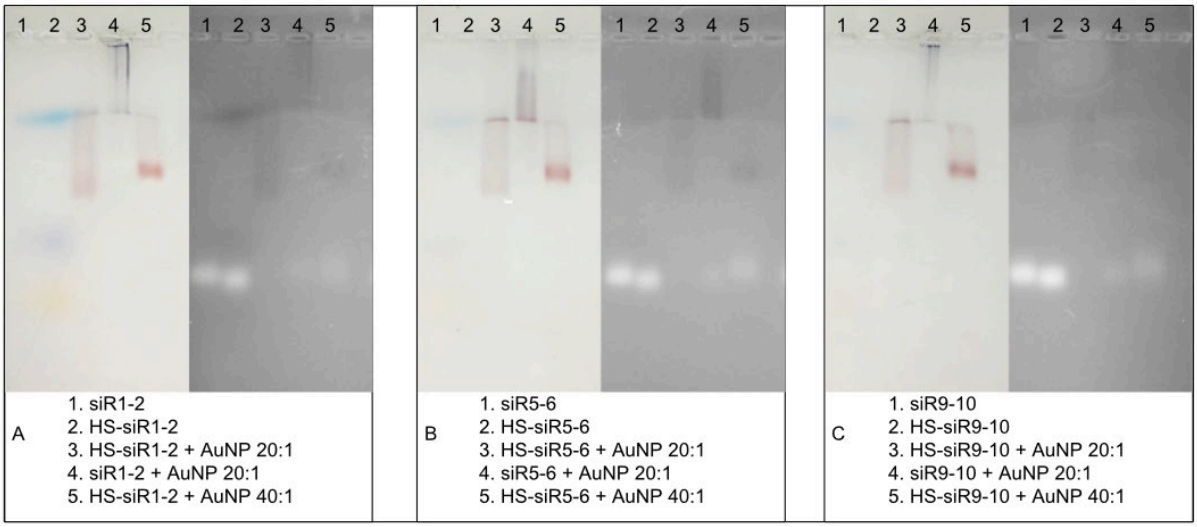

Figure 33. SNA hybridization (1.5% agarose gels, A- analysis of SNA formed with HS-siR1-2, B- analysis of SNA formed with HS-siR5-6, C- analysis of SNA formed with HS-siR9-10, results were visualized with the natural light to show AuNP (left panels) and under the UV light with EtBr (right panels))

This experiment juxtaposes AuNP complexes with selected HS-siRNAs duplexes. The corresponding siRNAs lacking the thiol group were used as a size reference (line 1); siRNA, which underwent AuNP hybridization protocol, was introduced to show hybridization dependence on a HS group presence. All HS-siRNAs duplexes form stable complexes with AuNP, migrating as one solid band (line 5 on panels A, B and C), while thiol-free siRNAs, with the same nucleotide sequence, cause AuNP precipitation and do not migrate in gel (line 4). Excess of RNA unbound to the AuNP is visible under UV light and migrates at the same level as the bare siRNA references. Lack of signal under the UV light in the case of siRNA-AuNP complexes is most likely caused by AuNP quenching affecting fluorophores located in the close proximity, such as EtBr intercalated in the attached siRNA.

In the experiments, for the RNA delivery purposes, between 20 and 40pmoles of RNA is attached to 1pmol of the 10nm AuNP. That was calculated in the following way:

1. 10nm AuNPs stock at a concentration of 60μg/mL contains an equivalent of $6x10^{12}$ particles/mL (data from Sigma Aldrich [400]) (1)
2. Using Avogadro's constant ($6.022x10^{23}$ particles = 1mole, or 1pmole = $6.022 x10^{11}$ particles) the amounts of RNA and AuNPs needed for reaction were calculated:

To make 20:1 or 40:1 RNA-AuNP ratio one needs to mix:

- 1pmol of AuNP (6 $x10^{11}$AuNPs) – 100µL from the main stock ($6x10^{12}$ particles/mL=$6x10^{9}$ particles/µL), is equal to approximately 6µg of gold (1)
- 20pmoles of RNA = $20x6.022\ x10^{11} = 1.2\ x10^{13}$ RNA particles
- 40pmoles of RNA = $40x6.022\ x10^{11} = 2.4\ x10^{13}$ RNA particles

For standard siRNA/RNAi experiment, a final concentration of siRNA ranges between 5 and 15nM in 200µL, which gives approximately 1 to 3pmoles of RNA in a well. **If 20 to 40pmoles of RNA is bound by 6µg of AuNPs, the amount of AuNPs needed to deliver 5-15nM of RNA is less than 1µg (6µg/20pmol = 0.3µg or 6µg/40pmol = 0.15µg).**
From the above calculations it becomes clear that the concentration of nanoparticle delivered with the RNA is below the IC50 for tested nanoparticles in cell lines.

tectoRNA-AuNP conjugates preparation

Having obtained the optimal condition to conjugate siRNA and AuNP, the next step was to attach structural RNA trimer to AuNP. This is achieved owing to the presence of the thiol linker introduced to the G3A monomer. The picture below shows a general scheme for T3-AuNP conjugation (Figure 34).

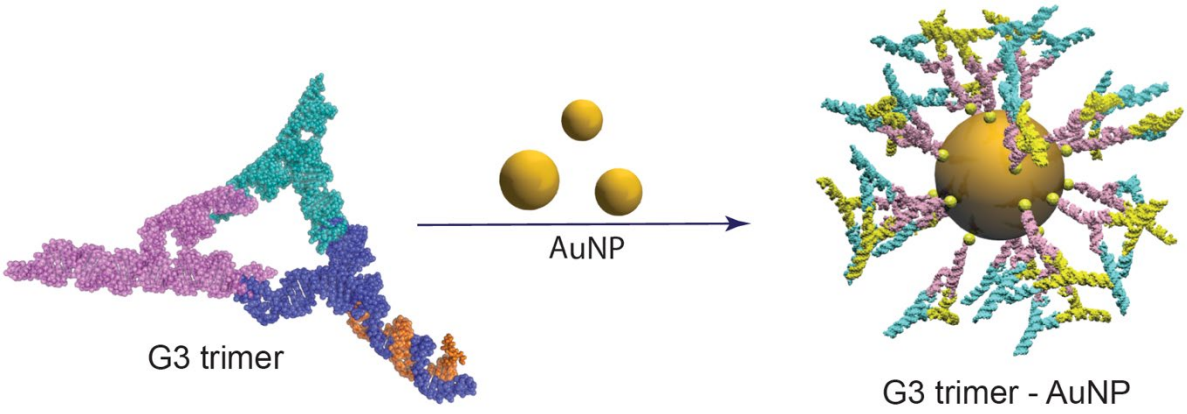

Figure 34. General scheme presenting the composition and conjugation of RNA trimer and AuNP. The salt ageing protocol was used [332].

To test this concept, first, the AuNP titration experiment was performed to select a tectroRNA:AuNP ratio allowing to saturate the nanoparticle and keep it stable. One G3 trimer, T3A7B1C1, was used for AuNP titration. Again, 1pmol of AuNP was

titrated with different amounts of RNA trimer, namely: 5, 10, 20, 30, 40 and 50pmol. The hybridization protocol was similar to the one used before for siRNA association with AuNPs. Hybridized tectoRNA-AuNP were concentrated by centrifugation and analyzed.

An agarose gel electrophoresis was run to evaluate the complex formation, with the 40pmol HS-siR5-6 used as a reference (left line) (Figure 35). The gel was visualized in the ambient light (panel A) to observe the migration of hybridized RNA - AuNP complex. The same gel was then visualized with the UV light to observe the dsRNA signal using ethidium bromide (panel B).

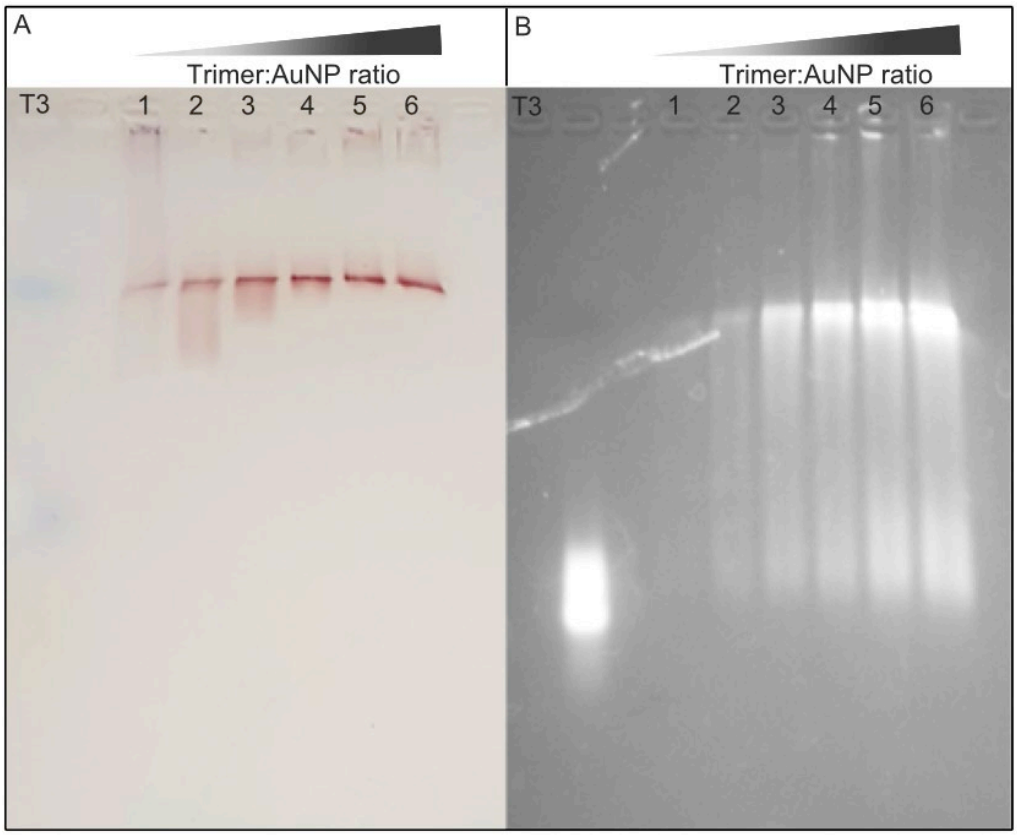

Figure 35. AuNPs titration with G3 trimer (1.5% agarose gel, A - natural light, B - UV light (EtBr), samples order: T3-control, 1-6 are samples with T3:AuNP ratio being 5:1, 10:1, 20:1, 30:1, 40:1 and 50:1 respectively)

It is visible that none of the samples precipitated, the way it was observed in the siRNA study. A faster migrating AuNP smear, visible in the natural light below the main band, may indicate formation of different population of RNA-AuNP. This suggest that due to electrostatic interactions between trimer's phosphates and the AuNP's surface there might be a different species at low concentration of RNA. As T3 concentration increases, the smear gets smaller, to disappear completely at 40:1 ratio (line 5) suggesting existence of single population, where electrostatic forces no

longer play a role. For this reason, the 40:1 ratio was selected to be used in the further studies.

Alongside with the titration experiment, a comparative experiment was performed to visualize differences in migration of: HS-siRNA-AuNP, G3 monomer-AuNP and G3 trimer- AuNP (Figure 36). As a control, a G1 trimer treated with AuNP was used, to assure that RNA without the thiol modification does not form a stable SNA nanoparticle.

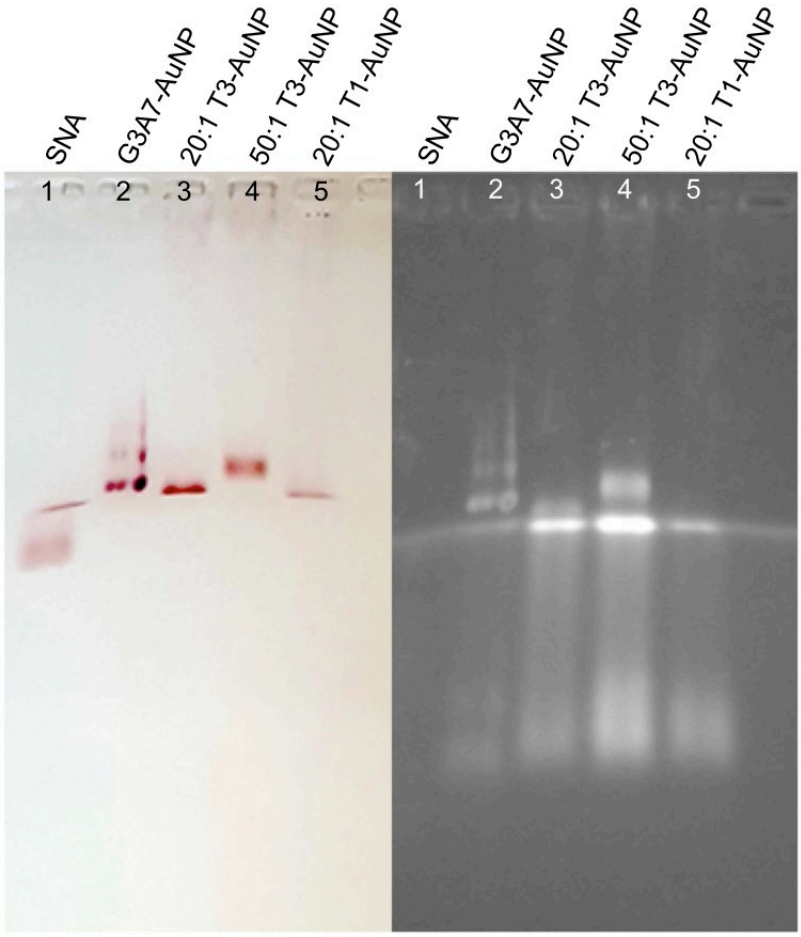

Figure 36. Formation of HS-siRNA, HS-monomer and HS-trimer hybrids with AuNP compared with thiol-free trimer interaction with AuNP (1.5% agarose gel, left panel - natural light, right panel - UV light (EtBr))

This gel experiment proved that in the absence of HS-RNA the conjugate is not formed and the AuNP smear and feeble band at the line 5 are visible due to electrostatic interaction between negatively charged RNA surface and AuNP. A G3 monomer can also be attached to AuNP, it is however less stable than tectoRNA trimer, likely owing to the stability of the 3WJ motif resulting from the monomer assembly.

RNA-AuNP characterization

Transmission electron microscopy of RNA-AuNP nanoparticles

Both siRNA-AuNP and Trimer-AuNP conjugates were analyzed with transmission electron microscopy (TEM). This has given the idea of nanoparticles' shape, dispersion and confirmed their average diameter (Figure 37). RNA coating could not be observed using high energy TEM due to the electron transparency of the nanoobjects, their 3D shape and high contrast of AuNP compared to the RNA part [401]. The functional assays were developed to observe the presence and the functionality of the introduced construct.

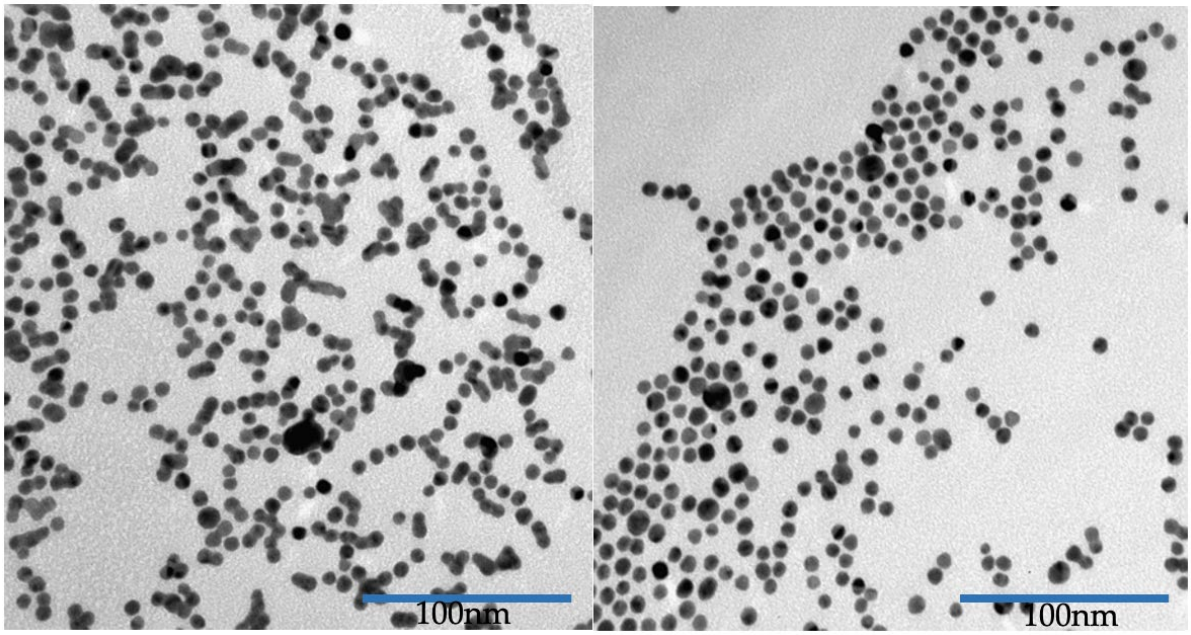

Figure 37. Electronogram presenting 10nm AuNP hybridized with siRNA (left) and RNA trimers (right) (300k magnification).

Dynamic Light Scattering analysis of RNA-AuNP

The dynamic light scattering technique was used to analyze RNA-AuNP conjugates and estimate their diameters and potential ζ. The mean particle diameter was determined for each construct following the volume - size distribution curves. As a result, the expected trend was observed, where AuNPs in solution have mean diameter of around 14nm, the siRNA-AuNP conjugate is 6nm greater and tectoRNA-AuNP's diameter is 20nm greater compared to naked AuNPs (Figure 38). The exact results are presented in the table below. Such increasing change in particles' diameters complies with expected outcome. The rough estimation of a siRNA length is 6nm, while the most simplistic, 'flat' model of the trimer should be approximately 16nm wide. The RNA fragments bound to

the AuNP in solution may be far from estimated flattened models and the RNA particles positioning on the AuNP surface may vary, thus altering the light scatters. This can explain the discrepancies in diameter changes observed with DLS. Overall diameter change, however is within the expected range and follows the expected tendency. Comparing to electrically neutral, naked AuNP the RNA-AuNP conjugates have low, negative ζ potential, -24mV for siRNA-AuNP and -12.7mV for trimer-AuNP. This, may account in some extent for nanoparticles' aggregation. However, it has never been an issue in experimental trials. The negative electrokinetic potential of RNA-conjugated samples also complies with their electrophoretic mobility. While naked AuNP doesn't migrate in gel, the RNA-AuNP does migrate towards the anode.

AuNPs < siRNA-AuNP < tectoRNA-AuNP

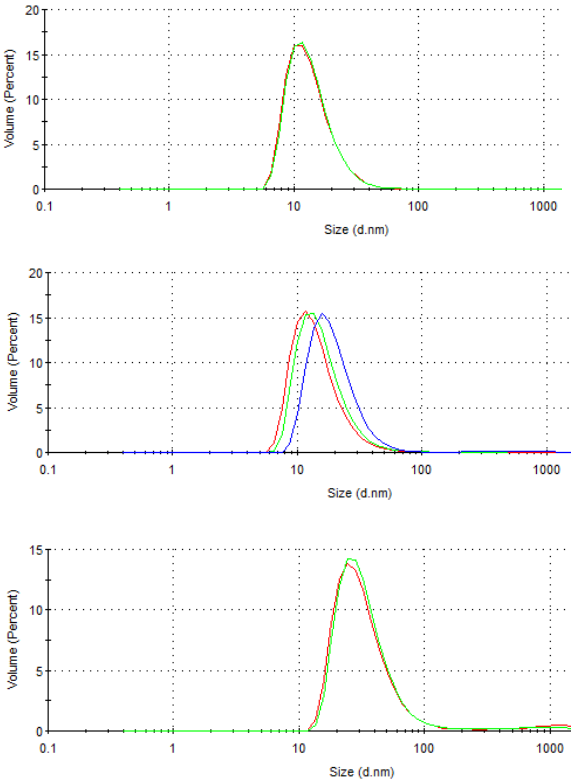

Sample	Size (volume)	SD
AuNP 0	14.18	7.85
siRNA-AuNP	20.19	10.19
tectoRNA-AuNP	34.61	24.46

Figure 38. Data collected with dynamic light scattering

siRNA-AuNP conjugate dissociation in the presence of thiols

The aim of these experiments was to determine whether the complexes assembled *via* a thiol linkage may be disassembled by introduction of another thiol molecule. It was suggested by Hong et al [252] that the GSH peptide, which is abundant among cells, contributes to the siRNA release from a spherical nucleic acid as it replaces it

on the AuNP surface. The Hong group presented results of the fluorescent RNA release from AuNP in living cells and after 2h in water.
Here, bioanalysis was used to verify release of RNA from newly created siRNA-AuNP complexes. The siRNA discharge from the complex was investigated under treatment with GSH or 2-mercapto ethanol (BME). The GSH or BME were applied to siRNA-AuNP in three concentrations and the solutions were incubated for 2, 4 or 24h to see how that affects the SNA.

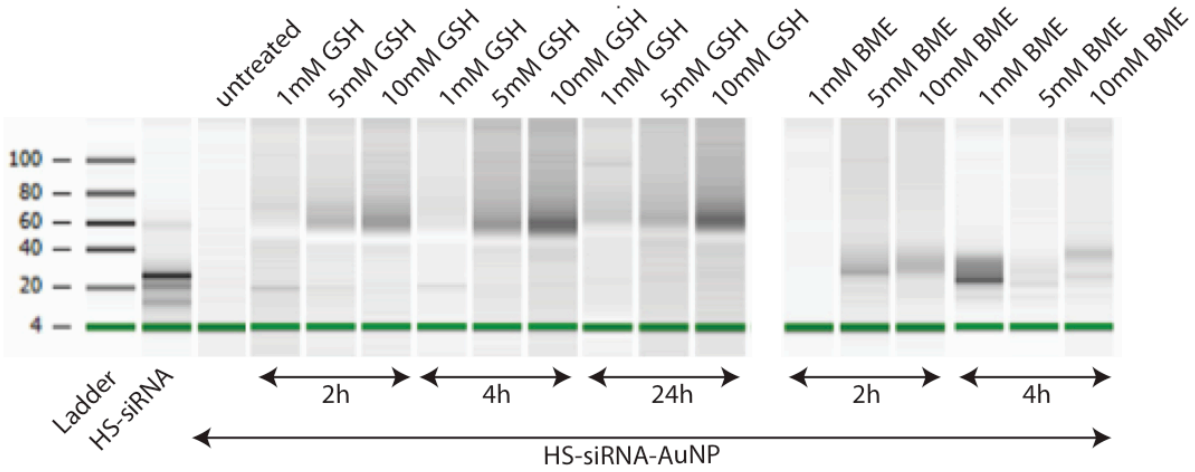

Figure 39. Bioanalysis of HS-siRNA-AuNP conjugates incubated for 2, 4 or 24h with GSH and 2, 4h with BME.

The bioanalysis indicated that both BME and GSH can cause dissociation of HS-siRNA from the AuNP surface (Figure 39). For BME, the length of incubation did not have a significant impact on the SNA disassembly. Immediately after BME addition the SNA solution turned blue suggesting some change, likely due to aggregation which leads to altered optical properties. Bioanalysis suggests that the addition of the lowest BME concentration (1mM) resulted in the best RNA removal, indicated by the strong band at the 21nt level, same as the HS-siRNA reference. The addition of GSH didn't cause any visible change in solution, even after 24h incubation. The lowest, 1mM concentration of the GSH peptide can cause partial dissociation of HS-siRNAs, visible as a thin band at 21nt reference level (2 and 4h incubation). Longer incubation does not influence the released siRNA amount. For the samples treated with GSH in a higher concentration, the lower band, corresponding to the 21nt reference, disappears and a higher band appears (~60nt). This may indicate formation of duplexes *via* thiol interactions between HS-siRNA and GSH, which was not observed for BME. As the incubation time increases, the upper band becomes more pronounced, suggesting that more HS-siRNA was removed but also there was more time to form duplexes. The untreated complexes

cannot be visualized due to the SYBR green fluorescence quenching in the presence of closely located AuNP (~6nm siRNA length), however, as the RNA is removed from the AuNP complex, the signal can be recorded. The result of this experiment lines up with the hypothesis that RNA-AuNP complexes can be disassembled by the GSH, or other thiols present in cytoplasm.

RNA-AuNP uptake in cells

The goal of this study was to show cellular uptake of the new tectoRNA-AuNP complexes. Cells were transfected once with the T3-AuNP (5nM) and analyzed with transmission electron microscopy, 72h post transfection. The electronograms are presented below (Figure 40).

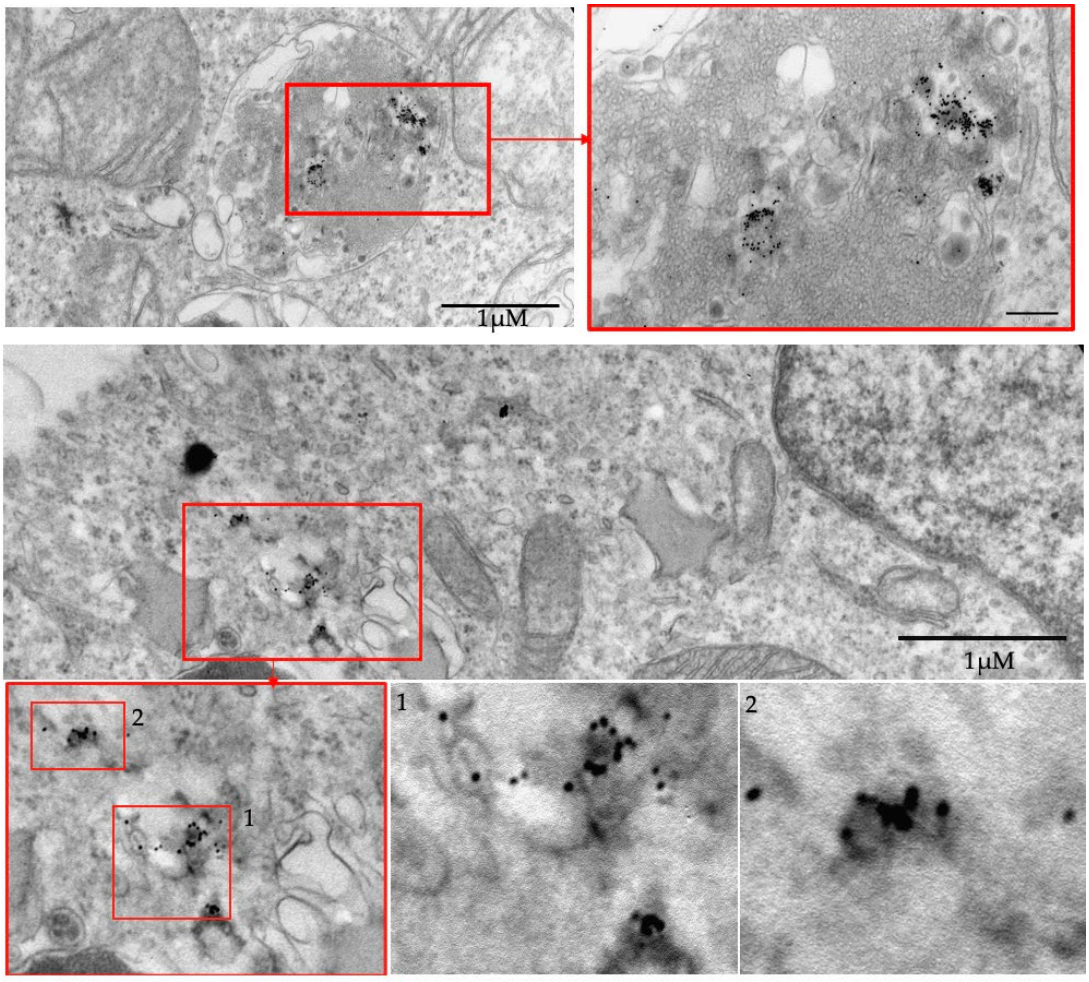

Figure 40. Electronogram of MDA-MB-231 GFP/RFP cells treated with TectoRNA-AuNP (captured at 30k magnification). Top panel represents nanoparticles placed inside of the membranous structure. Bottom panel shows nanoparticles dispersed in the cytoplasm and magnification of marked area, where dispersed free TectoRNA-AuNP are visible.

The TEM analysis has allowed to identify high electron density structures (AuNP) located in membranous structures as well as dispersed in cytoplasm. This, alongside with CopGFP gene expression regulation is a confirmation of cellular uptake of the complexes and their functionality.

Cell viability in the presence of selected RNA and RNA-AuNP

Cell viability was checked after treatment with selected RNA-AuNP complexes. This was done in addition to previously analyzed cytotoxic effect of AuNPs or regulatory RNAs, to assure lack of toxicity of the whole complex nanoparticles. The result of MTT assay confirms that none of the used components, nor their complexes are toxic to the model cell line (Figure 41).

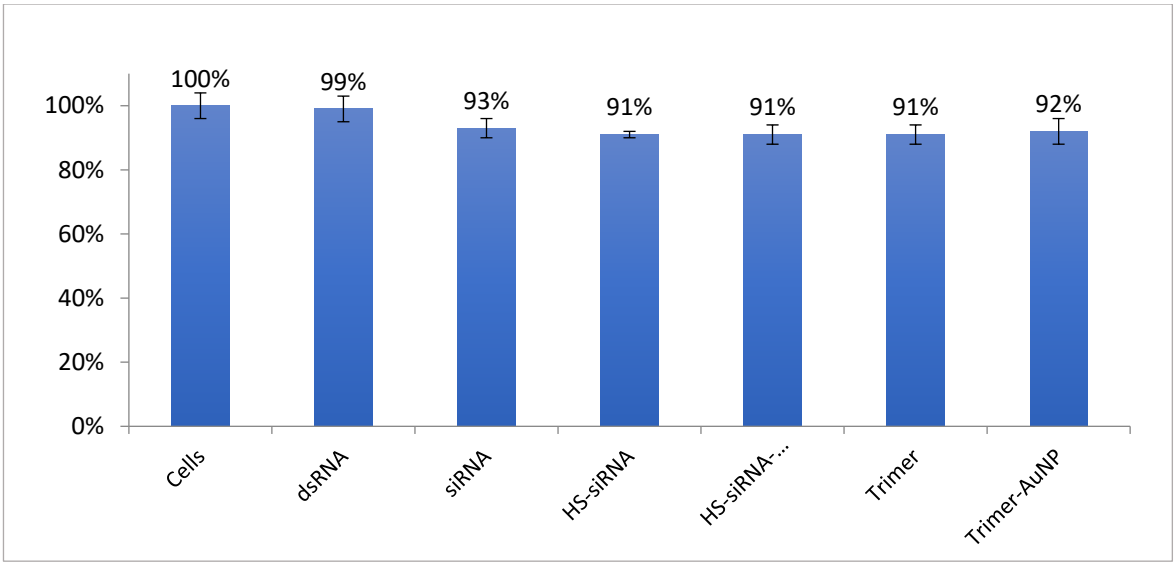

Figure 41. TectoRNA-AuNP cytotoxicity assay (MTT) results normalized to MDA-MB-231 GFP/RFP control cells, N=5.

Gene expression regulation studies in GFP model system

Gene expression regulation based on the RNAi may be induced by delivery of siRNA (~21nt duplex) to the cells, that is later taken up by RISC and cause degeneration of target mRNA [402]. Owing to the presence of DICER in cells, longer (>21nt) dsRNA or structural RNA may be processed and can enter RISC [403]. In this project a set of siRNAs and tectoRNA trimers with regulatory fragments were used in unmodified form and conjugated with AuNPs. The model cells were transfected with RNA elements to test the regulatory potential against GFP gene. The fundamental aim of this project was to show that the new generation of spherical nucleic acids – tectoRNA conjugated with AuNP (T3-AuNP) may be

introduced to the cells and is able to regulate gene expression without causing unwanted side effects to the cells.

MDA-MB-231 GFP expression system

The human cell line MDA-MB-231 GFP/RFP was used as a model cell line for all gene expression experiments. This line is a derivative of a human breast cancer cell line MDA-MB-231. MDA-MB-231 GFP/RFP are adherent cells where the green and red fluorescence may be easily be observed under the fluorescent microscope or measured using fluorometric methods.

GFP gene expression regulation with siRNA

A set of previously selected siRNAs was used in the preliminary gene expression regulation study in MDA-MB-231 stably expressing GFP and RFP. The three HS-siRNA duplexes and their unmodified equivalents were tested with two other siRNAs, that were previously proven to silence CopGFP expression in this model. Simultaneously for the siR5-6 sequence 3 variants were analyzed: classical siRNA duplex - siR5-6, siRNA duplex with 5'-thiol group HS-siR5-6 and AuNP conjugated with HS-siR5-6. This particular comparative element of the study was meant to prove that the presence of AuNP and introducing the same siRNA to the spherical framework would not change its regulatory efficacy. The gene expression regulation study was performed either with single addition of triple addition of the transfection mixture, after 72 or 144h of incubation, as 3 independent, consecutive experiments with 5 repetitions of each variant. The graphs (Figure 42-43) present GFP fluorescence data normalized to the fluorescence of untreated MDA-MB-231 GFP/RFP cells.

This experiment has shown that the siRNA-AuNP conjugates perform as well as siRNA and HS-siRNA of the same sequence. It can be also inferred from this study that there is practically no difference between single and triple addition protocol and neither of the tested conditions was toxic to the cells.

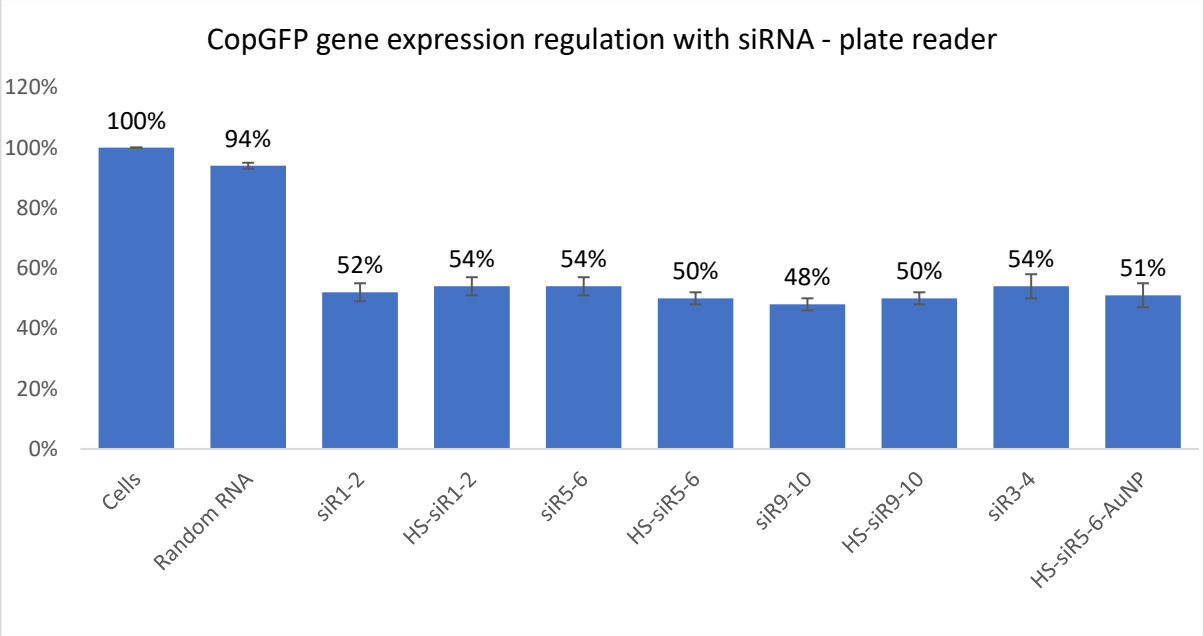

Figure 42. CopGFP expression regulation in MDA-MB-231 GFP/RFP, measured 72h post transfection with siRNAs, following the single addition protocol - plate reader measurement Cells were plated, 10 000cells/well, collected data was normalized to the fluorescence of untreated cells.

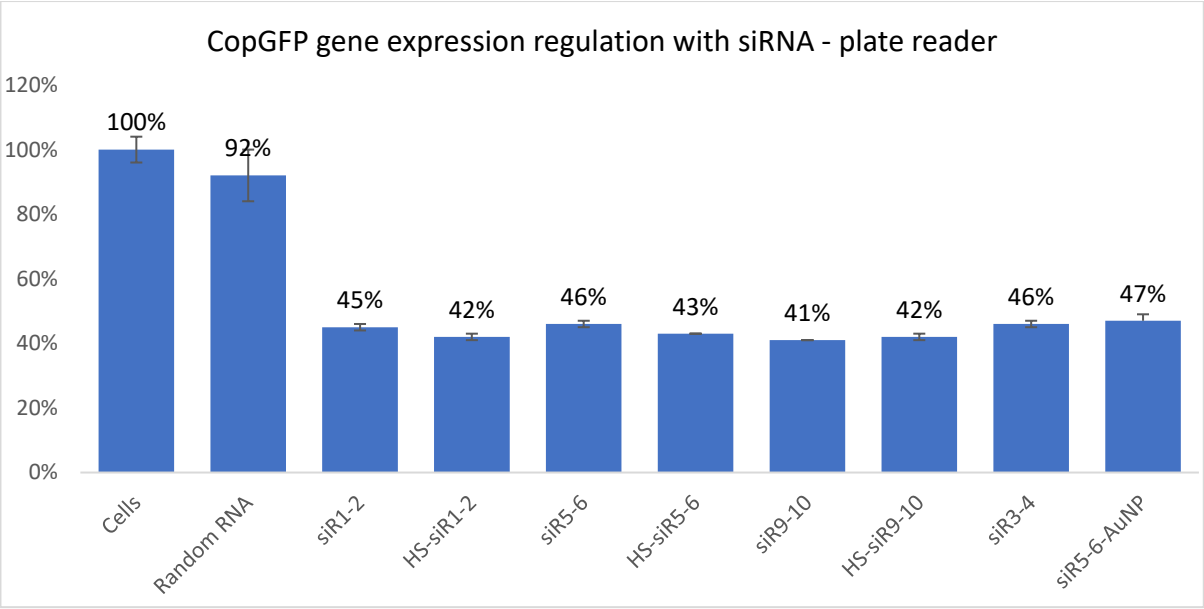

Figure 43. CopGFP expression regulation in MDA-MB-231 GFP/RFP, measured 144h post transfection with siRNAs, following the triple addition protocol - plate reader measurement. Cells were plated, 5 000cells/well, collected data was normalized to the fluorescence of untreated cells.

CopGFP gene regulation with RNA-AuNP

In this section a set of previously studied siRNA and trimers were introduced into the spherical shape by hybridization with 10nm AuNP. The siRNA-AuNP (siR1-2, siR5-6, siR9-10) and T3-AuNP (T3A1B1C1, T3A7B1C1, T3A9B1C1) samples were used for MDA-MB-231 GFP/RFP transfection. Unconjugated RNA structures, identical to hybridized ones, were used as controls. All samples were treated the same way and transfected in 3 portions of 5nM each, every 24h. Random RNA fragment was used as a negative control. The gene regulation effect was measured by GFP fluorescence, 144h after the first transfection. The graph below presents GFP fluorescence data normalized to the fluorescence of untreated MDA-MB-231 GFP/RFP cells.

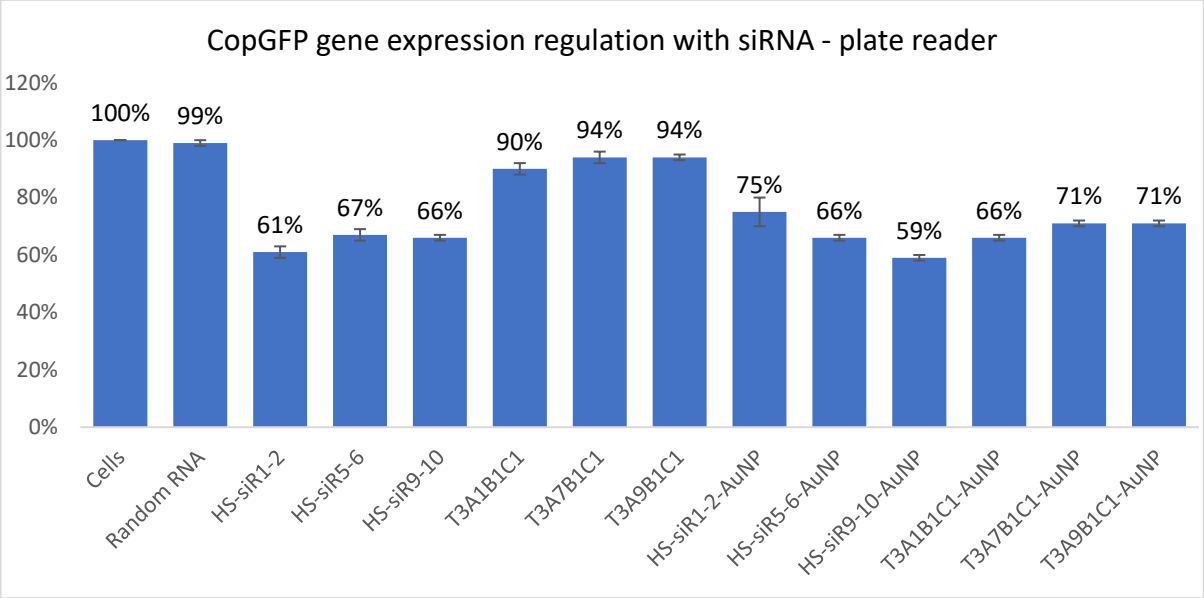

Figure 44. CopGFP expression regulation in MDA-MB-231 GFP/RFP, measured 72h post transfection with regulatory RNA or their AuNP conjugates, following the single addition protocol - plate reader measurement Cells were plated, 10 000cells/well, collected data was normalized to the fluorescence of untreated cells.

The above results suggest that following a single addition protocol the regulatory RNA trimer is more effective when conjugated to the AuNP when compared to the unmodified RNA. However, the 72h incubation time could be extended in order to allow for structural RNA processing. Therefore, a GFP regulation study in time intervals was performed.

CopGFP gene expression regulation in time intervals

This experiment aimed to select the optimal time for the CopGFP gene regulation with the new nanostructures. A set of siRNA and regulatory RNA constructs were applied to GFP model cells following the triple addition protocol, which means that cells were transfected 3 times, with 5nM siRNA or 5/3nM trimer, to get a final concentration of 15nM siRNA (equal to 5nM trimer). The gene expression regulation was monitored in time intervals by the GFP fluorescence measurement using plate reader, between 0 and 144h post transfection. Results of this experiment are presented in the schemes (Figure 45-46).

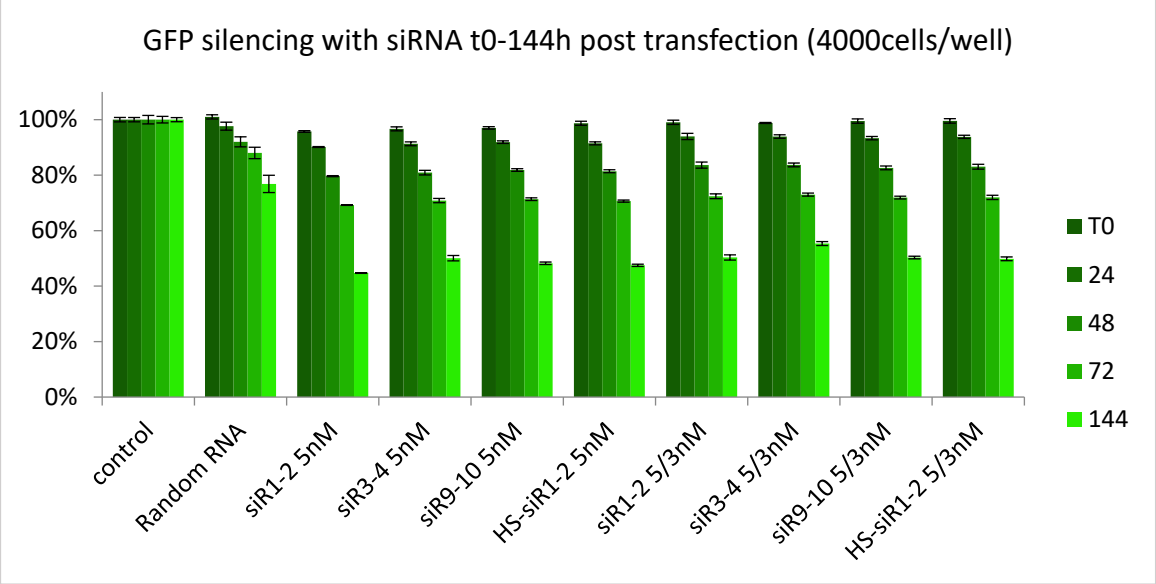

Figure 45. Change of GFP fluorescence in time after treatment with siRNA

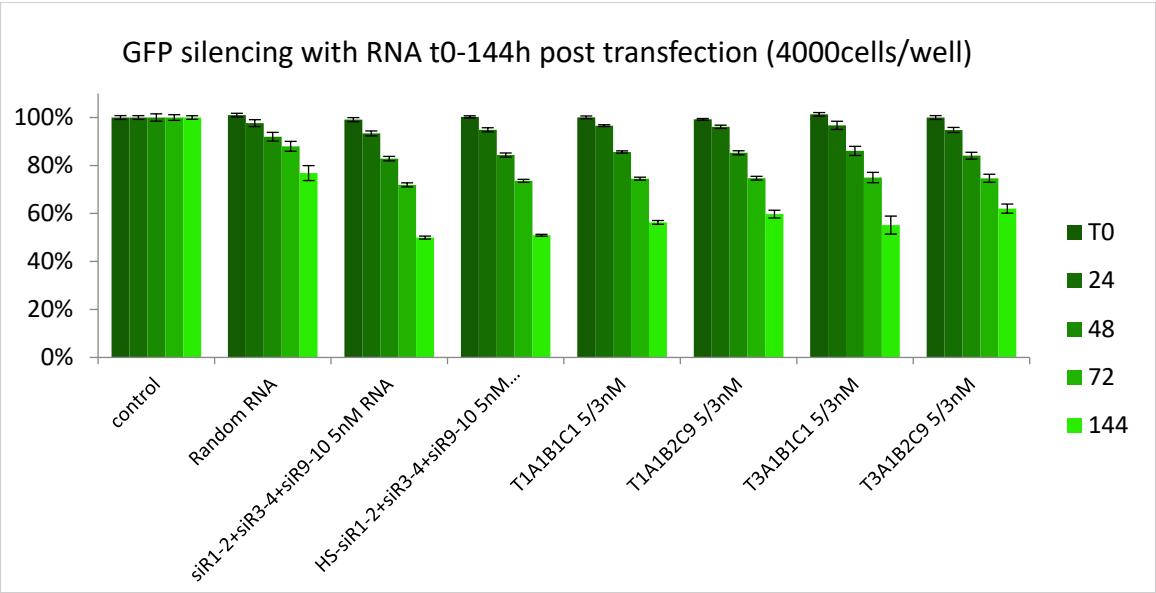

Figure 46. Change of GFP fluorescence in time after treatment with regulatory RNA nanoparticles

The plotted data is normalized to untreated cells (within a time point). It is clear, that there is a significant decrease in fluorescence in time, with 144h being the lowest. It suggests that, in the presence of regulatory RNAs, the GFP production is hindered enough to overcome doubling time of this cancer cell line. According to the obtained results, the 144h post transfection was selected for further investigations as it was the most practical time point in cell handling which allowed to keep reasonable cell density while showing the most optimal gene regulation effect in longer time period.

CopGFP expression regulation comparison of plate reader and flow cytometry studies

The concluding experiments were designed such that the final molar concentration of regulatory fragments delivered to cells was the same (15nM), regardless of the structure (siRNA, siRNA-AuNP, trimer, trimer-AuNP). Samples were delivered to cells in a triple addition protocol and analyzed using fluorescence plate reader (Figure 47) and flow cytometry (Figures 48-49) at 144h post transfection.

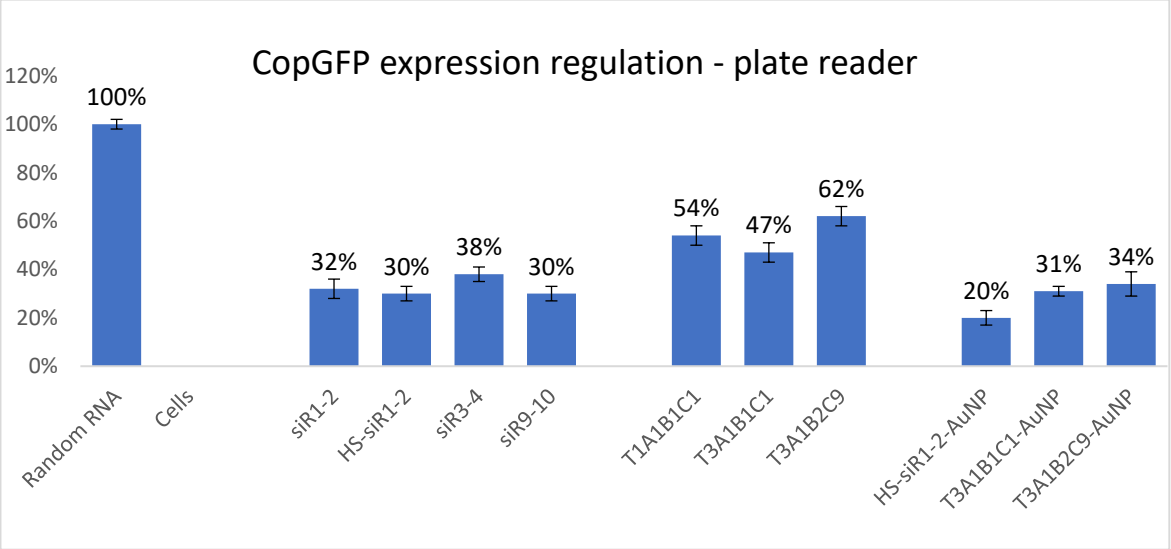

Figure 47. CopGFP gene expression regulation with regulatory RNA and RNA-AuNP conjugates, fluorescence plate reader results. Figure represents mean values from 3 separate experiments, error bars refer to standard error.

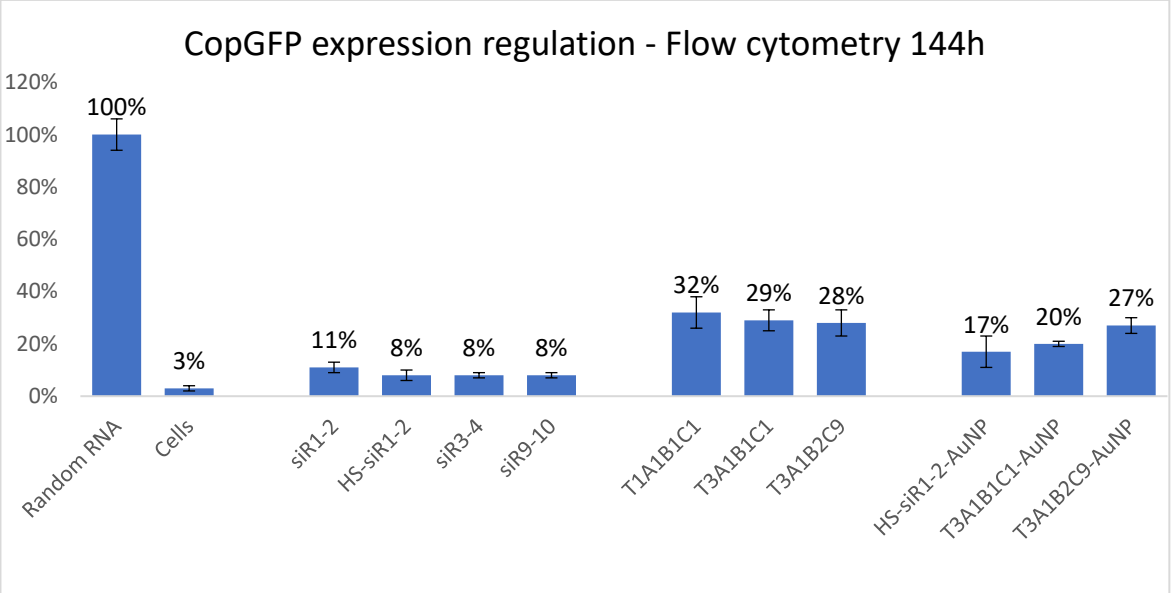

Figure 48. CopGFP gene expression regulation with regulatory RNA and RNA-AuNP conjugates, flow cytometry results. Figure represents mean values from 3 separate experiments, error bars refer to standard error.

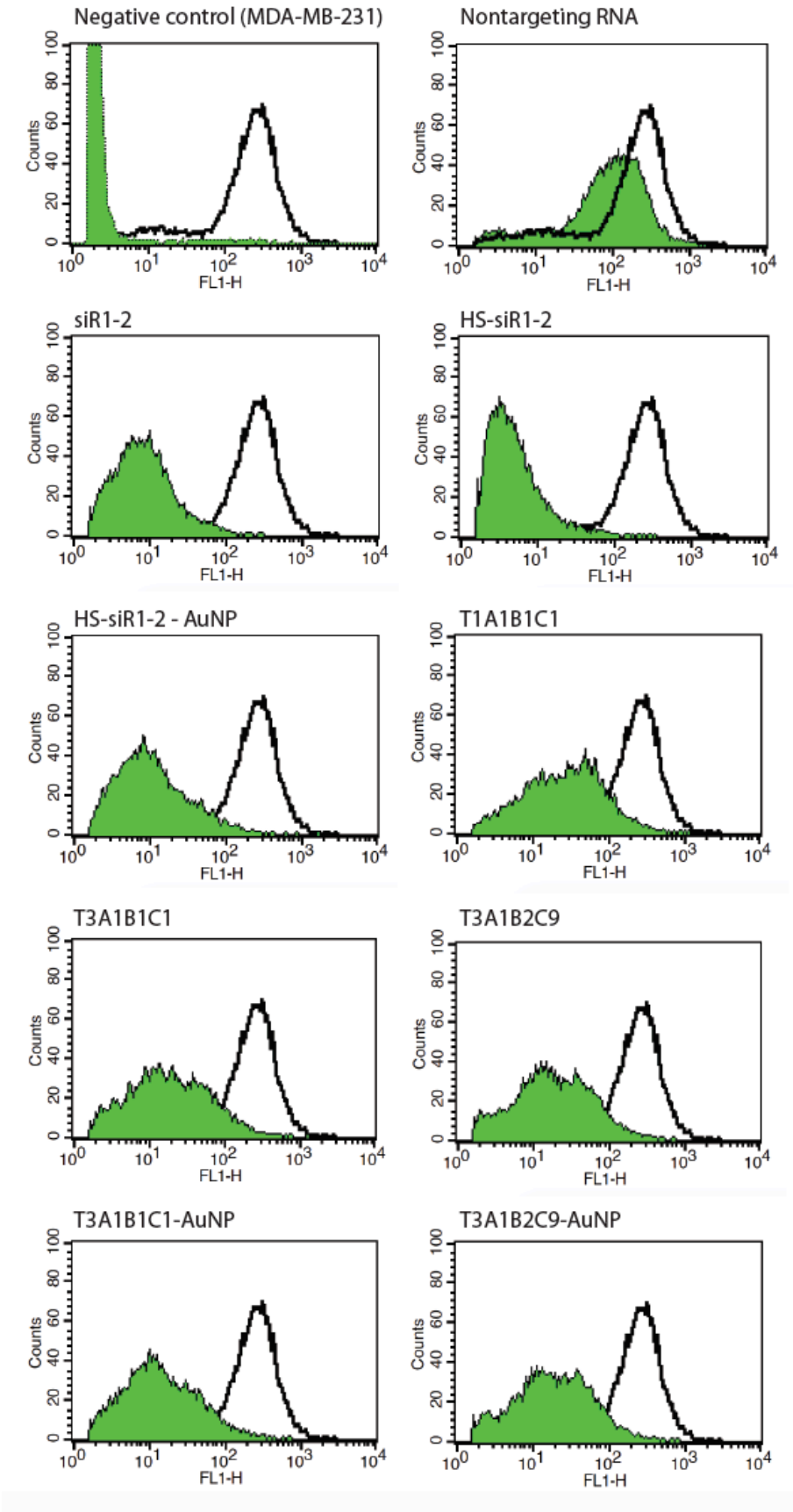

Figure 49. CopGFP gene expression regulation with RNA and RNA-AuNP conjugates, flow cytometry generated graphs overlaid with untreated control (100% fluorescence) marked with black line.

Results collected with both methods line up and allow to conclude that the new system based on structural RNA and AuNP is functional and leads to significant decrease in GFP fluorescence. While plate reader-based assay is a simpler method, the flow cytometry analysis allows to collect data only from restricted population of cells from the sample. In this setup, the sorting was focused on the healthy cells with minimal granularity, excluding potentially apoptotic or dead cells. With that in mind the observed results, presenting up to 80% decrease in GFP fluorescence, holds a great promise for applicability of trimer-AuNP design.

CopGFP expression regulation – fluorescence microscopy imaging

Cells treated with selected siRNA, trimers and their AuNP complexes were observed under the fluorescence microscope in order to get the full picture of the cells' morphology together with the GFP signal. Pictures were captured 144h post transfection (Figures 50-51) and comply with results obtained with plate reader and flow cytometry. A significant decrease of GFP fluorescence is visible for all transfected cells when compared to the controls. From the fluorescence images it can be deduced that the GFP fluorescence decrease after treatment with the trimer-AuNP conjugate (especially T3A1B2C9-AuNP) is at the similar level to the result obtained in cells treated with equal number of regulatory siRNAs. This shows that even though the structural RNA requires more time to be processed it still remains stable enough to regulate gene expression at the same level as similar siRNA, which requires much less processing post transfection. The obtained images comply with plate reader and flow cytometry results.

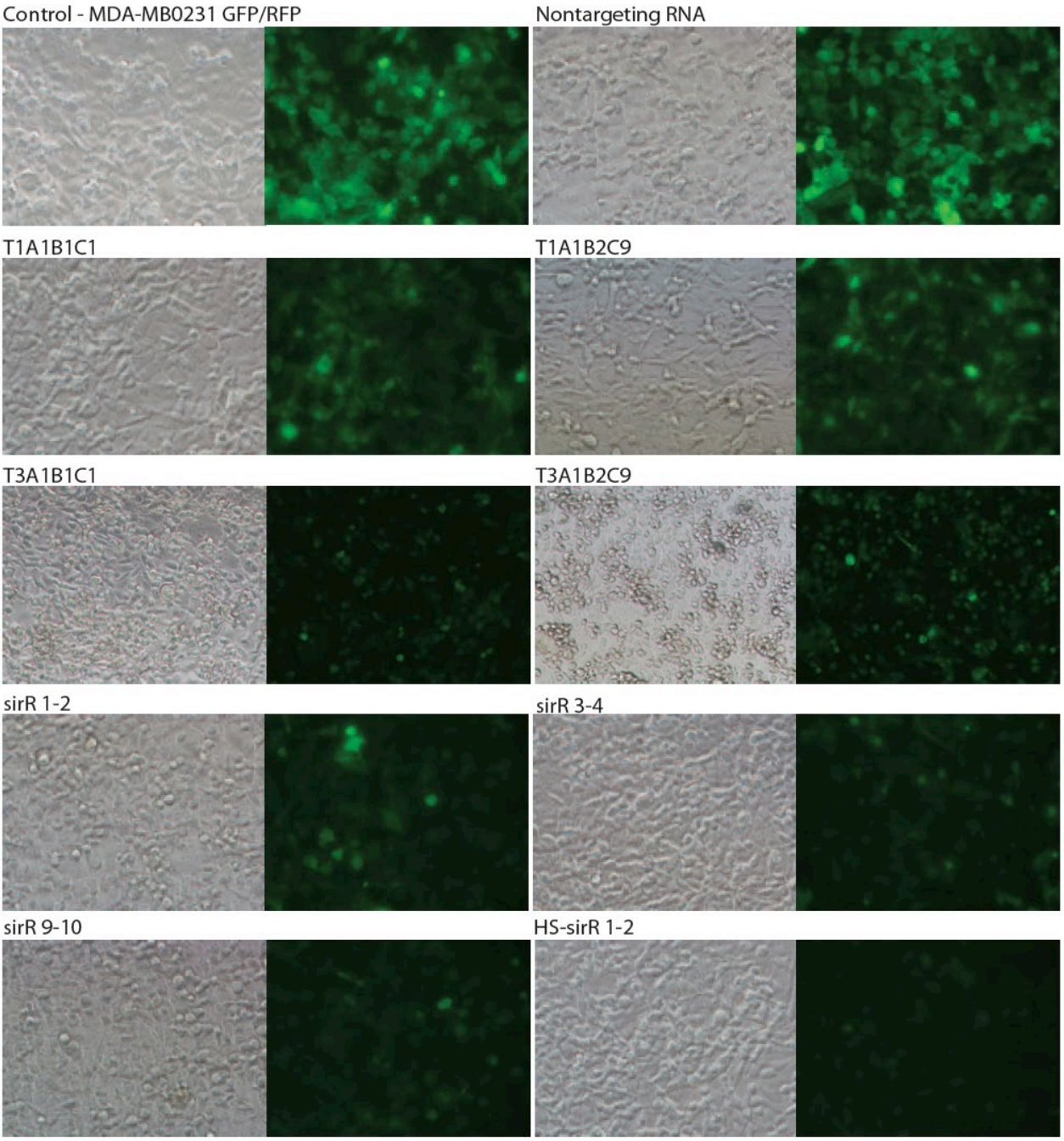

Figure 50. MDA-MB-231 GFP/RFP cells treated with regulatory RNA. The concentration of regulatory sequences is the same in each sample

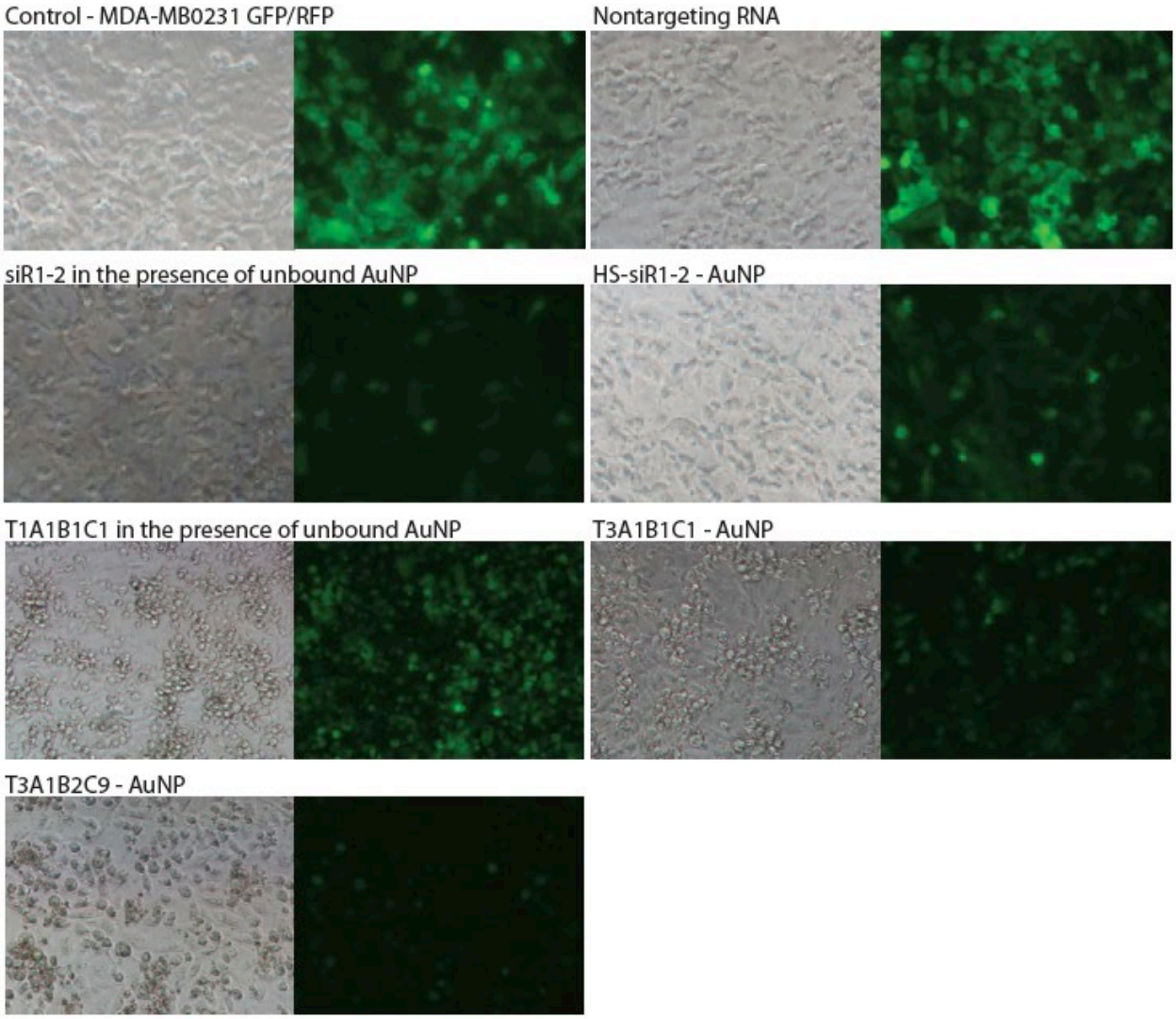

Figure 51. MDA-MB-231 cells treated with regulatory RNA-AuNP conjugates. The concentration of regulatory sequences is the same in each sample

Summary

In the presented study the new conjugate composed of tectoRNA trimer and the gold nanoparticle was designed, synthesized and investigated in human breast cancer cell model as a tool for gene expression regulation. The thiol modified RNA trimer was obtained by introducing a synthetic complementary RNA fragment bearing a thiol group at an aliphatic linker of the 5′ terminus of the monomer. The remaining RNA fragments were synthesized enzymatically by *in vitro* transcription with T7 RNA polymerase and were used to build a trimer. The RNA trimer was assembled by a one pot association protocol and evaluated electrophoretically. The trimer bears three regulatory fragments with sequences identical to previously selected siRNAs targeting CopGFP gene expressed in the model cell line. Presented methodology to use HS-RNA is a promising approach to modify larger RNA oligonucleotides that can only be produced enzymatically without the necessity of post-transcriptional modifications. In the following step the cytotoxicity of gold, platinum and silver nanoparticles was assayed in mammalian cell lines in order to select the non-toxic variant for conjugation with RNA. The 10nm AuNP was selected and used in subsequent studies. To make the RNA-AuNP conjugates, the thiol modified RNA (HS-RNA) and AuNP were incubated in the increasing salt concentration. The protocol was optimized for both, HS-siRNA and HS-trimer and the optimal RNA:AuNP composition was chosen based upon electrophoretic studies.

The effectivity of the regulatory RNA and their conjugates was tested by fluorescence methods: microscopy, plate reader and flow cytometry. As a result, up to 80% decrease of GFP fluorescence was observed after treatment with RNA-AuNP conjugates. The regulatory RNA trimers conjugated with AuNP regulate the CopGFP as well as the directly delivered, unconjugated siRNA, which shows that these constructs are stable for extended time (144h) and are processed inside the cells to induce regulatory effect. Moreover, the use of a trimer allows to introduce three or more different regulatory sequences, that are equally distributed in the nanoparticle which is important from the multi target therapeutic applications.

Materials and methods

Buffers used for the experiments

10x TB (50 mM TRIS, 50 mM boric acid)

The 54g of TRIS (Trizma base, Sigma) and 27.9g of boric acid were weighted and dissolved in milliQ water to a final volume of 500mL. Solution was filtered through 0.22µm filter and stored in the room temperature.

10x TBE (50 mM TRIS, 50 mM boric acid, 10mM EDTA)

The 54g of TRIS (Trizma base, Sigma) and 27.9g of boric acid were weighted and dissolved in milliQ water. The 10mL of 0.5M EDTA solution was added and solution was topped with milliQ water to a final volume of 500mL. Buffer was filtered through 0.22µm filter and stored in the room temperature.

10x citrate buffer, pH=6

To make 50mL citrate buffer (pH=6), 1.051g of citric acid monohydrate was mixed with 1.204g of sodium citrate dihydrate and topped with milliQ water to make 50mL. Buffer was filtered through 0.22µm syringe filter.

0.5M EDTA

The 95g of $Na_2EDTAx2\ H_2O$ (Sigma) was mixed with 400mL of milliQ water. pH was then adjusted to ~8.0 by addition of approximately 5g of NaOH pellets and the buffer was topped with milliQ water to make a final volume of 500mL. Solution was filtered through 0.22µm filter and stored in the room temperature.

8M Urea

To make 8M urea, 240g of urea (Sigma) was dissolved in water at a final volume of 500mL. Solution was filtered through 0.22µm filter and stored in the room temperature.

10% acrylamide: bis-acrylamide 19:1

Acrylamide solution was prepared by mixing 95g of acrylamide (Serva) and 5g of bis-acrylamide (Serva) in milliQ water at a final volume of 500mL. Solution was filtered through 0.22µm filter and stored in the fridge.

10% acrylamide: bis-acrylamide 19:1 in 8M urea

Acrylamide solution was prepared by mixing 95g of acrylamide (Serva), 5g of bis-acrylamide (Serva) and 240g of urea (Sigma) in milliQ water at a final volume of 500mL. Solution was filtered through 0.22µm filter and stored in the fridge.

Stains all dye solution – 100mL

Stains all dying solution was prepared by mixing 5mL of 1mg/mL stains-all (Sigma), 10% of formamide (Sigma), 25% of isopropanol (Stanlab), 1x TB or TBE and 50mL of milliQ water.

Cell lysis buffer – 20% SDS/50% DMF

Lysis buffer was prepared by mixing 100g of SDS (Sigma) with water and 250mL of DMF (Sigma) on the heat block at ~70°C. pH was adjusted to 4.7 with HCl and the solution was topped with milliQ water to a final volume of 500mL.

Gel loading buffer

Dye solution was prepared by mixing 200µL of 2.5% bromophenol blue, 200µL of xylene cyanol, 5mL of 10x TB and 2.5mL of 100% glycerol. Solution was adjusted with milliQ water to a final volume of 10mL.

UREA/EDTA loading buffer

The buffer was prepared by mixing 800µL of 0.5M EDTA and 9.2mL of 8M urea.

Polymerase Chain Reaction - DNA amplification

Two different PCR protocols were used in this project, which is due to the use of 2 different polymerases optimal for amplified templates. The G1 DNA sequences were amplified with the PCR mix (A&A Biotechnology) while the G3 DNA sequences were amplified with FIREPol DNA Polymerase (Solis Biodyne).

The DNA templates and primers for the G1 constructs were designed and synthesized in the Centre of Molecular and Macromolecular Studies, Polish Academy of Sciences. The T7 promoter sequence was introduced to a dsDNA templates in the forward primer followed by the sense siRNA sequence while the reverse primers carried the siRNA antisense strand. DNA template strand was universal for each monomer. The primers and templates used to make G1 PCR products are listed below and the sequences may be found in the appendix A.

Table 1 DNA primers and templates used for amplification

DNA template	*Primer.fwd*	*Primer. rev*	*PCR product*
CopA.tmp	siCop1	siCop1	CopA1
DJ_CopB.tmp	siCop1	siCop1C	CopB1
DJ_CopB.tmp	siCop2	siCop2	CopB2
CopC.tmp	siCop1	siCop1	CopC1
CopC.tmp	siCop9	siCop9	CopC9

Samples for PCR reactions were prepared in 100μL volume. The DNA template (final concentration 2nM) and primers (final concentration 1μM) were mixed with PCR water (provided with the polymerase) at a final volume of 50μL and topped with 50μL of 2x PCR Plus mixture solution (A&A Biotechnology). PCR solutions were mixed, spun down and the PCR program was run in the Mastercycler nexus (Eppendorf). The PCR program starts with 1min denaturation step at 94°C, then first 5 cycles are performed with 1min 30s denaturation at 94°C, 2min annealing at 54°C and 2min extension at 72°C and this is followed by second step with 30 cycles with 1min 30s denaturation at 94°C, 2min annealing at 62°C and 2min extension at 72°C; at the end of the PCR protocol, samples undergo a final denaturation step for 2min at 94°C and final extension for 20min at 72°C. After the PCR, samples were held at 4°C, prior to purification.

PCR products were purified with the Qiagen MinElute PCR purification kit, following the manufacturer's protocol and evaluated electrophoretically on 1.5% agarose gel with ethidium bromide (EtBr).

Agarose gel preparation:
The agarose gel was prepared by heat dissolving 1.5g of Agarose (Sigma) in 100mL of 0.5x TBE buffer. Agarose solution was supplemented with 10μL of 1% EtBr, poured into the gel cast with appropriate comb installed.
Alternative PCR protocol was used to make G3 DNA matrices. The DNA templates and primers were synthesized commercially (Genomed). The T7 promoter sequence was introduced to a dsDNA template on the forward primer, while the reverse primers carried the siRNA antisense strand. DNA template strand was universal for each monomer. The primers and templates used to make G3 PCR products are listed below and the sequences may be found in the appendix A.

Table 2 DNA primers and templates used for amplification

DNA template	*Primer.fwd*	*Primer. rev*	*PCR product*
CopA_Core.tmp	CopAcore	CopA1	CoreA1
CopA_Core.tmp	CopAcore	CopA7	CoreA7
CopA_Core.tmp	CopAcore	CopA9	CoreA9

Each PCR was prepared in 100µL total volume. At first, appropriate volume of water was added to the tubes, and mixed with 10µL of 10x polymerase buffer B (0.8 M Tris-HCl, 0.2 M $(NH_4)_2SO_4$, 0.2% w/v Tween-20; used at 1x final concentration), 8µL of 25mM $MgCl_2$ (2mM final concentration), 1µL 20mM dNTPs mix (0.2mM final concentration), 1µL of 0.4µM DNA template (4nM final concentration) and 0.5µL of 100µM primers forward and reverse (0.5µM final concentration of each primer). At the end, the 0.6µL of 5U/µL FIREPol DNA Polymerase was added to a final concentration of 0.03U/µL. All components were then mixed by vortexing, spun down and the PCR program was run in Mastercycler nexus (Eppendorf). All reagents used for the PCR, except from DNA sequences, were supplied with the polymerase kit (Solis Biodyne).

The PCR program starts with 1min initial denaturation step at 94°C, then first 5 cycles are performed with 1min 30s denaturation at 94°C, 2min annealing at 54°C and 2min extension at 72°C and this is followed by second step with 30 cycles of: 1min 30s denaturation at 94°C, 2min annealing at 62°C and 2min extension at 72°C; at the end of the PCR protocol, samples undergo a final denaturation step for 2min at 94°C and final extension for 20min at 72°C. After that, PCR samples are kept at 4°C, prior to purification.

PCR products were purified with the Qiagen MinElute PCR purification kit, following the manufacturer's protocol and evaluated on 1.5% agarose gel (same as above).

In vitro transcription

In vitro transcription with T7 RNA polymerase was performed to obtain long RNA fragments (94-120nt) from amplified dsDNA templates. Short RNA fragments (21-26nt) were synthesized by phosphoramidite method at the Bioorganic Chemistry Department, Centre of Molecular and Macromolecular Studies, Polish Academy of Sciences.

Each transcription reaction was prepared in the 300µL total volume. To make the transcription mix, sterile milliQ water was mixed with 30µL of 25mM NTP mix (2.5mM final concentration), 30µL of 10x T7 Buffer (1x final concentration) and 50µL of the PCR product (15-30µg DNA). At the end, 9µL of 50U/µL T7 RNA polymerase was added to a final concentration of 1.5U/µL. All reagents used for

the transcription were supplied from Lucigen. Reagents were mixed, vortexed, spun down and the transcription was performed for 4h at 37°C, with constant shaking - 450 rpm at the thermomixer.
After 3h of reaction, a 4µL aliquot from each transcription reaction was mixed with 1µL of 5x loading dye and analyzed on the 1.5% agarose gel for 1h at 90V to confirm whether transcription was successful.

10% denaturing PAGE preparation

The denaturing PAGE was prepared fresh before the electrophoresis. For RNA purification the thick gel was prepared (22mm by 16.5mm glass plates with 1.5mm spacers, 80mL solution) while for analytic purposes the thin gel was used (22mm by 16.5mm glass plates with 1mm spacers, 50mL solution). Prior to gel preparation, the gel cast was cleaned with 70% ethanol and assembled with appropriate spacers. For the RNA extraction gel, the thick 10% denaturing polyacrylamide gel (PAGE) solution was prepared fresh by mixing: 40mL of 20% acrylamide/bisacrylamide (19:1) in 8 M urea, 32mL of 8M urea (7.2M final concentration) and 8mL of 10x TBE buffer (final composition of 1x buffer: 50mM TRIS, 50mM boric acid, 1 mM EDTA). The 10mL from the gel solution was taken to prepare a gel stopper; 100µL of 10% ammonium persulfate solution (APS) and 20µL TEMED were added prior to applying the solution at the bottom of the cast. The 400µL APS and 40µL TEMED were added to the remaining 70mL of the gel mix and used to fill the rest of a cast. The 10-well comb was mounted and the gel was left to polymerize at the room temperature. Ready gel was mounted in the apparatus, with 1x TBE buffer in the top and bottom chambers. The protocol is identical for analytical gel preparation.

RNA purification

RNA products were purified by extraction from the polyacrylamide gel. After the transcription, 300µL samples were mixed with 150µL of buffer (0.5M EDTA/8M Urea), heated to 90°C for 3min, cooled down at the room temperature and applied on the freshly prepared 10% denaturing polyacrylamide gel (10% acrylamide/bisacrylamide (19:1), 8 M urea, 1x TBE). The electrophoresis was run for 2.5h at room temperature at 300V, 12 A (Labnet Power Station 300V).

RNA extraction from the gel:

After electrophoresis, the gel was carefully taken out of the cast and wrapped in the transparent foil. Gel was observed under the short UV light (254 nm) and selected RNA bands were cut out from the gel and placed in Eppendorf tubes with 600µL of "Crush and Soak" buffer (200mM NaCl, 10mM Tris, pH 7.5, 0.5mM NaEDTA). Gel samples were incubated overnight at 8°C with constant mixing 450 rpm.

RNA precipitation on ice:

The eluent from the overnight incubation was separated from the acrylamide gel pieces and gently mixed with 900µL of 100% ice cold ethanol and incubated in a freezer (-20°C) for minimum of 2h.

Washing:

Samples from the freezer were centrifuged for 20 min, 12000 rpm at 4°C and the liquid was removed leaving the precipitant at the bottom. Subsequently 600µL of 70% ethanol was added (without shaking) and samples were centrifuged for 10 min, 12000rpm at 4°C. Liquid was removed carefully and samples were dried in the vacuum concentrator (Eppendorf), then resuspended in 60µL of 1x TE buffer (pH 7.5 buffer (IDT Technologies)). The RNA concentration was measured with NanoDrop spectrophotometer (ThermoScientific). The molar extinction coefficients values were obtained with IDT oligoanalyzer tools (Integrated DNA Technologies) and used to calculate molar concentration of RNA according to the Beer's law.

RNA size confirmation and purity check with denaturing PAGE

This analysis was performed in order to check the quality and purity of transcribed RNA fragments. To prepare samples for analysis, stock solutions of monomers were diluted with water to obtain 20pmol of each monomer. Samples were mixed 1:1 with 0.5M EDTA/8M Urea buffer and heated at 90°C for 3min and cooled down at the room temperature. Samples were applied on the 10% denaturing PAGE (10% acrylamide/bisacrylamide (19:1), 8 M urea, 1x TBE). The gel was run for 3h at the room temperature, 300V (Labnet Power Station 300V) and stained overnight in the stains-all solution (Stains-all 50µg/mL (Sigma-Aldrich), 10% formamide, 25% isopropanol, 50mM TRIS, 50mM boric acid).

RNA association

RNA association study with agarose gel electrophoresis

For this experiment a T3A7B1C1 trimer was associated from equimolar amounts of G3A7 (HS-siR-5 + CoreA7), G1B1 and G1C1 varying Mg^{2+} concentrations, namely: 0.2mM, 1mM and 2mM of added $MgCl_2$. Two sets of these samples were prepared to associate RNA with one-pot protocol or a stepwise protocol.

The one-pot protocol was performed by mixing equimolar amounts (20pmoles) of each RNA fragment to assemble trimer. The samples were mixed and heated to 90°C for 3min and cooled down to 4°C. At the 4°C, each sample was supplemented with 0.2mM, 1mM or 2mM of $MgCl_2$ in 1xTE buffer and incubated by temperature ramping from 55°C to 22°C for 30min.

The stepwise protocol started from G3 monomer association. To do this, 3 samples were prepared, each containing 20pmoles of HS-siR5 and 20pmoles of CoreA7. Samples were mixed and incubated at 90°C for 3min, cooled down to 4°C and each sample was supplemented with either 0.2mM, 1mM or 2mM of $MgCl_2$ in 1x TE buffer, then incubated by temperature ramping from 55°C to 22°C for 30min. After the monomer association each of the 3 samples was supplemented with 20pmoles of separately pre-denatured (90°C, 3min) G1B1 and G1C1. Samples were mixed, spun down and incubated for 30min at 30°C.

Associated RNA constructs were analyzed on the nondenaturing 1.5% agarose gel (EtBr) in 0.5xTE buffer with 0.2mM Mg^{2+}.

RNA association studies with the nondenaturing (native) PAGE

Preparation of the nondenaturing (native) PAGE

The gel was prepared a day before and kept in the cold room (4°C) overnight. Prior to gel preparation the gel cast was cleaned with 70% ethanol and assembled with 1mm spacers. The 50mL of 10% native PAGE solution was prepared by mixing 25mL of 20% acrylamide/bisacrylamide (19:1) (10% final concentration), 20mL of water and 5mL of 10x TB buffer (final composition of 1x buffer: 50mM TRIS, 50mM boric acid). The solution was supplemented with 10µL of 1M $MgCl_2$ (0.2mM final concentration). The 10mL from the gel mix was taken to prepare a gel stopper; 100µL 10% ammonium persulfate solution (APS) and 20µL TEMED were added prior to applying the solution at the bottom of the cast. The 200µL of APS and 30µL of TEMED was added to the remaining 40mL of the gel mix and used to fill the rest of a cast. The comb was mounted and gel was left to polymerize at the room

temperature. Ready gel was mounted in the apparatus, with 1xTB buffer (with 0.2mM Mg^{2+}) left overnight at 4°C.

The siRNA association – electrophoretic mobility shift assay

Short RNA fragments were synthesized chemically from phosphoramidites at the Centre of Molecular and Macromolecular Studies, Polish Academy of Sciences. Oligonucleotides were purified chromatographically, dried and resuspended in 1xTE buffer (pH 7.5). Stock solutions of ssRNA were diluted and measured with NanoDrop spectrophotometer (ThermoScientific). Obtained OD values were used to calculate molar concentrations from molar extinction coefficients (IDT oligoanalyzer) according to the Beer's law. For the gel studies 50pmoles of dsRNA (siRNA) were prepared by mixing 50pmol of 2 appropriate monomers in sterile, filtered milliQ water (sequences and siRNA compositions may be found on the appendix). For example, to make 50pmoles of siR5-6, 50pmoles of siR5 was mixed with 50pmoles of siR6 and filled with water to make 30µL final volume.

To associate siRNA duplexes, prepared samples were heated to 90°C for 3min and cooled down to 4°C. Cool samples were then mixed with 5x loading buffer (final concentrations: 1xTE, 5% glycerol, 0.01% bromophenol, 0.01% xylene cyanol) and loaded on the 10% native polyacrylamide gel. The gel was run in the cold room (4°C), for 3h at 250V, 8 A (Labnet Power Station, 300V) and stained overnight in the stains-all solution (Stains-all 50µg/mL (Sigma-Aldrich), 10% formamide, 25% isopropanol, 50mM TRIS, 50mM boric acid).

T3 Trimer association - electrophoretic mobility shift assay

In this study RNA monomers, dimers and trimers were analyzed on the 10% native PAGE. Each RNA construct was prepared from frozen stocks of synthetic ssRNA and/or long RNA transcription products. Each sample contained total of 50pmol of RNA in water, regardless of its composition.

For example, to make a T3A7B1C1 trimer, 12.5pmoles of CoreA7, 12.5pmoles of siR-5, 12.5pmoles of G1B1 and 12.5pmoles of G1C1 were mixed in sterile water, giving a total 50pmoles of RNA in 25µL. To associate constructs, mixed samples were heat denatured at 90°C for 3min, cooled down to 4°C and supplemented with 5xTB/1mM $MgCl_2$ buffer (final concentration 0.2mM Mg^{2+} and 1xTB). Samples were then incubated by the temperature ramping, from 55°C to 22°C for 30min.

Associated constructs were mixed with 5xPAGE loading buffer (final concentrations: 1xTE, 5% glycerol, 0.01% bromophenol, 0.01% xylene cyanol) and

applied into the native PAGE (10% acrylamide/bisacrylamide (19:1), 1xTB, 0.2mM $MgCl_2$). The gel was run in the cold room (4°C), for 7h at 200V (Labnet Power Station, 300V) and stained overnight in the stains-all solution (Stains-all 50µg/mL (Sigma-Aldrich), 10% formamide, 25% isopropanol, 50mM TRIS, 50mM boric acid).

RNA-AuNP conjugates

Preparation of siRNA-AuNP conjugates

Titration of AuNP with siRNA to determine best siRNA-AuNP ratio

The RNA titration study was performed in order to select the best ratio of siRNA to 10nm AuNP, which will allow for saturation of the nanoparticle. For the hybridization study the following siRNA:AuNP mixes were prepared: 50:1, 40:1, 30:1, 20:1, 10:1 and 5:1pmol.

The siRNAs are composed of 2 strands: 1) 21nt long sense strand equipped with HS group and a C18 aliphatic linker at the 5' end and 2) 21nt long antisense strand (the exact sequences may be found in the appendix). In the AuNP titration experiment the HS-siR5-6 sequence was used as a model.
To prepare siRNAs for the experiment the appropriate picomolar amounts (5, 10, 20, 30, 40 or 50pmol) of HS-siR5-6 were prepared by mixing 2 complementary single stranded RNAs and water at a final volume of 25µL.
For example, to make 40pmoles of HS-siR5-6 40pmoles of siR5 or HS-siR5 were mixed with 40pmoles of siR6 and filled up with water to a final volume of 25µL.
Strands were associated by heating to 90°C for 3min and cooling down on ice.

AuNP mix preparation:

An AuNP master mix was prepared from the 10nm AuNP stock (Sigma-Aldrich). One portion of AuNP mix (equivalent of 1pmol of RNA), was prepared by mixing: 100µL of 60µg/mL 10nm AuNP, 20µL of 10x Citrate buffer pH=6 (1x final concentration), 6µL of 5M NaCl (150mM final concentration), 4µL of 10% Tween-20 (Sigma-Aldrich, 0.2% final concentration) and 37µL of sterile water. The 167µL from the AuNP mix was added to each 25µL of assembled HS-siRNA. Samples were mixed by vortexing, spun down and incubated at 30°C for 4h with constant shaking - 300rpm. After 4h samples were supplemented with 8µL of NaCl to a final concentration of 350mM NaCl and further incubated overnight.

The following day, samples were spun down at 13000rpm for 20min at 4°C and supernatant was removed, replaced with fresh 1xPBS and spun at 13000rpm for 20min again to wash out the unbound RNA and salt. Samples were washed 3 times and kept in 1xPBS at a desired volume. The hybridization protocol was adapted from [332]. Samples were analyzed with 1.5% agarose gel electrophoresis with EtBr for 1.5h at 80V.

siRNA-AuNP conjugation

All the further experiments were carried using 40:1pmol RNA-AuNP conjugate, prepared following the protocol above.

Preparation of tectoRNA-AuNP conjugates

AuNP titration with RNA trimer

Similar to the siRNA titration study, the titration study was performed to choose the amount of trimer, which will allow for saturation of the 10nm AuNP. For the hybridization study the following tectoRNA:AuNP mixes were prepared: 50:1, 40:1, 30:1, 20:1, 10:1 and 5:1pmol

The T3A7B1C1 trimer was used as a model in this study and prepared by mixing HS-siR5, CoreA7, G1B1 and G1C1 to obtain 5, 10, 20, 30, 40 or 50pmoles of trimer in 20μL of water. For example, to make 40 pmoles of T3A7B1C1 40 pmoles of HS-siR5, CoreA7, G1B1 and G1C1 were mixed with and filled up with water to make 20μL solution.

To associate trimers, the samples were heat denatured at 90°C for 3min, cooled down to 4°C and supplemented with 5μL of 5x $MgCl_2$/TB buffer (0.2mM Mg^{2+}, 1xTB final concentration) to make a final volume of 25μL. Samples were then incubated by the temperature ramping, from 55°C to 22°C for 30min. Prepared RNA aliquots were supplemented with 167μL of AuNP mix, vortexed, spun down and incubated following the protocol above (Preparation of siRNA-AuNP conjugates). Samples were analyzed with 1.5% agarose gel electrophoresis with EtBr for 2h at 80V.

RNA-AuNP conjugates preparation for cell transfection experiments

RNA-AuNP conjugates were hybridized at 40:1pmol RNA:AuNP ratio as described previously, washed with PBS three times and diluted to 1.25μM of RNA construct. The concentration was calculated assuming that the amount of RNA construct

added to AuNP does not change and that the loss of RNA at the hybridization and washing steps is neglectable.

Agarose gel studies for complex formation determination

For the agarose gel studies the siRNA-AuNP or tectoRNA-AuNP samples were spun down once, at 13000rpm for 30min at 4°C, to collect the AuNP-containing fraction. The supernatant was removed, leaving 40µL of the bottom fraction, which was mixed with 5x gel loading buffer (TB 1x, 5% glycerol final) and applied on the 1.5% agarose gel.

Agarose gel:

The 1.5% agarose gel was prepared by heat dissolving 3g of agarose (Sigma-Aldrich) in 200mL of 0.5x TBE buffer; 10µL of 1% ethidium bromide was added prior to pouring gel solution into the cast. 15-well comb was inserted into the gel solution and left in the room temperature to solidify.

Samples were loaded on the gel and the electrophoresis was run in the 0.5x TBE buffer at 80V for 1.5h. 20pmol siRNA was used as a reference. The gels were visualized under the UV light in the gel imaging device (UVTex, FireReader V10) to show mobility of the RNA fraction; the mobility of gold fractions conjugated with RNA is visible in the ambient light.

Bioanalysis of RNA samples

A fresh short RNA chip (Agilent) was unpacked and mounted into the provided loading station with a syringe. The analytic gel solution was prepared by mixing it with a dye, centrifugation and incubation in the room temperature. The gel solution was then loaded onto the chip according to the enclosed instruction. Each well was then supplemented with a dye and the preincubated DNA ladder was applied to the reference well. At the end, 1µL of the prepared test samples were applied to the wells. The chip was mixed by vortexing for 1min and placed into the pre-cleaned bioanalyzer. The chip specific bioanalysis program was run and results analyzed.

siRNA-AuNP conjugate treatment with GSH/BME

The siRNA-AuNP conjugates were treated with GSH or BME and examined with bioanalyzer. A set of siRNA-AuNP samples were prepared from HS-siR5-6 and

10nm AuNP, at the 40:1pmol ratio, as previously described. Ready conjugates were treated with GSH or BME (100mM stock solutions) added at a final concentration of 1, 5, 10mM in 40µL. Samples were incubated for 2, 4 or 24 hours at 37°C. The 1µM HS-siR5-6 and 1µM untreated conjugate solutions were used as references with water added instead. Each sample was incubated under the 3µL layer of mineral oil to prevent oxidation of thiols. In order to assure the best analytical conditions of bioanalysis, all tested solutions were prepared in the minimal possible salt concentration: SNA were washed with 0.05x PBS and GSH and BME were prepared in water. After incubation, samples were separated from the immersion oil by short spin and pipetting out the bottom fraction which was used for bioanalysis.

RNA cleavage study with Dicer

Monomer G1A1, trimer T1A1B1C1 and T3A7B1C1 were prepared following previously described protocol at a final concentration of 10µM. The 1uL from RNA samples was saved for bioanalysis and diluted 1:1 with water to make controls. For the enzymatic digestion study, the RNA samples were treated with Recombinant Turbo Dicer. All reagents were supplied with the Recombinant Turbo Dicer kit (Genlantis). Each experiment was prepared by mixing 6µL od 10µM RNA, 2µL of 50mM $MgCl_2$, 5x Turbo Dicer Reaction Buffer, 1µL of 10mM ATP, 1µL of 5x BSA and 1µL of 0.5U/µL Recombinant Turbo Dicer Enzyme. The final reaction volume was 12µL. Enzymatic reaction was performed for 2h 20min at 37°C, then was stopped by addition of 2µL of Turbo Dicer Stop Solution. Samples were analyzed with bioanalyzer (Agilent, RNA small chip). The 1µL of each experiment was applied on the chip and untreated RNA samples were used as controls.

Dynamic light scattering study

siRNA-AuNPs and tectoRNA-AuNPs were prepared as described previously. In this case for the experimental purposes, the higher concentration of conjugates was needed for dynamic light scattering (DLS) and 200pmoles of siRNA or tectoRNA were mixed with 5pmoles of AuNP (500µL of 60µg/µL citrate solution). Conjugates were washed twice and suspended in 1mL of 1x citrate buffer, pH=6. Such solution was then applied to the transparent cell and used for size and zeta potential measurement with DLS technique (Malvern). Samples were all analyzed at the

room temperature, with the same protocol and 170.8-255.1kcps (kilo counts per second) were collected for each analysis.

Cellular studies

Eukaryotic cell lines

Four cell lines were used in the project, including 3 adherent cell lines and one suspension cell line.

MDA-MB-231 GFP/RFP – adherent cell line

The human breast cancer cell line MDA-MB-231 and MDA-MB-231 GFP/RFP originate from M. D. Anderson Cancer Center, where the latter is a lentivirus modified line, stably expressing GFP and RFP (puromycin resistance). The MDA-MB-231 GFP/RFP (Cell Biolabs Inc) cells, stably expressing GFP and RFP was cultured in DMEM - high glucose (4.5g/L) medium (Dulbelcco's Modified Essential Medium, Gibco), enriched with 10% FBS (Biowest), 1% nonessential amino acids (Biowest) and 1% L-glutamine (Biowest). Two antibiotics were routinely added to media – 0.1mg/mL of penicillin and 100U/mL of streptomycin (Sigma Aldrich). The MDA-MB-231 cultures were incubated at the standard conditions and passaged when confluent (around 95% coverage) 2 times a week on average. The MDA-MB-231 GFP/RFP cell line was routinely observed under the fluorescent microscope (*Nikon Eclipse Ti-U microscope*) to check the GFP and RFP fluorescence.

Fibroblasts – adherent cell line

Human fibroblasts, CLTH human dermal foreskin fibroblasts (Celther) were cultured in DMEM - high glucose (4.5g/L) medium (Dulbelcco's Modified Essential Medium, Gibco), enriched with 10% FBS (Biowest), 1% nonessential amino acids (Biowest) and 1% L-glutamine (Biowest). Two antibiotics were routinely added to media – 0.1mg/mL of penicillin and 100U/mL of streptomycin (Sigma Aldrich). Fibroblasts were incubated at the standard conditions and passaged when confluent (around 95% coverage) once a week on average.

MCF-7 – adherent cell line

The human breast cancer cell line MCF-7 (Michigan Cancer Foundation-7 – name referring to the institute where the cell line was established, obtained from ATCC) was cultured in MEM (Eagle's Minimum Essential Medium, Gibco) medium

enriched with 10% FBS (Biowest), in the presence of two antibiotics – 0.1mg/mL of penicillin and 100U/mL of streptomycin (Sigma Aldrich). MCF-7 were incubated at the standard conditions and passaged when confluent (around 95% coverage) 2 times a week on average.

Molt-4 – suspension cell line

The T-lymphoblast cell line Molt-4 (ATCC), derived from leukemic cells of a patient with acute lymphoblastic leukaemia, was cultured in RPMI1620 medium (Gibco), enriched with 2g/L glucose (Biowest), 1mg/L glutathione (Biowest), 10% FBS (Biowest) and two antibiotics – 0.1mg/mL of penicillin and 100U/mL of streptomycin (Sigma Aldrich). Molt-4 cells were incubated at the standard conditions and passaged 2 times a week on average

Methods used for cell cultures handling

Cell cultures were kept in 25cm^2 flat bottom bottles (Nunc) in 10mL of appropriate medium at the standard conditions of 37°C with 5% CO_2 (LAB-LINE, Binder incubator).

Cell culture from frozen stock

The cell cultures were thawed from frozen stock (~10^6 cells frozen in the cultivation media with 10% dimethyl sulfoxide (DMSO)). Frozen stock was resuspended with the warm cultivation media and transferred to the falcon tube. Cell suspension was centrifuged at 900rpm for 3min at room temperature. The supernatant containing DMSO was removed, cells were resuspended in 5mL of cultivation medium and transferred to the 25cm^2 bottle. Cells were incubated at 37°C, 5% CO_2 and medium were replaced after 24h.

Cells passage

Adherent cells:

Adherent cell lines were passaged by removing the old media from above the cell monolayer and washing the monolayer with HBSS solution (without Ca^{2+} and Mg^{2+} ions, Biowest). Cells were detached from the bottom of the bottle by trypsin treatment with 300µL 10x trypsin EDTA (Biowest) for 2min at 37°C. Detachment progress was checked under the microscope and once cells detached, 5mL of the growth media was used to transfer cells to a falcon tube. Cells were collected by

centrifugation at 900rpm for 3min at the room temperature. The supernatant was removed and sedimented cells were resuspended in 5mL of warm cultivation medium. Depending upon desired cell concentration, appropriate amount was transferred to the new bottle/plate with fresh cultivation medium. The cells were incubated at 37°C with 5% CO_2.

Suspension cells – Molt-4

For subculturing the cell suspension was transferred from the bottle do 15mL falcon tube and centrifuged at 900rpm for 3min at the room temperature. The supernatant was removed and sedimented cells were resuspended in 5mL of cultivation medium. Depending upon desired cell concentration, appropriate amount was transferred to the new bottle/plate to with fresh cultivation medium. The cells were incubated at 37°C with 5% CO_2.

Counting cells for the experiment

Cells were counted with the automatic cell counter - Scepter cell counter (Scepter 2.0, Millipore) prior to seeding. The 200µL of cells resuspended in a fresh medium was transferred to a fresh Eppendorf tube and diluted 4-fold by adding 600µL of medium. A cell counter sensor (60µm) was attached to the counter and submerged in the prepared cell suspension. Counter aspirates around 50-60µL of the solution for analysis and, as a result, gives a histogram and averaged cell concentration in cell/mL units. The cell concentration given by the cell counter was multiplied by 4 to get the real concentration in the falcon tube.

Cells seeding

Counted cell suspension in a falcon tube was diluted with the appropriate medium to a desired cell concentration, mixed and placed in a sterile reservoir. The 100µL of the cell suspension was pipetted with a multichannel pipette into a selected plate. The cells were incubated at 37°C with 5% CO_2.

Cells freezing

Prepared cell suspension in a falcon tube that hasn't been used for experiments could be frozen for storage. Cells' suspensions of approximately 10^6 cells/mL were mixed with appropriate medium, supplemented with 10% DMSO and 1mL from the mix was poured into volume to cryogenic tubes (Nunc). Tubes were sealed with cups and transferred to a freezing container CoolCell (BioCision) allowing for

controlled freezing (-1°C /min). The container was placed in -80°C freezer and after 24h tubes were transferred to a Dewar's container with liquid nitrogen (Thermolyne Locator 4 plus, ThermoFisher Scientific) for long term storage.

Metal nanoparticles impact on cell viability

Selected cells were collected from cultivation bottles, counted with the Scepter cell counter and plated on transparent 96-well plates (Nunc), each in the amount of 7000 cells/well in 100µL of appropriate media. Cells were incubated for 24h at 37°C with 5% CO_2 prior to cytotoxicity experiments.

For the cytotoxicity studies spherical nanoparticles of 3 noble metals were selected, namely: gold nanoparticles (AuNP: 10, 50 and 100nm diameter, citrate water solutions), silver (AgNP 100nm – powder dissolved in water) and platinum (PtNP 50nm - powder dissolved in water). All nanoparticles were purchased from Sigma Aldrich. Cytotoxicity of selected nanoparticles was tested with the MTT assay in 4 cell lines: MDA-MB-231 GFP/RFP, Molt-4, MCF-7, human fibroblasts. Nanoparticles' concentrations, from 0 to 50µg/mL were analyzed. For this experiment nanoparticles stocks were diluted with the cultivation media containing 0.2% Tween-20 to make a final concentration of 0, 0.5, 1, 2.5, 5, 10, 20 or 50µg/mL of nanoparticles in a final volume of 200µL. The medium was removed by aspiration from the plate prepared a day before. The 200µL from the nanoparticle dilutions were added to the experimental wells at the 96-well plate. The prepared 96-well culture plates were incubated for 48h at 37°C with 5% CO_2 prior to the MTT assay.

MTT assay

The MTT assay was used to evaluate the metabolic activity of the tested cells by colorimetric change observation of the yellow tetrazolium dye 3-(4,5-dimethylthiazol-2-yl)-2,5-diphenyltetrazolium bromide (MTT) to its insoluble purple formazan salt as a consequence of NAD(P)H-dependent cellular oxidoreductase enzymes activity. The color change, indicative of the metabolic activity of the living and active cells, was measured on the plate reader at 570 nm, with a background reference measured at 650nm. Each cell line was tested at minimum of 10 repetitions in 2 or 3 consecutive passages.

To initiate the MTT assay 25µL of MTT (5mg/mL) was added to each well and incubated at 37°C with 5% CO_2 for 2h. Subsequently cells were lysed by incubation with 95µL of SDS lysis buffer per well (20% SDS, 50% DMF) for 2h with shaking. The absorbance of the cell lysates was measured at the FLUOstar Omega plate reader (BMG Labtech) at 570 with the reference at 650 nm.

Collected data was analyzed using the Microsoft Excel software. First the background absorbance at 650nm was subtracted from 570nm absorbance for each experiment. Average absorbance of the untreated cells was calculated and used as a 100% cell viability - reference for normalization. Repetitions within the same experiments were normalized to their control (100%) and then the normalized data from subsequent experiments for a given cell line was averaged together to prepare the diagrams. Error bars correspond to the standard error calculated from standard deviation divided by square root of sample size – N.

Gene expression regulation studies in GFP model system

Transfecting cells with selected RNA components

The RNA constructs were delivered to MDA-MB-231 GFP/RFP model cells to study the CopGFP gene expression regulation while the RFP gene was used as a reference. The study was performed for RNA-only substances: siRNA (duplexes), tectoRNA monomers, trimers and for RNA-AuNP conjugates. The RNA constructs were delivered to cells following one of 2 protocols: 1) single addition, where cells were transfected with RNA once, to a final concentration of 15nM siRNA (equal to 5nM trimer) or 2) triple addition, where cells were transfected with RNA sample 3 times (5nM siRNA or 5/3nM trimer each time), to get a final concentration of 15nM siRNA (equal to 5nM trimer). Each transfection mixture contained 3 parts: RNA construct, HBSS+ (with Mg2+ and Ca2+ ions, Life Technologies) and SAINT-sRNA (Synvolux).

The siRNA transfection was performed following a single addition or triple addition protocol. Random RNA fragment (nontargeting RNA fragment) was used as a transfection control.

MDA-MB-231 GFP/RFP cells' transfection in 96-well plate (plate reader):

Transfection mix preparation:

The transfection master mix was prepared for 4 to 5 repetitions of each experiment. RNA samples were associated following previously described protocol, at a final concentration of 1.25μM. To prepare a transfection mix, a 10-fold dilution of SAINT -sRNA in HBSS+ was prepared in a fresh Eppendorf tube. In the second step the associated RNA stock (1.25μM) was diluted appropriately in HBSS+, depending upon desired final concentration. The SAINT-sRNA solution was added 1:1 to each of the RNA solutions, mixed, incubated for 15min at the room temperature and used for transfection. For example, to prepare a transfection solution to deliver a final 5nM RNA to 200μL medium, in 5 repetitions, the following reagents are mixed: 1.4μL of 1.25μM RNA, 95.5μL of HBSS+ and 5.1μL of SAINT -sRNA (2% overhead accounting for pipetting error).

Cell delivery

For the single addition protocol, the MDA-MB-231 GFP/RFP cells were counted with the automatic cell counter (Scepter 2.0, Millipore) and 60μL sensor, then plated on a fluorescent 96-well plate (Nunc) at a concentration of 10000 cells/well, 24h prior to transfection. At the transfection day, the medium was removed from wells by aspiration and 20μL of a transfection mixture was added on top of the cell monolayer. Next, 80μL of warm HBSS+ (with Mg^{2+} and Ca^{2+} ions, Life Technologies) was added to the wells and incubated for 5h at 37°C with 5% CO_2. After 5h incubation, 100μL of warm cultivation medium was added to each well, the plate was returned to incubator and left for 72h. After 72h the GFP gene expression silencing was evaluated by GFP fluorescence measurement on the fluorescence plate reader (FLUOstar Omega, BMG Labtech).

In the triple addition protocol, the cells were counted and seeded 5000 cells/well and prepared in the same way as described above. At the first transfection day (t0), the cultivation medium was removed from wells by aspiration and 20μL of a fresh transfection mixture was added on top of the cell monolayer. Next 80μL of warm HBSS+ (with Mg^{2+} and Ca^{2+} ions, Life Technologies) was added to the wells and incubated for 5h in 37°C with 5% CO_2. After 5h incubation, 60μL of warm cultivation medium was added to each well and plate was returned to incubator. The next day, 24h after the 1st transfection (t1=24h), another 20μL of freshly prepared transfection mix was added to wells, without removing the medium and the plate was returned to the incubator. The following day, 48h after the 1st

transfection (t2=48h), another 20µL of freshly prepared transfection mix was added to wells, without removing the medium and the plate was returned to the incubator. At the 96h after the 1st transfection, 100µL of a fresh medium was added to all wells, without removal of the old medium. The plates were incubated for the total of 144h from the 1st transfection.

MDA-MB-231 cells' transfection in 48-well plate (flow cytometry experiments):

RNA preparation:

This experiment was scaled up, 3-fold from the 96-well plate experiment and prepared accordingly. For the transfection, RNA samples were mixed with SAINT-sRNA transfection agent in HBSS+ (with Mg^{2+} and Ca^{2+} ions, Life Technologies) and 60µL of mix was applied to cells, 3 times every 24h. For example, for 2 repetitions of one experiment: 4.9µL of 1.25µM RNA, 110.28µL of HBSS+ and 3.06µL of Saint-sRNA were mixed (2% overhead accounting for pipetting error) and incubated at the room temperature for 15min.

Cell delivery:

The experiment is scaled up from 96-well plate experiment by multiplying volumes and cells by the factor of 3, following thermofisher.com instructions. For the experiments, concentration of cells was measured with the cell counter (Scepter 2.0, Millipore) and 60µL sensor. The cells were plated on a 48-well plate (Greiner) 12000 cells/well, in 200µL of warm medium and cultivated at 37°C with 5% CO_2 for 24h prior to experiment. At the t0, old medium was removed and 60µL of the transfection solution was added per well, topped with 180µL of pre-warmed HBSS+ and incubated for 5h at 37°C with 5% CO_2. After 5h incubation, 240µL of pre-warmed cultivation medium was added to each well and plate was returned to the incubator. The next 2 days, 24h and 48h after the 1st transfection, another 60µL of freshly prepared transfection solution were added to wells, without removing the medium and the plate was returned to the incubator. The 96h after the 1st transfection, 300µL of a fresh medium was added to all wells, without removal of the old medium. The plates were incubated for the total of 144h from the 1st transfection.

After the fluorescence measurement selected transfection experiments were tested for the cytotoxicity by MTT assay.

GFP fluorescence assay with the plate reader

The efficiency of the CopGFP regulation was studied by the GFP fluorescence intensity measurement (ex: 485nm, em: 520nm) with the fluorescence plate reader (FLUOstar Omega, BMG Labtech). Cells were analyzed at different time points after transfection.

All calculations for the gene expression regulation studies were done in Microsoft Excel software. Normalization to cell viability was achieved by 1) subtracting the normalized GFP fluorescence from 100% to get a percent of fluorescence decrease (%F) for each well related to 100% - average of untreated cells fluorescence 2) the %F obtained for each well was then multiplied by the % value of normalized MTT results giving the final result – % GFP fluorescence decrease normalized to cell viability.

Fluorescence microscopy

Fluorescence microscopy was used for routine evaluation of MDA-MB-231 GFP/RFP cells' fluorescence and for observation of GFP fluorescence decay in the RNAi gene regulation experiments. GFP fluorescence was observed at the following microscope setup: excitation wavelength = 465–495nm, dichroic mirror wavelength = 505nm, absorption filter wavelength = 515–555nm, with exposition time >300ms. Images were recorded and analyzed using NisElement software. Equipment used: Nikon Eclipse Ti-U microscope with metal, halide lamp (Lumen 200, Prior Scientific), 10x magnification lens and 10x ocular lens.

Fluorescence Associated Cells Sorting – flow cytometry

The 48-well plate experiments were set up for the flow cytometry study. Prior to flow cytometry experiment medium was removed from wells and the cells were collected by trypsin treatment, where 100µL of 1x trypsin EDTA (Biowest) was added per each well and incubated for 2min at 37°C. Detached cells were resuspended in 1000µL of 1xPBS (without Mg^{2+} and Ca^{2+} ions, Sigma) and transferred to the 1.5 mL tubes. Cells were collected by centrifugation at 1500 rpm, 4°C for 10 min. Supernatant was removed and the cells were resuspended in 1000µL of 1xPBS and washed once more. Finally, cells were resuspended in 1000µL of 1xPBS and transferred to FACS tubes and kept on ice and in dark. The fluorescence-activated cell sorting measurements were run with FACSCalibur flow cytometer (BD Bioscience) collecting data from forward and side scatters and green and

yellow fluorescence. Each experiment was prepared in 2 repetitions and counted at least 2 times, collecting 10000 counts each. Three independent experiments were done. The gene regulation efficiency was inferred from the mean GFP fluorescence intensity (ex:485nm, em: 520nm) output from flow cytometry. Gathered fluorescence means were plotted in Excel software, normalized to cells treated with a random RNA and averaged within 3 independent experiments. Standard error was calculated for each sample.

Real time-RT-PCR

Selected cells from RNAi experiments were treated with TriPure reagent (Roche) for RNA isolation (following the manufacturer's instructions). Isolated RNA fraction was dissolved in 30μL of DEPEC water and RNA concentration was measured with the NanoDrop. All samples were brought to a final concentration of 100ng/μL. The 25ng of isolated RNA were applied to PCR strips and supplemented with 2.5mM of primers for CopGFP mRNA and appropriate amount of PCR-grade water to make a final reaction volume of 10μL. The reaction master mix was prepared by mixing SYBR Green, enzyme blend and magnesium solution. Master mix was mixed, spun down and added to each tube. PCR strips were covered, spun down and inserted to the real time RT-PCR machine (Roche LightCycler 96).

The following program was run: 55°C 10min → 95°C 30s → (95°C 10s - 60°C 10s - 72°C 10s)x20 → Melting curve (95°C 10s → 65°C 1min → 97°C temp. ramping) → 37°C hold.

RNA-AuNP delivery to cells – transmission electron microscopy

For the TEM analysis cells were prepared in 24-well plates and transfected once with 5nM of T3A1B2C9-AuNP accordingly to a single addition protocol. The 72h after transfection cells were fixed with 2.5% glutaraldehyde, 2% paraformaldehyde solution (provided by TEM facility) and incubated for 1h at 4°C. In the next step, cells were washed three times with 0.1M cacodylate buffer (provided by TEM facility) for 10min to remove fixative solution. Post fixation was handled at the TEM facility (Nencki Institute of Experimental Biology of Polish Academy of Sciences, Warsaw, Poland), where fixed samples were treated with 1% osmium tetroxide for 1h at the room temperature, washed three times with water for 10min and stained

with 2% uranyl acetate water solution. For dehydration samples were incubated in the increasing ethanol concentrations, then in pure propylene oxide. At the end, cells were embedded in the propylene oxide and Epon resin, then in pure Epon resin. The 70nm sections were collected on TEM copper grids. Samples were analyzed and electron micrographs were captured with Morada camera on a JEM 1400 transmission electron microscope at 80 kV (JEOL Co., Japan).

Appendix A

1. DNA sequences used in the project

name	**DNA used for PCR**	**Length [nt]**
CopA_core.tmp	CATCAACAAGAGGCGTGCAGGCTTCACCTCTTGTTGATTTGGGCACAGGGACTGC GTGCCTCCTTCACAGTCC	73
CopA_core.fwd	TTCTAATACGACTCACTATAGGACTGTGAAGGAGGCACGC	40
CopA1.rev	GGACAGCGTGATCTTCACCGACATCAACAAGAGGCGTGC	39
CopA7.rev	CGACAAGATCATCCGCAGCAA**CATCAACAAGAGGCGTGC**	39
CopA9.rev	AGACACCCGCAUCGAGAAGUACATCAACAAGAGGCGTGC	39
CopA.tmp	CATCAACAAGAGGCGTGCAGGCTTCACCTCTTGTTGATTTGGGCACAGACTCTGC GTGCCTCCTTCACAGAGTCTGTGCGTGTCGGTGAAGATC	94
dj_CopB.tmp	CATCAACAAGAGGCGTGGAGGCTTCACCTCTTGTTGATTTGGGCACAGACTCTGC GTGCTCGCTTCACAGAGTCTGTGCGTGTCGGTGAAGATC	94
CopC.tmp	CATCAACAAGAGGCGTGCGAGCTTCACCTCTTGTTGATTTGGGCACAGACTCTGC GTGCCTGCTTCACAGAGTCTGTGCGTGTCGGTGAAGATC	94
siCop1.fwd	TTCTAATACGACTCACTATAGGCGTGATCTTCACCGACACGCAC	44
siCop1.rev	GGAGCGTGATCTTCACCGACACATCAACAAGAGGCGTGC	39
siCop1C.rev	GGAGCGTGATCTTCACCGACACATCAACAAGAGGCGTGG	39
siCop2.fwd	TTCTAATACGACTCACTATAGGACCAACAAGATGAAGAGCGCACAGACTCTGTGA AG	44
siCop2.rev	GGAGACCAACAAGATGAAGAGCATCAACAAGAGGCGTG	44
siCop9.fwd	TTCTAATACGACTCACTATAGGACCCGCATCGAGAAGTACGCACAGACTCTGTGA AG	44
siCop9.rev	GGAGACCCGCATCGAGAAGTACATCAACAAGAGGCGTG	44

name	PCR products	Length [nt]
CopA1core.tmp PCR product (CopA_core.fwd,CopA_core.tmp, CopA1.rev)	TTCTAATACGACTCACTATAGGACTGTGAAGGAGGCACGCAGTCCCTGTGCCCAAATC AACAAGAGGTGAAGCCTGCACGCCTCTTGTTGATGTCGGTGAAGATCACGCTGTCC GGACAGCGTGATCTTCACCGACATCAACAAGAGGCGTGCAGGCTTCACCTCTTGTTGA TTTGGGCACAGGGACTGCGTGCCTCCTTCACAGTCCTATAGTGAGTCGTATTAGAA	114
CopA7core.tmp PCR product (CopA_core.fwd,CopA_core.tmp, CopA7.rev)	TTCTAATACGACTCACTATAGGACTGTGAAGGAGGCACGCAGTCCCTGTGCCCAAATC AACAAGAGGTGAAGCCTGCACGCCTCTTGTTGATGTTGCTGCGGATGATCTTGTCG CGACAAGATCATCCGCAGCAACATCAACAAGAGGCGTGCAGGCTTCACCTCTTGTTGA TTTGGGCACAGGGACTGCGTGCCTCCTTCACAGTCCTATAGTGAGTCGTATTAGAA	114
CopA9core.tmp PCR product (CopA_core.fwd,CopA_core.tmp, CopA9.rev)	TTCTAATACGACTCACTATAGGACTGTGAAGGAGGCACGCAGTCCCTGTGCCCAAATC AACAAGAGGTGAAGCCTGCACGCCTCTTGTTGATGTACTTCTCGATGCGGGTGTCT AGACACCCGCATCGAGAAGTACATCAACAAGAGGCGTGCAGGCTTCACCTCTTGTTGA TTTGGGCACAGGGACTGCGTGCCTCCTTCACAGTCCTATAGTGAGTCGTATTAGAA	114
CopA.tmp PCR product (siCop1.fwd CopA.tmp siCop1.rev)	TTCTAATACGACTCACTATAGGCGTGATCTTCACCGACACGCACAGACTCTGTGAAGG AGGCACGCAGAGTCTGTGCCCAAATCAACAAGAGGTGAAGCCTGCACGCCTCTTGTTG ATGTGTCGGTGAAGATCACGCTCC GGAGCGTGATCTTCACCGACACATCAACAAGAGGCGTGCAGGCTTCACCTCTTGTTGA TTTGGGCACAGACTCTGCGTGCCTCCTTCACAGAGTCTGTGCGTGTCGGTGAAGATCA CGCCTATAGTGAGTCGTATTAGAA	140
CopB.tmp PCR product (siCop1.fwd dj_CopB.tmp siCop1C.rev)	TTCTAATACGACTCACTATAGGCGTGATCTTCACCGACACGCACAGACTCTGTGAAGC GAGCACGCAGAGTCTGTGCCCAAATCAACAAGAGGTGAAGCCTCCACGCCTCTTGTTG ATGTGTCGGTGAAGATCACGCTCC GGAGCGTGATCTTCACCGACACATCAACAAGAGGCGTGGAGGCTTCACCTCTTGTTGA TTTGGGCACAGACTCTGCGTGCTCGCTTCACAGAGTCTGTGCGTGTCGGTGAAGATCA CGCCTATAGTGAGTCGTATTAGAA	140
CopB.tmp PCR product (siCop2.fwd dj_CopB.tmp siCop2.rev)	GGAGACCAACAAGATGAAGAGCATCAACAAGAGGCGTGGAGGCTTCACCTCTTGTTGA TTTGGGCACAGACTCTGCGTGCTCGCTTCACAGAGTCTGTGCGCTCTTCATCTTGTTG GTCCTATAGTGAGTCGTATTAGAA CCTCTGGTTGTTCTACTTCTCGTAGTTGTTCTCCGCACCTCCGAAGTGGAGAACAACT AAACCCGTGTCTGAGACGCACGAGCGAAGTGTCTCAGACACGCGAGAAGTAGAACAAC CAGGATATCACTCAGCATAATCTT	140
CopC.tmp PCR product (siCop1.fwd CopC.tmp siCop1.rev)	TTCTAATACGACTCACTATAGGCGTGATCTTCACCGACACGCACAGACTCTGTGAAGC AGGCACGCAGAGTCTGTGCCCAAATCAACAAGAGGTGAAGCTCGCACGCCTCTTGTTG ATGTGTCGGTGAAGATCACGCTCC GGAGCGTGATCTTCACCGACACATCAACAAGAGGCGTGCGAGCTTCACCTCTTGTTGA TTTGGGCACAGACTCTGCGTGCCTGCTTCACAGAGTCTGTGCGTGTCGGTGAAGATCA CGCCTATAGTGAGTCGTATTAGAA	140

CopC.tmp PCR product (siCop9.fwd CopC.tmp siCop9.rev)	TTCTAATACGACTCACTATAGGACCCGCATCGAGAAGTACGCACAGACTCTGTGAAGC AGGCACGCAGAGTCTGTGCCCAAATCAACAAGAGGTGAAGCTCGCACGCCTCTTGTTG ATGTACTTCTCGATGCGGGTCTCC GGAGACCCGCATCGAGAAGTACATCAACAAGAGGCGTGCGAGCTTCACCTCTTGTTGA TTTGGGCACAGACTCTGCGTGCCTGCTTCACAGAGTCTGTGCGTACTTCTCGATGCGG GTCCTATAGTGAGTCGTATTAGAA	140

2. RNA – structural RNA building blocks

name	Sequence	Length [nt]	Generation
CopA1 (G1A1)	GGCGUGAUCUUCACCGACACGCACAGACUCUGUGAAGGAGGCACGCA GAGUCUGUGCCCAAAUCAACAAGAGGUGAAGCCUGCACGCCUCUUGU UGAUGUGUCGGUGAAGAUCACGCUCC	120	1G
CopB1 (G1B1)	GGCGUGAUCUUCACCGACACGCACAGACUCUGUGAAGCGAGCACGCA GAGUCUGUGCCCAAAUCAACAAGAGGUGAAGCCUCCACGCCUCUUGU UGAUGUGUCGGUGAAGAUCACGCUCC	120	1G
CopC1 (G1C1)	GGCGUGAUCUUCACCGACACGCACAGACUCUGUGAAGCAGGCACGCA GAGUCUGUGCCCAAAUCAACAAGAGGUGAAGCUCGCACGCCUCUUGU UGAUGUGUCGGUGAAGAUCACGCUCC	120	1G
CopA2 (G1A2)	GGACCAACAAGAUGAAGAGCGCACAGACUCUGUGAAGGAGGCACGCA GAGUCUGUGCCCAAAUCAACAAGAGGUGAAGCCUGCACGCCUCUUGU UGAUGCUCUUCAUCUUGUUGGUCUCC	120	1G
CopC9(G1C 9)	GGACCCGCAUCGAGAAGUACGCACAGACUCUGUGAAGCAGGCACGCA GAGUCUGUGCCCAAAUCAACAAGAGGUGAAGCUCGCACGCCUCUUGU UGAUGUACUUCUCGAUGCGGGUCUCC	120	1G
CORE_CopA 1 (G3A1)	GGACUGUGAAGGAGGCACGCAGUCCCUGUGCCCAAAUCAACAAGAGG UGAAGCCUGCACGCCUCUUGUUGAUGUCGGUGAAGAUCACGCUGUCC	94	3G
CORE_CopA 7 (G3A7)	GGACUGUGAAGGAGGCACGCAGUCCCUGUGCCCAAAUCAACAAGAGG UGAAGCCUGCACGCCUCUUGUUGAUGUUGCUGCGGAUGAUCUUGUCG	94	3G
CORE_CopA 9 (G3A9)	GGACUGUGAAGGAGGCACGCAGUCCCUGUGCCCAAAUCAACAAGAGG UGAAGCCUGCACGCCUCUUGUUGAUGUACUUCUCGAUGCGGGUGUGA	94	3G

3. siRNA

name	Sequence	Length [nt]	dsRNA (siRNA)
siR1 (Same as HS-1)	ACAGCGUGAUCUUCACCGATT	21	siR1-2
siR2(Complement HS-1)	UCGGUGAAGAUCACGCUGUTT	21	
siR3	AUGACCAACAAGAUGAAGATT	21	siR3-4
siR4	UCUUCAUCUUGUUGGUCAUTT	21	
siR5*	GGACAGCGUGAUCUUCACCTT	21	siCop7
siR6*	GGUGAAGAUCACGCUGUCCTT	21	
siR7	GGAUGAUCUUGUCGGUGAATT	21	siR7-8
siR8	UUCACCGACAAGAUCAUCCTT	21	
siR1*	GCAUGACCAACAAGAUGAATT	21	siCop5
siR2*	UUCAUCUUGUUGGUCAUGCTT	21	
siR3*	CAAGAUGAAGAGCACCAAATT	21	siCop6

siR4*	UUUGGUGCUCUUCAUCUUGTT	21	
siR5 (Same as HS-7)	ACAAGAUCAUCCGCAGCAATT	21	siR5-6
siR6(Complement HS-7)	UUGCUGCGGAUGAUCUUGUTT	21	
siR7*	ACAGCCACAUGCACUUCAATT	21	siCop8
siR8*	UUGAAGUGCAUGUGGCUGUTT	21	
siR9 (Same as HS-9)	ACACCCGCAUCGAGAAGUATT	21	siR9-10
siR10(Complement HS-9)	UACUUCUCGAUGCGGGUGUTT	21	
dj_siR_11	GAGAUCGAGUGCCGCAUCATT	21	siCop10
dj_siR_12	UGAUGCGGCACUCGAUCUCTT	21	

modified:

name	Sequence	Length [nt]	modification
SHsiRNA-1 (HS-siR1)	ACAGCGUGAUCUUCACCG ATT	21	*Thiol linker C6 SH, spacer 18*
SHsiRNA-7 (HS-siR5)	ACAAGAUCAUCCGCAGCA A**TT**	21	*Thiol linke C6 SH, spacer 18*
FAM-siRNA-7 (FAM-siR5)	ACAAGAUCAUCCGCAGCA A**TT**	21	*2'F modification, FAM – luorescein 5'end*
SHsiRNA-9 (HS-siR9)	ACACCCGCAUCGAGAAGU A**TT**	21	*Thiol linker C6 SH, spacer 18*

GFP GENE -> copGFP mRNA:

AUGGAGAGCGACGAGAGCGGCCUGCCCGCCAUGGAGAUCGAGUGCCGCAUCACCGGCACC
CUGAACGGCGUGGAGUUCGAGCUGGUGGGCGGCGGAGAGGGCACCCCCAAGCAGGGCCGC
AUGACCAACAAGAUGAAGAGCACCAAAGGCGCCCUGACCUUCAGCCCCUACCUGCUGAGC
CACGUGAUGGGCUACGGCUUCUACCACUUCGGCACCUACCCCAGCGGCUACGAGAACCCC
UUCCUGCACGCCAUCAACAACGGCGGCUACACCAACACCCGCAUCGAGAAGUACGAGGAC
GGCGGCGUGCUGCACGUGAGCUUCAGCUACCGCUACGAGGCCGGCCGCGUGAUCGGCGAC
UUCAAGGUGGUGGGCACCGGCUUCCCCGAGG**ACAGCGUGAUCUUCACCGA**CAAGAUCAUC
CGCAGCAACGCCACCGUGGAGCACCUGCACCCCAUGGGCGAUAACGUGCUGGUGGGCAGC
UUCGCCCGCACCUUCAGCCUGCGCGACGGCGGCUACUACAGCUUCGUGGUGGACAGCCAC
AUGCACUUCAAGAGCGCCAUCCACCCCAGCAUCCUGCAGAACGGGGGCCCCAUGUUCGCC
UUCCGCCGCGUGGAGGAGCUGCACAGCAACACCGAGCUGGGCAUCGUGGAGUACCAGCAC
GCCUUCAAGACCCCCAUCGCCUUCGCCAGAUCCCGCGCUCAGUCGUCCAAUUCUGCCGUG
GACGGCACCGCCGGACCCGGCUCCACCGGAUCUCGCUAA

References

1. Jedrzejczyk, D.; Chworos, A., Self-Assembling RNA Nanoparticle for Gene Expression Regulation in a Model System. *Acs Synth Biol* **2019,** *8* (3), 491-497.
2. Watson, J. D.; Crick, F. H., The structure of DNA. *Cold Spring Harb Symp Quant Biol* **1953,** *18*, 123-31.
3. Franklin, R. E.; Gosling, R. G., Evidence for 2-chain helix in crystalline structure of sodium deoxyribonucleate. *Nature* **1953,** *172* (4369), 156-7.
4. Jackson, R. J.; Hellen, C. U.; Pestova, T. V., The mechanism of eukaryotic translation initiation and principles of its regulation. *Nat Rev Mol Cell Biol* **2010,** *11* (2), 113-27.
5. Dever, T. E.; Green, R., The elongation, termination, and recycling phases of translation in eukaryotes. *Cold Spring Harb Perspect Biol* **2012,** *4* (7), a013706.
6. Crick, F. H., On protein synthesis. *Symp Soc Exp Biol* **1958,** *12*, 138-63.
7. Consortium, E. P., An integrated encyclopedia of DNA elements in the human genome. *Nature* **2012,** *489* (7414), 57-74.
8. Leppek, K.; Das, R.; Barna, M., Functional 5' UTR mRNA structures in eukaryotic translation regulation and how to find them. *Nat Rev Mol Cell Biol* **2018,** *19* (3), 158-174.
9. Mayr, C., What Are 3' UTRs Doing? *Cold Spring Harb Perspect Biol* **2019,** *11* (10).
10. Decroly, E.; Ferron, F.; Lescar, J.; Canard, B., Conventional and unconventional mechanisms for capping viral mRNA. *Nat Rev Microbiol* **2011,** *10* (1), 51-65.
11. Ray, P. D.; Fry, R. C., The Cell: The Fundamental Unit in Systems Biology. In *Systems Biology in Toxicology and Environmental Health*, Academic Press: 2015; pp 11-42.
12. Ramanathan, A.; Robb, G. B.; Chan, S. H., mRNA capping: biological functions and applications. *Nucleic Acids Res* **2016,** *44* (16), 7511-26.
13. Patel, S.; Athirasala, A.; Menezes, P. P.; Ashwanikumar, N.; Zou, T.; Sahay, G.; Bertassoni, L. E., Messenger RNA Delivery for Tissue Engineering and Regenerative Medicine Applications. *Tissue Eng Part A* **2019,** *25* (1-2), 91-112.
14. O'Donoghue, P.; Ling, J.; Soll, D., Transfer RNA function and evolution. *RNA Biol* **2018,** *15* (4-5), 423-426.
15. Hoagland, M. B.; Stephenson, M. L.; Scott, J. F.; Hecht, L. I.; Zamecnik, P. C., A soluble ribonucleic acid intermediate in protein synthesis. *J Biol Chem* **1958,** *231* (1), 241-57.
16. Moras, D.; Comarmond, M. B.; Fischer, J.; Weiss, R.; Thierry, J. C.; Ebel, J. P.; Giege, R., Crystal structure of yeast tRNAAsp. *Nature* **1980,** *288* (5792), 669-74.
17. Burton, Z. F., transfer RNA. In *Evolution since Coding: Cradles, Halos, Barrels, and Wings*, Academic Press: 2018.
18. Harvey Lodish, A. B., S. Lawrence Zipursky, Paul Matsudaira, David Baltimore and James Darnell, *Molecular Cell Biology*. 4th ed.; W. H. Freeman and Company: NY, 2000.
19. Betat, H.; Morl, M., The CCA-adding enzyme: A central scrutinizer in tRNA quality control. *Bioessays* **2015,** *37* (9), 975-82.
20. Goldman, E., *tRNA and the Human Genome*. 2011.
21. Nishimura, J. A. M. a. S., Modified nucleosides in transfer RNA. *Accounts of Chemical Research* **1977,** *10*.
22. Suzuki, T., The expanding world of tRNA modifications and their disease relevance. *Nat Rev Mol Cell Biol* **2021,** *22* (6), 375-392.
23. Translation. https://www.genome.gov/genetics-glossary/Translation.
24. Yoshihama, M.; Uechi, T.; Asakawa, S.; Kawasaki, K.; Kato, S.; Higa, S.; Maeda, N.; Minoshima, S.; Tanaka, T.; Shimizu, N.; Kenmochi, N., The human ribosomal protein genes: sequencing and comparative analysis of 73 genes. *Genome Res* **2002,** *12* (3), 379-90.

25. Moore, P. B.; Steitz, T. A., The involvement of RNA in ribosome function. *Nature* **2002,** *418* (6894), 229-35.
26. Lee, R. C.; Feinbaum, R. L.; Ambros, V., The C. elegans heterochronic gene lin-4 encodes small RNAs with antisense complementarity to lin-14. *Cell* **1993,** *75* (5), 843-54.
27. Pasquinelli, A. E.; Reinhart, B. J.; Slack, F.; Martindale, M. Q.; Kuroda, M. I.; Maller, B.; Hayward, D. C.; Ball, E. E.; Degnan, B.; Muller, P.; Spring, J.; Srinivasan, A.; Fishman, M.; Finnerty, J.; Corbo, J.; Levine, M.; Leahy, P.; Davidson, E.; Ruvkun, G., Conservation of the sequence and temporal expression of let-7 heterochronic regulatory RNA. *Nature* **2000,** *408* (6808), 86-9.
28. Lee, R. C.; Ambros, V., An extensive class of small RNAs in Caenorhabditis elegans. *Science* **2001,** *294* (5543), 862-4.
29. Lagos-Quintana, M.; Rauhut, R.; Lendeckel, W.; Tuschl, T., Identification of novel genes coding for small expressed RNAs. *Science* **2001,** *294* (5543), 853-8.
30. Lee, Y.; Ahn, C.; Han, J.; Choi, H.; Kim, J.; Yim, J.; Lee, J.; Provost, P.; Radmark, O.; Kim, S.; Kim, V. N., The nuclear RNase III Drosha initiates microRNA processing. *Nature* **2003,** *425* (6956), 415-9.
31. Yang, J. S.; Lai, E. C., Alternative miRNA biogenesis pathways and the interpretation of core miRNA pathway mutants. *Mol Cell* **2011,** *43* (6), 892-903.
32. Filipow, S.; Laczmanski, L., Blood Circulating miRNAs as Cancer Biomarkers for Diagnosis and Surgical Treatment Response. *Front Genet* **2019,** *10*, 169.
33. Rupaimoole, R.; Calin, G. A.; Lopez-Berestein, G.; Sood, A. K., miRNA Deregulation in Cancer Cells and the Tumor Microenvironment. *Cancer Discov* **2016,** *6* (3), 235-46.
34. Tomasz P. Lehmann, J. M., Natalia Szostak, Marta Szachniuk, Sylwia Grodecka-Gazdecka, Paweł P. Jagodziński, In Vitro and in Silico Analysis of miR-125a with rs12976445 Polymorphism in Breast Cancer Patients. *Applied Sciences* **2020,** *10* (20).
35. Meng, L.; Liu, C.; Lu, J.; Zhao, Q.; Deng, S.; Wang, G.; Qiao, J.; Zhang, C.; Zhen, L.; Lu, Y.; Li, W.; Zhang, Y.; Pestell, R. G.; Fan, H.; Chen, Y. H.; Liu, Z.; Yu, Z., Small RNA zippers lock miRNA molecules and block miRNA function in mammalian cells. *Nat Commun* **2017,** *8*, 13964.
36. Lennox, K. A.; Behlke, M. A., Chemical modification and design of anti-miRNA oligonucleotides. *Gene Ther* **2011,** *18* (12), 1111-20.
37. Chen, Y.; Gao, D. Y.; Huang, L., In vivo delivery of miRNAs for cancer therapy: challenges and strategies. *Adv Drug Deliv Rev* **2015,** *81*, 128-41.
38. Carthew, R. W.; Sontheimer, E. J., Origins and Mechanisms of miRNAs and siRNAs. *Cell* **2009,** *136* (4), 642-55.
39. Tomari, Y.; Zamore, P. D., Perspective: machines for RNAi. *Genes Dev* **2005,** *19* (5), 517-29.
40. Lisowiec-Wachnicka, J.; Bartys, N.; Pasternak, A., A systematic study on the influence of thermodynamic asymmetry of 5'-ends of siRNA duplexes in relation to their silencing potency. *Sci Rep* **2019,** *9* (1), 2477.
41. Hu, B.; Zhong, L.; Weng, Y.; Peng, L.; Huang, Y.; Zhao, Y.; Liang, X. J., Therapeutic siRNA: state of the art. *Signal Transduct Target Ther* **2020,** *5* (1), 101.
42. Saw, P. E.; Song, E. W., siRNA therapeutics: a clinical reality. *Sci China Life Sci* **2020,** *63* (4), 485-500.
43. Yang, J., Patisiran for the treatment of hereditary transthyretin-mediated amyloidosis. *Expert Rev Clin Pharmacol* **2019,** *12* (2), 95-99.
44. Ozata, D. M.; Gainetdinov, I.; Zoch, A.; O'Carroll, D.; Zamore, P. D., PIWI-interacting RNAs: small RNAs with big functions. *Nat Rev Genet* **2019,** *20* (2), 89-108.
45. Klattenhoff, C.; Theurkauf, W., Biogenesis and germline functions of piRNAs. *Development* **2008,** *135* (1), 3-9.
46. Han, B. W.; Zamore, P. D., piRNAs. *Curr Biol* **2014,** *24* (16), R730-3.
47. Siomi, M. C.; Sato, K.; Pezic, D.; Aravin, A. A., PIWI-interacting small RNAs: the vanguard of genome defence. *Nat Rev Mol Cell Biol* **2011,** *12* (4), 246-58.

48. Czech, B.; Munafo, M.; Ciabrelli, F.; Eastwood, E. L.; Fabry, M. H.; Kneuss, E.; Hannon, G. J., piRNA-Guided Genome Defense: From Biogenesis to Silencing. *Annu Rev Genet* **2018,** *52*, 131-157.
49. Seto, A. G.; Kingston, R. E.; Lau, N. C., The coming of age for Piwi proteins. *Mol Cell* **2007,** *26* (5), 603-9.
50. Kuramochi-Miyagawa, S.; Watanabe, T.; Gotoh, K.; Totoki, Y.; Toyoda, A.; Ikawa, M.; Asada, N.; Kojima, K.; Yamaguchi, Y.; Ijiri, T. W.; Hata, K.; Li, E.; Matsuda, Y.; Kimura, T.; Okabe, M.; Sakaki, Y.; Sasaki, H.; Nakano, T., DNA methylation of retrotransposon genes is regulated by Piwi family members MILI and MIWI2 in murine fetal testes. *Genes Dev* **2008,** *22* (7), 908-17.
51. Aravin, A. A.; Bourc'his, D., Small RNA guides for de novo DNA methylation in mammalian germ cells. *Genes Dev* **2008,** *22* (8), 970-5.
52. Liu, J.; Zhang, S.; Cheng, B., Epigenetic roles of PIWIinteracting RNAs (piRNAs) in cancer metastasis (Review). *Oncol Rep* **2018,** *40* (5), 2423-2434.
53. Weng, W.; Liu, N.; Toiyama, Y.; Kusunoki, M.; Nagasaka, T.; Fujiwara, T.; Wei, Q.; Qin, H.; Lin, H.; Ma, Y.; Goel, A., Novel evidence for a PIWI-interacting RNA (piRNA) as an oncogenic mediator of disease progression, and a potential prognostic biomarker in colorectal cancer. *Mol Cancer* **2018,** *17* (1), 16.
54. Mai, D.; Zheng, Y.; Guo, H.; Ding, P.; Bai, R.; Li, M.; Ye, Y.; Zhang, J.; Huang, X.; Liu, D.; Sui, Q.; Pan, L.; Su, J.; Deng, J.; Wu, G.; Li, R.; Deng, S.; Bai, Y.; Ligu, Y.; Tan, W.; Wu, C.; Wu, T.; Zheng, J.; Lin, D., Serum piRNA-54265 is a New Biomarker for early detection and clinical surveillance of Human Colorectal Cancer. *Theranostics* **2020,** *10* (19), 8468-8478.
55. Yamashiro, H.; Siomi, M. C., PIWI-Interacting RNA in Drosophila: Biogenesis, Transposon Regulation, and Beyond. *Chem Rev* **2018,** *118* (8), 4404-4421.
56. Ravasi, T.; Suzuki, H.; Pang, K. C.; Katayama, S.; Furuno, M.; Okunishi, R.; Fukuda, S.; Ru, K.; Frith, M. C.; Gongora, M. M.; Grimmond, S. M.; Hume, D. A.; Hayashizaki, Y.; Mattick, J. S., Experimental validation of the regulated expression of large numbers of non-coding RNAs from the mouse genome. *Genome Res* **2006,** *16* (1), 11-9.
57. Carninci, P.; Kasukawa, T.; Katayama, S.; Gough, J.; Frith, M. C.; Maeda, N.; Oyama, R.; Ravasi, T.; Lenhard, B.; Wells, C.; Kodzius, R.; Shimokawa, K.; Bajic, V. B.; Brenner, S. E.; Batalov, S.; Forrest, A. R.; Zavolan, M.; Davis, M. J.; Wilming, L. G.; Aidinis, V.; Allen, J. E.; Ambesi-Impiombato, A.; Apweiler, R.; Aturaliya, R. N.; Bailey, T. L.; Bansal, M.; Baxter, L.; Beisel, K. W.; Bersano, T.; Bono, H.; Chalk, A. M.; Chiu, K. P.; Choudhary, V.; Christoffels, A.; Clutterbuck, D. R.; Crowe, M. L.; Dalla, E.; Dalrymple, B. P.; de Bono, B.; Della Gatta, G.; di Bernardo, D.; Down, T.; Engstrom, P.; Fagiolini, M.; Faulkner, G.; Fletcher, C. F.; Fukushima, T.; Furuno, M.; Futaki, S.; Gariboldi, M.; Georgii-Hemming, P.; Gingeras, T. R.; Gojobori, T.; Green, R. E.; Gustincich, S.; Harbers, M.; Hayashi, Y.; Hensch, T. K.; Hirokawa, N.; Hill, D.; Huminiecki, L.; Iacono, M.; Ikeo, K.; Iwama, A.; Ishikawa, T.; Jakt, M.; Kanapin, A.; Katoh, M.; Kawasawa, Y.; Kelso, J.; Kitamura, H.; Kitano, H.; Kollias, G.; Krishnan, S. P.; Kruger, A.; Kummerfeld, S. K.; Kurochkin, I. V.; Lareau, L. F.; Lazarevic, D.; Lipovich, L.; Liu, J.; Liuni, S.; McWilliam, S.; Madan Babu, M.; Madera, M.; Marchionni, L.; Matsuda, H.; Matsuzawa, S.; Miki, H.; Mignone, F.; Miyake, S.; Morris, K.; Mottagui-Tabar, S.; Mulder, N.; Nakano, N.; Nakauchi, H.; Ng, P.; Nilsson, R.; Nishiguchi, S.; Nishikawa, S.; Nori, F.; Ohara, O.; Okazaki, Y.; Orlando, V.; Pang, K. C.; Pavan, W. J.; Pavesi, G.; Pesole, G.; Petrovsky, N.; Piazza, S.; Reed, J.; Reid, J. F.; Ring, B. Z.; Ringwald, M.; Rost, B.; Ruan, Y.; Salzberg, S. L.; Sandelin, A.; Schneider, C.; Schonbach, C.; Sekiguchi, K.; Semple, C. A.; Seno, S.; Sessa, L.; Sheng, Y.; Shibata, Y.; Shimada, H.; Shimada, K.; Silva, D.; Sinclair, B.; Sperling, S.; Stupka, E.; Sugiura, K.; Sultana, R.; Takenaka, Y.; Taki, K.; Tammoja, K.; Tan, S. L.; Tang, S.; Taylor, M. S.; Tegner, J.; Teichmann, S. A.; Ueda, H. R.; van Nimwegen, E.; Verardo, R.; Wei, C. L.; Yagi, K.; Yamanishi, H.; Zabarovsky, E.; Zhu, S.; Zimmer, A.; Hide, W.; Bult, C.; Grimmond, S. M.; Teasdale, R. D.; Liu, E. T.; Brusic, V.; Quackenbush, J.; Wahlestedt, C.; Mattick, J. S.; Hume, D. A.; Kai, C.; Sasaki, D.; Tomaru, Y.; Fukuda, S.; Kanamori-Katayama,

M.; Suzuki, M.; Aoki, J.; Arakawa, T.; Iida, J.; Imamura, K.; Itoh, M.; Kato, T.; Kawaji, H.; Kawagashira, N.; Kawashima, T.; Kojima, M.; Kondo, S.; Konno, H.; Nakano, K.; Ninomiya, N.; Nishio, T.; Okada, M.; Plessy, C.; Shibata, K.; Shiraki, T.; Suzuki, S.; Tagami, M.; Waki, K.; Watahiki, A.; Okamura-Oho, Y.; Suzuki, H.; Kawai, J.; Hayashizaki, Y.; Consortium, F.; Group, R. G. E. R.; Genome Science, G., The transcriptional landscape of the mammalian genome. *Science* **2005,** *309* (5740), 1559-63.

58. Ma, L.; Cao, J.; Liu, L.; Du, Q.; Li, Z.; Zou, D.; Bajic, V. B.; Zhang, Z., LncBook: a curated knowledgebase of human long non-coding RNAs. *Nucleic Acids Res* **2019,** *47* (D1), D128-D134.

59. Statello, L.; Guo, C. J.; Chen, L. L.; Huarte, M., Gene regulation by long non-coding RNAs and its biological functions. *Nat Rev Mol Cell Biol* **2021,** *22* (2), 96-118.

60. Katayama, S.; Tomaru, Y.; Kasukawa, T.; Waki, K.; Nakanishi, M.; Nakamura, M.; Nishida, H.; Yap, C. C.; Suzuki, M.; Kawai, J.; Suzuki, H.; Carninci, P.; Hayashizaki, Y.; Wells, C.; Frith, M.; Ravasi, T.; Pang, K. C.; Hallinan, J.; Mattick, J.; Hume, D. A.; Lipovich, L.; Batalov, S.; Engstrom, P. G.; Mizuno, Y.; Faghihi, M. A.; Sandelin, A.; Chalk, A. M.; Mottagui-Tabar, S.; Liang, Z.; Lenhard, B.; Wahlestedt, C.; Group, R. G. E. R.; Genome Science, G.; Consortium, F., Antisense transcription in the mammalian transcriptome. *Science* **2005,** *309* (5740), 1564-6.

61. Wilusz, J. E.; Freier, S. M.; Spector, D. L., 3' end processing of a long nuclear-retained noncoding RNA yields a tRNA-like cytoplasmic RNA. *Cell* **2008,** *135* (5), 919-32.

62. Dieci, G.; Preti, M.; Montanini, B., Eukaryotic snoRNAs: a paradigm for gene expression flexibility. *Genomics* **2009,** *94* (2), 83-8.

63. Pamudurti, N. R.; Bartok, O.; Jens, M.; Ashwal-Fluss, R.; Stottmeister, C.; Ruhe, L.; Hanan, M.; Wyler, E.; Perez-Hernandez, D.; Ramberger, E.; Shenzis, S.; Samson, M.; Dittmar, G.; Landthaler, M.; Chekulaeva, M.; Rajewsky, N.; Kadener, S., Translation of CircRNAs. *Mol Cell* **2017,** *66* (1), 9-21 e7.

64. Jeck, W. R.; Sorrentino, J. A.; Wang, K.; Slevin, M. K.; Burd, C. E.; Liu, J.; Marzluff, W. F.; Sharpless, N. E., Circular RNAs are abundant, conserved, and associated with ALU repeats. *Rna* **2013,** *19* (2), 141-57.

65. Yao, R. W.; Wang, Y.; Chen, L. L., Cellular functions of long noncoding RNAs. *Nat Cell Biol* **2019,** *21* (5), 542-551.

66. Kruger, K.; Grabowski, P. J.; Zaug, A. J.; Sands, J.; Gottschling, D. E.; Cech, T. R., Self-splicing RNA: autoexcision and autocyclization of the ribosomal RNA intervening sequence of Tetrahymena. *Cell* **1982,** *31* (1), 147-57.

67. Cecilia Guerrier-Takada, K. G., Terry Marsh, Norman Pace, Sidney Altman, The RNA moiety of ribonuclease P is the catalytic subunit of the enzyme. *Cell* **1983,** *35* (3).

68. Moore, P. B.; Steitz, T. A., After the ribosome structures: how does peptidyl transferase work? *Rna* **2003,** *9* (2), 155-9.

69. R.K.O.Sigel, M. S. S. Z.-P., Ribozymes. In *Reference Module in Life Sciences*, Elsevier: 2017.

70. A.Lescoute, E. W., Ribozymes. In *Encyclopedia of Virology*, Academic Press: 2008.

71. de la Pena, M.; Garcia-Robles, I.; Cervera, A., The Hammerhead Ribozyme: A Long History for a Short RNA. *Molecules* **2017,** *22* (1).

72. Fedor, M. J., Structure and function of the hairpin ribozyme. *J Mol Biol* **2000,** *297* (2), 269-91.

73. Been, M. D.; Wickham, G. S., Self-cleaving ribozymes of hepatitis delta virus RNA. *Eur J Biochem* **1997,** *247* (3), 741-53.

74. Saldanha, R.; Mohr, G.; Belfort, M.; Lambowitz, A. M., Group I and group II introns. *Faseb J* **1993,** *7* (1), 15-24.

75. Lilley, D. M., The ribosome functions as a ribozyme. *Chembiochem* **2001,** *2* (1), 31-5.

76. Park, S. V.; Yang, J. S.; Jo, H.; Kang, B.; Oh, S. S.; Jung, G. Y., Catalytic RNA, ribozyme, and its applications in synthetic biology. *Biotechnol Adv* **2019,** *37* (8), 107452.

77. Kashani-Sabet, M., Ribozyme therapeutics. *J Investig Dermatol Symp Proc* **2002,** *7* (1), 76-8.

78. Schmitz, S. U.; Grote, P.; Herrmann, B. G., Mechanisms of long noncoding RNA function in development and disease. *Cell Mol Life Sci* **2016,** *73* (13), 2491-509.

79. Felletti, M.; Bieber, A.; Hartig, J. S., The 3'-untranslated region of mRNAs as a site for ribozyme cleavage-dependent processing and control in bacteria. *RNA Biol* **2017,** *14* (11), 1522-1533.
80. Wieland, M.; Auslander, D.; Fussenegger, M., Engineering of ribozyme-based riboswitches for mammalian cells. *Methods* **2012,** *56* (3), 351-7.
81. Hieronymus, R.; Muller, S., Engineering of hairpin ribozyme variants for RNA recombination and splicing. *Ann N Y Acad Sci* **2019,** *1447* (1), 135-143.
82. Lee, R. T.; Ng, A. S.; Ingham, P. W., Ribozyme Mediated gRNA Generation for In Vitro and In Vivo CRISPR/Cas9 Mutagenesis. *PLoS One* **2016,** *11* (11), e0166020.
83. Tang, W.; Hu, J. H.; Liu, D. R., Aptazyme-embedded guide RNAs enable ligand-responsive genome editing and transcriptional activation. *Nat Commun* **2017,** *8*, 15939.
84. Silverman, S. K., *Nucleic Acid Switches and Sensors*. Springer: 2006.
85. Zhang, Y.; Wang, J.; Cheng, H.; Sun, Y.; Liu, M.; Wu, Z.; Pei, R., Conditional control of suicide gene expression in tumor cells with theophylline-responsive ribozyme. *Gene Ther* **2017,** *24* (2), 84-91.
86. Germer, K.; Leonard, M.; Zhang, X., RNA aptamers and their therapeutic and diagnostic applications. *Int J Biochem Mol Biol* **2013,** *4* (1), 27-40.
87. Tuerk, C.; Gold, L., Systematic evolution of ligands by exponential enrichment: RNA ligands to bacteriophage T4 DNA polymerase. *Science* **1990,** *249* (4968), 505-10.
88. Ellington, A. D.; Szostak, J. W., In vitro selection of RNA molecules that bind specific ligands. *Nature* **1990,** *346* (6287), 818-22.
89. Long, S. B.; Long, M. B.; White, R. R.; Sullenger, B. A., Crystal structure of an RNA aptamer bound to thrombin. *Rna* **2008,** *14* (12), 2504-12.
90. Potty, A. S.; Kourentzi, K.; Fang, H.; Schuck, P.; Willson, R. C., Biophysical characterization of DNA and RNA aptamer interactions with hen egg lysozyme. *Int J Biol Macromol* **2011,** *48* (3), 392-7.
91. de-los-Santos-Alvarez, N.; Lobo-Castanon, M. J.; Miranda-Ordieres, A. J.; Tunon-Blanco, P., Modified-RNA aptamer-based sensor for competitive impedimetric assay of neomycin B. *J Am Chem Soc* **2007,** *129* (13), 3808-9.
92. Jeong, S.; Han, S. R.; Lee, Y. J.; Lee, S. W., Selection of RNA aptamers specific to active prostate-specific antigen. *Biotechnol Lett* **2010,** *32* (3), 379-85.
93. Walsh, R.; DeRosa, M. C., Retention of function in the DNA homolog of the RNA dopamine aptamer. *Biochem Biophys Res Commun* **2009,** *388* (4), 732-5.
94. Hanif, A.; Farooq, R.; Rehman, M. U.; Khan, R.; Majid, S.; Ganaie, M. A., Aptamer based nanobiosensors: Promising healthcare devices. *Saudi Pharm J* **2019,** *27* (3), 312-319.
95. Kim, M. Y.; Jeong, S., In vitro selection of RNA aptamer and specific targeting of ErbB2 in breast cancer cells. *Nucleic Acid Ther* **2011,** *21* (3), 173-8.
96. Bagalkot, V.; Zhang, L.; Levy-Nissenbaum, E.; Jon, S.; Kantoff, P. W.; Langer, R.; Farokhzad, O. C., Quantum dot-aptamer conjugates for synchronous cancer imaging, therapy, and sensing of drug delivery based on bi-fluorescence resonance energy transfer. *Nano Lett* **2007,** *7* (10), 3065-70.
97. Boussebayle, A.; Groher, F.; Suess, B., RNA-based Capture-SELEX for the selection of small molecule-binding aptamers. *Methods* **2019,** *161*, 10-15.
98. Henderson, C. A.; Rail, C. A.; Butt, L. E.; Vincent, H. A.; Callaghan, A. J., Generation of small molecule-binding RNA arrays and their application to fluorogen-binding RNA aptamers. *Methods* **2019,** *167*, 39-53.
99. Ferapontova, E. E.; Olsen, E. M.; Gothelf, K. V., An RNA aptamer-based electrochemical biosensor for detection of theophylline in serum. *J Am Chem Soc* **2008,** *130* (13), 4256-8.
100. Mao, K.; Zhang, H.; Pan, Y.; Zhang, K.; Cao, H.; Li, X.; Yang, Z., Nanomaterial-based aptamer sensors for analysis of illicit drugs and evaluation of drugs consumption for wastewater-based epidemiology. *Trends Analyt Chem* **2020,** *130*, 115975.

101. Pfeiffer, F.; Mayer, G., Selection and Biosensor Application of Aptamers for Small Molecules. *Front Chem* **2016,** *4*, 25.
102. Ning, Y.; Hu, J.; Lu, F., Aptamers used for biosensors and targeted therapy. *Biomed Pharmacother* **2020,** *132*, 110902.
103. Mondragon, E.; Maher, L. J., 3rd, RNA aptamer inhibitors of a restriction endonuclease. *Nucleic Acids Res* **2015,** *43* (15), 7544-55.
104. Urak, K. T.; Blanco, G. N.; Shubham, S.; Lin, L. H.; Dassie, J. P.; Thiel, W. H.; Chen, Y.; Sonkar, V. K.; Lei, B.; Murthy, S.; Gutierrez, W. R.; Wilson, M. E.; Stiber, J. A.; Klesney-Tait, J.; Dayal, S.; Miller, F. J., Jr.; Giangrande, P. H., RNA inhibitors of nuclear proteins responsible for multiple organ dysfunction syndrome. *Nat Commun* **2019,** *10* (1), 116.
105. Farokhzad, O. C.; Cheng, J.; Teply, B. A.; Sherifi, I.; Jon, S.; Kantoff, P. W.; Richie, J. P.; Langer, R., Targeted nanoparticle-aptamer bioconjugates for cancer chemotherapy in vivo. *Proc Natl Acad Sci U S A* **2006,** *103* (16), 6315-20.
106. Wan, L. Y.; Yuan, W. F.; Ai, W. B.; Ai, Y. W.; Wang, J. J.; Chu, L. Y.; Zhang, Y. Q.; Wu, J. F., An exploration of aptamer internalization mechanisms and their applications in drug delivery. *Expert Opin Drug Deliv* **2019,** *16* (3), 207-218.
107. Karagiannis, P.; Fujita, Y.; Saito, H., RNA-based gene circuits for cell regulation. *Proc Jpn Acad Ser B Phys Biol Sci* **2016,** *92* (9), 412-422.
108. Panchal, V.; Brenk, R., Riboswitches as Drug Targets for Antibiotics. *Antibiotics (Basel)* **2021,** *10* (1).
109. Winkler, W. C.; Breaker, R. R., Genetic control by metabolite-binding riboswitches. *Chembiochem* **2003,** *4* (10), 1024-32.
110. Lee, C. H.; Han, S. R.; Lee, S. W., Therapeutic Applications of Aptamer-Based Riboswitches. *Nucleic Acid Ther* **2016,** *26* (1), 44-51.
111. Hallberg, Z. F.; Su, Y.; Kitto, R. Z.; Hammond, M. C., Engineering and In Vivo Applications of Riboswitches. *Annu Rev Biochem* **2017,** *86*, 515-539.
112. Yu, A. M.; Choi, Y. H.; Tu, M. J., RNA Drugs and RNA Targets for Small Molecules: Principles, Progress, and Challenges. *Pharmacol Rev* **2020,** *72* (4), 862-898.
113. Schmidt, C. M.; Smolke, C. D., RNA Switches for Synthetic Biology. *Cold Spring Harb Perspect Biol* **2019,** *11* (1).
114. Sharma, V.; Nomura, Y.; Yokobayashi, Y., Engineering complex riboswitch regulation by dual genetic selection. *J Am Chem Soc* **2008,** *130* (48), 16310-5.
115. Ogawa, A., Rational design of artificial riboswitches based on ligand-dependent modulation of internal ribosome entry in wheat germ extract and their applications as label-free biosensors. *Rna* **2011,** *17* (3), 478-88.
116. Townshend, B.; Kennedy, A. B.; Xiang, J. S.; Smolke, C. D., High-throughput cellular RNA device engineering. *Nat Methods* **2015,** *12* (10), 989-94.
117. Schoukroun-Barnes, L. R.; Wagan, S.; White, R. J., Enhancing the analytical performance of electrochemical RNA aptamer-based sensors for sensitive detection of aminoglycoside antibiotics. *Anal Chem* **2014,** *86* (2), 1131-7.
118. Chauvier, A.; Picard-Jean, F.; Berger-Dancause, J. C.; Bastet, L.; Naghdi, M. R.; Dube, A.; Turcotte, P.; Perreault, J.; Lafontaine, D. A., Transcriptional pausing at the translation start site operates as a critical checkpoint for riboswitch regulation. *Nat Commun* **2017,** *8*, 13892.
119. Finke, M.; Brecht, D.; Stifel, J.; Gense, K.; Gamerdinger, M.; Hartig, J. S., Efficient splicing-based RNA regulators for tetracycline-inducible gene expression in human cell culture and C. elegans. *Nucleic Acids Res* **2021,** *49* (12), e71.
120. Savinov, A.; Block, S. M., Self-cleavage of the glmS ribozyme core is controlled by a fragile folding element. *Proc Natl Acad Sci U S A* **2018,** *115* (47), 11976-11981.
121. Kornberg, R. D., The molecular basis of eukaryotic transcription. *Proc Natl Acad Sci U S A* **2007,** *104* (32), 12955-61.

122. Caruthers, M. H.; Beaucage, S. L.; Becker, C.; Efcavitch, J. W.; Fisher, E. F.; Galluppi, G.; Goldman, R.; deHaseth, P.; Matteucci, M.; McBride, L.; et al., Deoxyoligonucleotide synthesis via the phosphoramidite method. *Gene Amplif Anal* **1983,** *3*, 1-26.
123. Caruthers, M. H., Gene synthesis machines: DNA chemistry and its uses. *Science* **1985,** *230* (4723), 281-5.
124. Matteucci, M. D.; Caruthers, M. H., Synthesis of deoxyoligonucleotides on a polymer support. 1981. *Biotechnology* **1992,** *24*, 92-8.
125. Hill, D. J.; Mio, M. J.; Prince, R. B.; Hughes, T. S.; Moore, J. S., A field guide to foldamers. *Chem Rev* **2001,** *101* (12), 3893-4012.
126. Jaeger, L.; Westhof, E.; Leontis, N. B., TectoRNA: modular assembly units for the construction of RNA nano-objects. *Nucleic Acids Res* **2001,** *29* (2), 455-63.
127. Nasalean, L.; Baudrey, S.; Leontis, N. B.; Jaeger, L., Controlling RNA self-assembly to form filaments. *Nucleic Acids Res* **2006,** *34* (5), 1381-92.
128. Xia, G.; Chen, L.; Sera, T.; Fa, M.; Schultz, P. G.; Romesberg, F. E., Directed evolution of novel polymerase activities: mutation of a DNA polymerase into an efficient RNA polymerase. *Proc Natl Acad Sci U S A* **2002,** *99* (10), 6597-602.
129. Padilla, R.; Sousa, R., A Y639F/H784A T7 RNA polymerase double mutant displays superior properties for synthesizing RNAs with non-canonical NTPs. *Nucleic Acids Res* **2002,** *30* (24), e138.
130. Chelliserrykattil, J.; Ellington, A. D., Evolution of a T7 RNA polymerase variant that transcribes 2'-O-methyl RNA. *Nat Biotechnol* **2004,** *22* (9), 1155-60.
131. Kawai, R.; Kimoto, M.; Ikeda, S.; Mitsui, T.; Endo, M.; Yokoyama, S.; Hirao, I., Site-specific fluorescent labeling of RNA molecules by specific transcription using unnatural base pairs. *J Am Chem Soc* **2005,** *127* (49), 17286-95.
132. Pardi, N.; Muramatsu, H.; Weissman, D.; Kariko, K., In vitro transcription of long RNA containing modified nucleosides. *Methods Mol Biol* **2013,** *969*, 29-42.
133. Moore, M. J.; Query, C. C., Joining of RNAs by splinted ligation. *Methods Enzymol* **2000,** *317*, 109-23.
134. Wang, Z.; Shah, K.; Rana, T. M., Probing Tat peptide-TAR RNA interactions by psoralen photo-cross-linking. *Biochemistry* **2001,** *40* (21), 6458-64.
135. Buchmueller, K. L.; Hill, B. T.; Platz, M. S.; Weeks, K. M., RNA-tethered phenyl azide photocrosslinking via a short-lived indiscriminant electrophile. *J Am Chem Soc* **2003,** *125* (36), 10850-61.
136. Seelig, B.; Jaschke, A., Ternary conjugates of guanosine monophosphate as initiator nucleotides for the enzymatic synthesis of 5'-modified RNAs. *Bioconjug Chem* **1999,** *10* (3), 371-8.
137. Sengle, G.; Jenne, A.; Arora, P. S.; Seelig, B.; Nowick, J. S.; Jaschke, A.; Famulok, M., Synthesis, incorporation efficiency, and stability of disulfide bridged functional groups at RNA 5'-ends. *Bioorg Med Chem* **2000,** *8* (6), 1317-29.
138. Merino, E. J.; Weeks, K. M., Facile conversion of aptamers into sensors using a 2'-ribose-linked fluorophore. *J Am Chem Soc* **2005,** *127* (37), 12766-7.
139. Merino, E. J.; Wilkinson, K. A.; Coughlan, J. L.; Weeks, K. M., RNA structure analysis at single nucleotide resolution by selective 2'-hydroxyl acylation and primer extension (SHAPE). *J Am Chem Soc* **2005,** *127* (12), 4223-31.
140. Gherghe, C. M.; Krahn, J. M.; Weeks, K. M., Crystal structures, reactivity and inferred acylation transition states for 2'-amine substituted RNA. *J Am Chem Soc* **2005,** *127* (39), 13622-8.
141. Benjamin D. Fairbanks, E. A. S., Kristi S. Anseth, Christopher N. Bowman, Reaction Rates and Mechanisms for Radical, Photoinitated Addition of Thiols to Alkynes, and Implications for Thiol−Yne Photopolymerizations and Click Reactions. *Macromolecules* **2010,** *43* (9).
142. Paredes, E.; Das, S. R., Click chemistry for rapid labeling and ligation of RNA. *Chembiochem* **2011,** *12* (1), 125-31.

143. Winz, M. L.; Samanta, A.; Benzinger, D.; Jaschke, A., Site-specific terminal and internal labeling of RNA by poly(A) polymerase tailing and copper-catalyzed or copper-free strain-promoted click chemistry. *Nucleic Acids Res* **2012,** *40* (10), e78.
144. Sawant, A. A.; Tanpure, A. A.; Mukherjee, P. P.; Athavale, S.; Kelkar, A.; Galande, S.; Srivatsan, S. G., A versatile toolbox for posttranscriptional chemical labeling and imaging of RNA. *Nucleic Acids Res* **2016,** *44* (2), e16.
145. Winz, M. L.; Linder, E. C.; Becker, J.; Jaschke, A., Site-specific one-pot triple click labeling for DNA and RNA. *Chem Commun (Camb)* **2018,** *54* (83), 11781-11784.
146. staff, B. c., In *Blausen.com*, WikiJournal of Medicine: Medical gallery of Blausen Medical 2014, 2014.
147. Freier, S. M.; Kierzek, R.; Jaeger, J. A.; Sugimoto, N.; Caruthers, M. H.; Neilson, T.; Turner, D. H., Improved free-energy parameters for predictions of RNA duplex stability. *Proc Natl Acad Sci U S A* **1986,** *83* (24), 9373-7.
148. Egli, M., Structural Aspects of Nucleic Acid Analogs and Antisense Oligonucleotides. *Angewandte Chemie* **1996,** *35* (17).
149. Zuker, M., Mfold web server for nucleic acid folding and hybridization prediction. *Nucleic Acids Res* **2003,** *31* (13), 3406-15.
150. Hofacker, I. L., Vienna RNA secondary structure server. *Nucleic Acids Res* **2003,** *31* (13), 3429-31.
151. Andronescu, M.; Fejes, A. P.; Hutter, F.; Hoos, H. H.; Condon, A., A new algorithm for RNA secondary structure design. *J Mol Biol* **2004,** *336* (3), 607-24.
152. Andronescu, M.; Zhang, Z. C.; Condon, A., Secondary structure prediction of interacting RNA molecules. *J Mol Biol* **2005,** *345* (5), 987-1001.
153. Leontis, N. B.; Westhof, E., Geometric nomenclature and classification of RNA base pairs. *Rna* **2001,** *7* (4), 499-512.
154. Leontis, N. B.; Westhof, E., The annotation of RNA motifs. *Comp Funct Genomics* **2002,** *3* (6), 518-24.
155. Leontis, N. B.; Stombaugh, J.; Westhof, E., The non-Watson-Crick base pairs and their associated isostericity matrices. *Nucleic Acids Res* **2002,** *30* (16), 3497-531.
156. Leontis, N. B.; Westhof, E., Analysis of RNA motifs. *Curr Opin Struct Biol* **2003,** *13* (3), 300-8.
157. Crick, F. H., Codon--anticodon pairing: the wobble hypothesis. *J Mol Biol* **1966,** *19* (2), 548-55.
158. Huang, L.; Lilley, D. M. J., The kink-turn in the structural biology of RNA. *Q Rev Biophys* **2018,** *51*, e5.
159. Chworos, A., Rational Design of RNA Nanoparticles and Nanoarrays. In *RNA Nanotechnology*, Pan Stanford Publishing Pte. Ltd.: 2014.
160. Woodson, S. A., Recent insights on RNA folding mechanisms from catalytic RNA. *Cell Mol Life Sci* **2000,** *57* (5), 796-808.
161. Holbrook, S. R., RNA structure: the long and the short of it. *Curr Opin Struct Biol* **2005,** *15* (3), 302-8.
162. Leontis, N. B.; Lescoute, A.; Westhof, E., The building blocks and motifs of RNA architecture. *Curr Opin Struct Biol* **2006,** *16* (3), 279-87.
163. Hendrix, D. K.; Brenner, S. E.; Holbrook, S. R., RNA structural motifs: building blocks of a modular biomolecule. *Q Rev Biophys* **2005,** *38* (3), 221-43.
164. Popenda, M.; Szachniuk, M.; Blazewicz, M.; Wasik, S.; Burke, E. K.; Blazewicz, J.; Adamiak, R. W., RNA FRABASE 2.0: an advanced web-accessible database with the capacity to search the three-dimensional fragments within RNA structures. *BMC Bioinformatics* **2010,** *11*, 231.
165. Gandhi, M.; Caudron-Herger, M.; Diederichs, S., RNA motifs and combinatorial prediction of interactions, stability and localization of noncoding RNAs. *Nat Struct Mol Biol* **2018,** *25* (12), 1070-1076.

166. Chworos, A.; Severcan, I.; Koyfman, A. Y.; Weinkam, P.; Oroudjev, E.; Hansma, H. G.; Jaeger, L., Building programmable jigsaw puzzles with RNA. *Science* **2004,** *306* (5704), 2068-72.
167. Lescoute, A.; Westhof, E., Topology of three-way junctions in folded RNAs. *Rna* **2006,** *12* (1), 83-93.
168. Staple, D. W.; Butcher, S. E., Pseudoknots: RNA structures with diverse functions. *PLoS Biol* **2005,** *3* (6), e213.
169. Cao, S.; Chen, S. J., Structure and stability of RNA/RNA kissing complex: with application to HIV dimerization initiation signal. *Rna* **2011,** *17* (12), 2130-43.
170. De Jaeger, K.; Kavanagh, M. C.; Hill, R. P., Relationship of hypoxia to metastatic ability in rodent tumours. *Br J Cancer* **2001,** *84* (9), 1280-5.
171. Fay, M. M.; Lyons, S. M.; Ivanov, P., RNA G-Quadruplexes in Biology: Principles and Molecular Mechanisms. *J Mol Biol* **2017,** *429* (14), 2127-2147.
172. Seeman, N. C., Nucleic acid junctions and lattices. *J Theor Biol* **1982,** *99* (2), 237-47.
173. Neville R. Kallenbach, R.-I. M., Nadrian C. Seeman An immobile nucleic acid junction constructed from oligonucleotides. *Nature* **1983,** *305*.
174. Westhof, E.; Masquida, B.; Jaeger, L., RNA tectonics: towards RNA design. *Fold Des* **1996,** *1* (4), R78-88.
175. Jaeger, L., Leontis, N.B., Tecto-RNA: One-Dimensional Self-Assembly through Tertiary Interactions. *Angewandte Chemie* **2000**.
176. Seeman, N. C., Structural DNA nanotechnology: an overview. *Methods Mol Biol* **2005,** *303*, 143-66.
177. Birac, J. J.; Sherman, W. B.; Kopatsch, J.; Constantinou, P. E.; Seeman, N. C., Architecture with GIDEON, a program for design in structural DNA nanotechnology. *J Mol Graph Model* **2006,** *25* (4), 470-80.
178. Jaeger, L.; Chworos, A., The architectonics of programmable RNA and DNA nanostructures. *Curr Opin Struct Biol* **2006,** *16* (4), 531-43.
179. Yingling, Y. G.; Shapiro, B. A., Computational design of an RNA hexagonal nanoring and an RNA nanotube. *Nano Lett* **2007,** *7* (8), 2328-34.
180. Afonin, K. A.; Bindewald, E.; Yaghoubian, A. J.; Voss, N.; Jacovetty, E.; Shapiro, B. A.; Jaeger, L., In vitro assembly of cubic RNA-based scaffolds designed in silico. *Nat Nanotechnol* **2010,** *5* (9), 676-82.
181. Dirks, R. M.; Lin, M.; Winfree, E.; Pierce, N. A., Paradigms for computational nucleic acid design. *Nucleic Acids Res* **2004,** *32* (4), 1392-403.
182. Mathews, D. H.; Turner, D. H., Prediction of RNA secondary structure by free energy minimization. *Curr Opin Struct Biol* **2006,** *16* (3), 270-8.
183. Hansma, H. G.; Oroudjev, E.; Baudrey, S.; Jaeger, L., TectoRNA and 'kissing-loop' RNA: atomic force microscopy of self-assembling RNA structures. *J Microsc* **2003,** *212* (Pt 3), 273-9.
184. Geary, C.; Chworos, A.; Verzemnieks, E.; Voss, N. R.; Jaeger, L., Composing RNA Nanostructures from a Syntax of RNA Structural Modules. *Nano Lett* **2017,** *17* (11), 7095-7101.
185. Dey, S., Fan, C., Gothelf, K.V. et al., DNA origami. *Nat Rev Methods Primers* **2021,** *1* (13).
186. Rothemund, P. W., Folding DNA to create nanoscale shapes and patterns. *Nature* **2006,** *440* (7082), 297-302.
187. Douglas, S. M.; Dietz, H.; Liedl, T.; Hogberg, B.; Graf, F.; Shih, W. M., Self-assembly of DNA into nanoscale three-dimensional shapes. *Nature* **2009,** *459* (7245), 414-8.
188. Geary, C.; Rothemund, P. W.; Andersen, E. S., A single-stranded architecture for cotranscriptional folding of RNA nanostructures. *Science* **2014,** *345* (6198), 799-804.
189. Geary, C.; Grossi, G.; McRae, E. K. S.; Rothemund, P. W. K.; Andersen, E. S., RNA origami design tools enable cotranscriptional folding of kilobase-sized nanoscaffolds. *Nat Chem* **2021,** *13* (6), 549-558.

190. Hoiberg, H. C.; Sparvath, S. M.; Andersen, V. L.; Kjems, J.; Andersen, E. S., An RNA Origami Octahedron with Intrinsic siRNAs for Potent Gene Knockdown. *Biotechnol J* **2019,** *14* (1), e1700634.
191. Krissanaprasit, A.; Key, C.; Fergione, M.; Froehlich, K.; Pontula, S.; Hart, M.; Carriel, P.; Kjems, J.; Andersen, E. S.; LaBean, T. H., Genetically Encoded, Functional Single-Strand RNA Origami: Anticoagulant. *Adv Mater* **2019,** *31* (21), e1808262.
192. Krissanaprasit, A.; Key, C. M.; Froehlich, K.; Pontula, S.; Mihalko, E.; Dupont, D. M.; Andersen, E. S.; Kjems, J.; Brown, A. C.; LaBean, T. H., Multivalent Aptamer-Functionalized Single-Strand RNA Origami as Effective, Target-Specific Anticoagulants with Corresponding Reversal Agents. *Adv Healthc Mater* **2021,** *10* (11), e2001826.
193. Fire, A.; Xu, S.; Montgomery, M. K.; Kostas, S. A.; Driver, S. E.; Mello, C. C., Potent and specific genetic interference by double-stranded RNA in Caenorhabditis elegans. *Nature* **1998,** *391* (6669), 806-11.
194. Elbashir, S. M.; Lendeckel, W.; Tuschl, T., RNA interference is mediated by 21- and 22-nucleotide RNAs. *Genes Dev* **2001,** *15* (2), 188-200.
195. Kim, V. N., Small RNAs: classification, biogenesis, and function. *Mol Cells* **2005,** *19* (1), 1-15.
196. Vermeulen, A.; Behlen, L.; Reynolds, A.; Wolfson, A.; Marshall, W. S.; Karpilow, J.; Khvorova, A., The contributions of dsRNA structure to Dicer specificity and efficiency. *Rna* **2005,** *11* (5), 674-82.
197. Bergeron, L., Jr.; Perreault, J. P.; Abou Elela, S., Short RNA duplexes guide sequence-dependent cleavage by human Dicer. *Rna* **2010,** *16* (12), 2464-73.
198. Nakanishi, K., Anatomy of RISC: how do small RNAs and chaperones activate Argonaute proteins? *Wiley Interdiscip Rev RNA* **2016,** *7* (5), 637-60.
199. Reynolds, A.; Leake, D.; Boese, Q.; Scaringe, S.; Marshall, W. S.; Khvorova, A., Rational siRNA design for RNA interference. *Nat Biotechnol* **2004,** *22* (3), 326-30.
200. Zamore, P. D., Ancient pathways programmed by small RNAs. *Science* **2002,** *296* (5571), 1265-9.
201. Burton, N. O.; Burkhart, K. B.; Kennedy, S., Nuclear RNAi maintains heritable gene silencing in Caenorhabditis elegans. *Proc Natl Acad Sci U S A* **2011,** *108* (49), 19683-8.
202. Holen, T.; Amarzguioui, M.; Wiiger, M. T.; Babaie, E.; Prydz, H., Positional effects of short interfering RNAs targeting the human coagulation trigger Tissue Factor. *Nucleic Acids Res* **2002,** *30* (8), 1757-66.
203. Chiu, Y. L.; Rana, T. M., RNAi in human cells: basic structural and functional features of small interfering RNA. *Mol Cell* **2002,** *10* (3), 549-61.
204. Hu, B.; Weng, Y.; Xia, X. H.; Liang, X. J.; Huang, Y., Clinical advances of siRNA therapeutics. *J Gene Med* **2019,** *21* (7), e3097.
205. Saw, P. E.; Xu, X.; Chen, J.; Song, E. W., Non-coding RNAs: the new central dogma of cancer biology. *Sci China Life Sci* **2021,** *64* (1), 22-50.
206. Guo, S.; Tschammer, N.; Mohammed, S.; Guo, P., Specific delivery of therapeutic RNAs to cancer cells via the dimerization mechanism of phi29 motor pRNA. *Hum Gene Ther* **2005,** *16* (9), 1097-109.
207. Khaled, A.; Guo, S.; Li, F.; Guo, P., Controllable self-assembly of nanoparticles for specific delivery of multiple therapeutic molecules to cancer cells using RNA nanotechnology. *Nano Lett* **2005,** *5* (9), 1797-808.
208. Tarapore, P.; Shu, Y.; Guo, P.; Ho, S. M., Application of phi29 motor pRNA for targeted therapeutic delivery of siRNA silencing metallothionein-IIA and survivin in ovarian cancers. *Mol Ther* **2011,** *19* (2), 386-94.
209. Shu, D.; Moll, W. D.; Deng, Z.; Mao, C.; Guo, P., Bottom-up Assembly of RNA Arrays and Superstructures as Potential Parts in Nanotechnology. *Nano Lett* **2004,** *4* (9), 1717-23.

210. Grabow, W. W.; Zakrevsky, P.; Afonin, K. A.; Chworos, A.; Shapiro, B. A.; Jaeger, L., Self-Assembling RNA Nanorings Based on RNAI/II Inverse Kissing Complexes. *Nano Lett* **2011,** *11* (2), 878-887.
211. Khisamutdinov, E. F.; Jasinski, D. L.; Guo, P., RNA as a boiling-resistant anionic polymer material to build robust structures with defined shape and stoichiometry. *ACS Nano* **2014,** *8* (5), 4771-81.
212. Fujita, Y.; Furushima, R.; Ohno, H.; Sagawa, F.; Inoue, T., Cell-surface receptor control that depends on the size of a synthetic equilateral-triangular RNA-protein complex. *Sci Rep* **2014,** *4*, 6422.
213. Bindewald, E.; Afonin, K.; Jaeger, L.; Shapiro, B. A., Multistrand RNA secondary structure prediction and nanostructure design including pseudoknots. *ACS Nano* **2011,** *5* (12), 9542-51.
214. Ohuchi, S. J.; Sagawa, F.; Sakamoto, T.; Inoue, T., A trifunctional, triangular RNA-protein complex. *Febs Lett* **2015,** *589* (18), 2424-8.
215. Bui, M. N.; Brittany Johnson, M.; Viard, M.; Satterwhite, E.; Martins, A. N.; Li, Z.; Marriott, I.; Afonin, K. A.; Khisamutdinov, E. F., Versatile RNA tetra-U helix linking motif as a toolkit for nucleic acid nanotechnology. *Nanomedicine* **2017,** *13* (3), 1137-1146.
216. Guo, P. X.; Erickson, S.; Anderson, D., A small viral RNA is required for in vitro packaging of bacteriophage phi 29 DNA. *Science* **1987,** *236* (4802), 690-4.
217. Guo, P.; Zhang, C.; Chen, C.; Garver, K.; Trottier, M., Inter-RNA interaction of phage phi29 pRNA to form a hexameric complex for viral DNA transportation. *Mol Cell* **1998,** *2* (1), 149-55.
218. Guo, S.; Huang, F.; Guo, P., Construction of folate-conjugated pRNA of bacteriophage phi29 DNA packaging motor for delivery of chimeric siRNA to nasopharyngeal carcinoma cells. *Gene Ther* **2006,** *13* (10), 814-20.
219. Stewart, J. M.; Viard, M.; Subramanian, H. K.; Roark, B. K.; Afonin, K. A.; Franco, E., Programmable RNA microstructures for coordinated delivery of siRNAs. *Nanoscale* **2016,** *8* (40), 17542-17550.
220. Ohno, H.; Kobayashi, T.; Kabata, R.; Endo, K.; Iwasa, T.; Yoshimura, S. H.; Takeyasu, K.; Inoue, T.; Saito, H., Synthetic RNA-protein complex shaped like an equilateral triangle. *Nat Nanotechnol* **2011,** *6* (2), 116-20.
221. Osada, E.; Suzuki, Y.; Hidaka, K.; Ohno, H.; Sugiyama, H.; Endo, M.; Saito, H., Engineering RNA-protein complexes with different shapes for imaging and therapeutic applications. *ACS Nano* **2014,** *8* (8), 8130-40.
222. Ohuchi, S. J.; Sagawa, F.; Sakamoto, T.; Inoue, T., Altering the orientation of a fused protein to the RNA-binding ribosomal protein L7Ae and its derivatives through circular permutation. *Biochem Biophys Res Commun* **2015,** *466* (3), 388-92.
223. Jedrzejczyk, D. J., Chworos, A., Structural identification of the novel
3 way-junction motif. *DNA and RNA Nanotechnology* **2015**.
224. Ishikawa, J.; Furuta, H.; Ikawa, Y., RNA tectonics (tectoRNA) for RNA nanostructure design and its application in synthetic biology. *Wiley Interdiscip Rev RNA* **2013,** *4* (6), 651-64.
225. Severcan, I.; Geary, C.; Verzemnieks, E.; Chworos, A.; Jaeger, L., Square-shaped RNA particles from different RNA folds. *Nano Lett* **2009,** *9* (3), 1270-7.
226. Dibrov, S. M.; McLean, J.; Parsons, J.; Hermann, T., Self-assembling RNA square. *Proc Natl Acad Sci U S A* **2011,** *108* (16), 6405-8.
227. Lee, J. B.; Hong, J.; Bonner, D. K.; Poon, Z.; Hammond, P. T., Self-assembled RNA interference microsponges for efficient siRNA delivery. *Nat Mater* **2012,** *11* (4), 316-22.
228. Koyfman, A. Y.; Braun, G.; Magonov, S.; Chworos, A.; Reich, N. O.; Jaeger, L., Controlled spacing of cationic gold nanoparticles by nanocrown RNA. *J Am Chem Soc* **2005,** *127* (34), 11886-7.
229. Ohno, H.; Inoue, T., Designed Regular Tetragon-Shaped RNA-Protein Complexes with Ribosomal Protein L1 for Bionanotechnology and Synthetic Biology. *ACS Nano* **2015,** *9* (5), 4950-6.
230. Lee, A. J.; Crothers, D. M., The solution structure of an RNA loop-loop complex: the ColE1 inverted loop sequence. *Structure* **1998,** *6* (8), 993-1005.

231. Afonin, K. A.; Kireeva, M.; Grabow, W. W.; Kashlev, M.; Jaeger, L.; Shapiro, B. A., Co-transcriptional assembly of chemically modified RNA nanoparticles functionalized with siRNAs. *Nano Lett* **2012,** *12* (10), 5192-5.
232. Afonin, K. A.; Viard, M.; Koyfman, A. Y.; Martins, A. N.; Kasprzak, W. K.; Panigaj, M.; Desai, R.; Santhanam, A.; Grabow, W. W.; Jaeger, L.; Heldman, E.; Reiser, J.; Chiu, W.; Freed, E. O.; Shapiro, B. A., Multifunctional RNA nanoparticles. *Nano Lett* **2014,** *14* (10), 5662-71.
233. Afonin, K. A.; Viard, M.; Tedbury, P.; Bindewald, E.; Parlea, L.; Howington, M.; Valdman, M.; Johns-Boehme, A.; Brainerd, C.; Freed, E. O.; Shapiro, B. A., The Use of Minimal RNA Toeholds to Trigger the Activation of Multiple Functionalities. *Nano Lett* **2016,** *16* (3), 1746-53.
234. Schwarz-Schilling, M.; Dupin, A.; Chizzolini, F.; Krishnan, S.; Mansy, S. S.; Simmel, F. C., Optimized Assembly of a Multifunctional RNA-Protein Nanostructure in a Cell-Free Gene Expression System. *Nano Lett* **2018,** *18* (4), 2650-2657.
235. Johnson, M. B.; Halman, J. R.; Satterwhite, E.; Zakharov, A. V.; Bui, M. N.; Benkato, K.; Goldsworthy, V.; Kim, T.; Hong, E.; Dobrovolskaia, M. A.; Khisamutdinov, E. F.; Marriott, I.; Afonin, K. A., Programmable Nucleic Acid Based Polygons with Controlled Neuroimmunomodulatory Properties for Predictive QSAR Modeling. *Small* **2017,** *13* (42).
236. Ke, W.; Hong, E.; Saito, R. F.; Rangel, M. C.; Wang, J.; Viard, M.; Richardson, M.; Khisamutdinov, E. F.; Panigaj, M.; Dokholyan, N. V.; Chammas, R.; Dobrovolskaia, M. A.; Afonin, K. A., RNA-DNA fibers and polygons with controlled immunorecognition activate RNAi, FRET and transcriptional regulation of NF-kappaB in human cells. *Nucleic Acids Res* **2019,** *47* (3), 1350-1361.
237. Jeong, E. H.; Kim, H.; Jang, B.; Cho, H.; Ryu, J.; Kim, B.; Park, Y.; Kim, J.; Lee, J. B.; Lee, H., Technological development of structural DNA/RNA-based RNAi systems and their applications. *Adv Drug Deliv Rev* **2016,** *104*, 29-43.
238. Grabow, W. W.; Zakrevsky, P.; Afonin, K. A.; Chworos, A.; Shapiro, B. A.; Jaeger, L., Self-assembling RNA nanorings based on RNAI/II inverse kissing complexes. *Nano Lett* **2011,** *11* (2), 878-87.
239. Afonin, K. A.; Kasprzak, W.; Bindewald, E.; Puppala, P. S.; Diehl, A. R.; Hall, K. T.; Kim, T. J.; Zimmermann, M. T.; Jernigan, R. L.; Jaeger, L.; Shapiro, B. A., Computational and experimental characterization of RNA cubic nanoscaffolds. *Methods* **2014,** *67* (2), 256-65.
240. Afonin, K. A.; Viard, M.; Kagiampakis, I.; Case, C. L.; Dobrovolskaia, M. A.; Hofmann, J.; Vrzak, A.; Kireeva, M.; Kasprzak, W. K.; KewalRamani, V. N.; Shapiro, B. A., Triggering of RNA interference with RNA-RNA, RNA-DNA, and DNA-RNA nanoparticles. *ACS Nano* **2015,** *9* (1), 251-9.
241. Halman, J. R.; Satterwhite, E.; Roark, B.; Chandler, M.; Viard, M.; Ivanina, A.; Bindewald, E.; Kasprzak, W. K.; Panigaj, M.; Bui, M. N.; Lu, J. S.; Miller, J.; Khisamutdinov, E. F.; Shapiro, B. A.; Dobrovolskaia, M. A.; Afonin, K. A., Functionally-interdependent shape-switching nanoparticles with controllable properties. *Nucleic Acids Res* **2017,** *45* (4), 2210-2220.
242. Azharuddin, M.; Zhu, G. H.; Das, D.; Ozgur, E.; Uzun, L.; Turner, A. P. F.; Patra, H. K., A repertoire of biomedical applications of noble metal nanoparticles. *Chem Commun (Camb)* **2019,** *55* (49), 6964-6996.
243. Connor, E. E.; Mwamuka, J.; Gole, A.; Murphy, C. J.; Wyatt, M. D., Gold nanoparticles are taken up by human cells but do not cause acute cytotoxicity. *Small* **2005,** *1* (3), 325-7.
244. Yeh, Y. C.; Creran, B.; Rotello, V. M., Gold nanoparticles: preparation, properties, and applications in bionanotechnology. *Nanoscale* **2012,** *4* (6), 1871-80.
245. Amendola, V.; Pilot, R.; Frasconi, M.; Marago, O. M.; Iati, M. A., Surface plasmon resonance in gold nanoparticles: a review. *J Phys Condens Matter* **2017,** *29* (20), 203002.
246. Khan, A. K., Rashid, R., Murtaza, G., Zahra, A., Gold Nanoparticles: Synthesis and Applications in Drug Delivery. **2014**.
247. Yue, J.; Feliciano, T. J.; Li, W.; Lee, A.; Odom, T. W., Gold Nanoparticle Size and Shape Effects on Cellular Uptake and Intracellular Distribution of siRNA Nanoconstructs. *Bioconjug Chem* **2017,** *28* (6), 1791-1800.

248. Steckiewicz, K. P.; Barcinska, E.; Malankowska, A.; Zauszkiewicz-Pawlak, A.; Nowaczyk, G.; Zaleska-Medynska, A.; Inkielewicz-Stepniak, I., Impact of gold nanoparticles shape on their cytotoxicity against human osteoblast and osteosarcoma in in vitro model. Evaluation of the safety of use and anti-cancer potential. *J Mater Sci Mater Med* **2019,** *30* (2), 22.
249. Han, G.; Martin, C. T.; Rotello, V. M., Stability of gold nanoparticle-bound DNA toward biological, physical, and chemical agents. *Chem Biol Drug Des* **2006,** *67* (1), 78-82.
250. Minakshi Das, K. H. S., Seong Soo A An, Dong Kee Yi, Review on gold nanoparticles and their applications. *Toxicology and Environmental Health Sciences* **2011**.
251. Weintraub, K., Biomedicine: The new gold standard. *Nature* **2013,** *495* (7440), S14-6.
252. Hong, R.; Han, G.; Fernandez, J. M.; Kim, B. J.; Forbes, N. S.; Rotello, V. M., Glutathione-mediated delivery and release using monolayer protected nanoparticle carriers. *J Am Chem Soc* **2006,** *128* (4), 1078-9.
253. L. Dziawer, P. K., S. Męczyńska-Wielgosz, M. Pruszyński, M. Łyczko, B. Wąs, G. Celichowski, J. Grobelny, J. Jastrzębski, A. Bilewicz, Gold nanoparticle bioconjugates labelled with 211At for targeted alpha therapy. *Rsc Adv* **2017,** (65).
254. Wang, Y.; Ni, Y., Combination of UV-vis spectroscopy and chemometrics to understand protein-nanomaterial conjugate: a case study on human serum albumin and gold nanoparticles. *Talanta* **2014,** *119*, 320-30.
255. Sotnikov, D. V.; Berlina, A. N.; Ivanov, V. S.; Zherdev, A. V.; Dzantiev, B. B., Adsorption of proteins on gold nanoparticles: One or more layers? *Colloids Surf B Biointerfaces* **2019,** *173*, 557-563.
256. Liu, F.; Wang, L.; Wang, H.; Yuan, L.; Li, J.; Brash, J. L.; Chen, H., Modulating the activity of protein conjugated to gold nanoparticles by site-directed orientation and surface density of bound protein. *ACS Appl Mater Interfaces* **2015,** *7* (6), 3717-24.
257. Czechowska, E.; Ranoszek-Soliwoda, K.; Tomaszewska, E.; Pudlarz, A.; Celichowski, G.; Gralak-Zwolenik, D.; Szemraj, J.; Grobelny, J., Comparison of the antioxidant activity of catalase immobilized on gold nanoparticles via specific and non-specific adsorption. *Colloids Surf B Biointerfaces* **2018,** *171*, 707-714.
258. Pudlarz, A. M.; Czechowska, E.; Ranoszek-Soliwoda, K.; Tomaszewska, E.; Celichowski, G.; Grobelny, J.; Szemraj, J., Immobilization of Recombinant Human Catalase on Gold and Silver Nanoparticles. *Appl Biochem Biotechnol* **2018,** *185* (3), 717-735.
259. Khashayar, P.; Amoabediny, G.; Larijani, B.; Hosseini, M.; Vanfleteren, J., Fabrication and Verification of Conjugated AuNP-Antibody Nanoprobe for Sensitivity Improvement in Electrochemical Biosensors. *Sci Rep* **2017,** *7* (1), 16070.
260. Busch, R. T.; Karim, F.; Weis, J.; Sun, Y.; Zhao, C.; Vasquez, E. S., Optimization and Structural Stability of Gold Nanoparticle-Antibody Bioconjugates. *ACS Omega* **2019,** *4* (12), 15269-15279.
261. Dykman, L. A.; Khlebtsov, N. G., Gold nanoparticles in chemo-, immuno-, and combined therapy: review [Invited]. *Biomed Opt Express* **2019,** *10* (7), 3152-3182.
262. Lupusoru, R. V.; Pricop, D. A.; Uritu, C. M.; Arvinte, A.; Coroaba, A.; Esanu, I.; Zaltariov, M. F.; Silion, M.; Stefanescu, C.; Pinteala, M., Effect of TAT-DOX-PEG irradiated gold nanoparticles conjugates on human osteosarcoma cells. *Sci Rep* **2020,** *10* (1), 6591.
263. Camerin, M.; Magaraggia, M.; Soncin, M.; Jori, G.; Moreno, M.; Chambrier, I.; Cook, M. J.; Russell, D. A., The in vivo efficacy of phthalocyanine-nanoparticle conjugates for the photodynamic therapy of amelanotic melanoma. *Eur J Cancer* **2010,** *46* (10), 1910-8.
264. Labala, S.; Jose, A.; Venuganti, V. V., Transcutaneous iontophoretic delivery of STAT3 siRNA using layer-by-layer chitosan coated gold nanoparticles to treat melanoma. *Colloids Surf B Biointerfaces* **2016,** *146*, 188-97.
265. Mohammadi, Z.; Sazgarnia, A.; Rajabi, O.; Seilanian Toosi, M., Comparative study of X-ray treatment and photodynamic therapy by using 5-aminolevulinic acid conjugated gold nanoparticles in a melanoma cell line. *Artif Cells Nanomed Biotechnol* **2017,** *45* (3), 467-473.

266. Huang, X.; Li, M.; Xu, Y.; Zhang, J.; Meng, X.; An, X.; Sun, L.; Guo, L.; Shan, X.; Ge, J.; Chen, J.; Luo, Y.; Wu, H.; Zhang, Y.; Jiang, Q.; Ning, X., Novel Gold Nanorod-Based HR1 Peptide Inhibitor for Middle East Respiratory Syndrome Coronavirus. *ACS Appl Mater Interfaces* **2019,** *11* (22), 19799-19807.
267. Huang, X.; Jain, P. K.; El-Sayed, I. H.; El-Sayed, M. A., Plasmonic photothermal therapy (PPTT) using gold nanoparticles. *Lasers Med Sci* **2008,** *23* (3), 217-28.
268. Kennedy, L. C.; Bickford, L. R.; Lewinski, N. A.; Coughlin, A. J.; Hu, Y.; Day, E. S.; West, J. L.; Drezek, R. A., A new era for cancer treatment: gold-nanoparticle-mediated thermal therapies. *Small* **2011,** *7* (2), 169-83.
269. Day, E. S.; Zhang, L.; Thompson, P. A.; Zawaski, J. A.; Kaffes, C. C.; Gaber, M. W.; Blaney, S. M.; West, J. L., Vascular-targeted photothermal therapy of an orthotopic murine glioma model. *Nanomedicine (Lond)* **2012,** *7* (8), 1133-48.
270. Vines, J. B.; Yoon, J. H.; Ryu, N. E.; Lim, D. J.; Park, H., Gold Nanoparticles for Photothermal Cancer Therapy. *Front Chem* **2019,** *7*, 167.
271. Huefner, A.; Septiadi, D.; Wilts, B. D.; Patel, II; Kuan, W. L.; Fragniere, A.; Barker, R. A.; Mahajan, S., Gold nanoparticles explore cells: cellular uptake and their use as intracellular probes. *Methods* **2014,** *68* (2), 354-63.
272. D'Acunto, M., Detection of Intracellular Gold Nanoparticles: An Overview. *Materials (Basel)* **2018,** *11* (6).
273. Song, K. H.; Kim, C.; Cobley, C. M.; Xia, Y.; Wang, L. V., Near-infrared gold nanocages as a new class of tracers for photoacoustic sentinel lymph node mapping on a rat model. *Nano Lett* **2009,** *9* (1), 183-8.
274. Rogers, N. J.; Jeffery, H. C.; Claire, S.; Lewis, D. J.; Zikeli, G.; Hodges, N. J.; Egginton, S.; Nash, G. B.; Pikramenou, Z., Tailoring iridium luminescence and gold nanoparticle size for imaging of microvascular blood flow. *Nanomedicine (Lond)* **2017,** *12* (22), 2725-2740.
275. Bagheri, S.; Yasemi, M.; Safaie-Qamsari, E.; Rashidiani, J.; Abkar, M.; Hassani, M.; Mirhosseini, S. A.; Kooshki, H., Using gold nanoparticles in diagnosis and treatment of melanoma cancer. *Artif Cells Nanomed Biotechnol* **2018,** *46* (sup1), 462-471.
276. Meola, A.; Rao, J.; Chaudhary, N.; Sharma, M.; Chang, S. D., Gold Nanoparticles for Brain Tumor Imaging: A Systematic Review. *Front Neurol* **2018,** *9*, 328.
277. Cichomski, M., Tomaszewska, E., Kośla, K., Kozłowski, W., Kowalczyk, P.J., Grobelny, J., Study of dithiol monolayer as the interface for controlled deposition of gold nanoparticles. *Materials Characterization* **2011,** *62*.
278. Chen, X.; Wei, M.; Jiang, S.; Forster, S., Two Growth Mechanisms of Thiol-Capped Gold Nanoparticles Controlled by Ligand Chemistry. *Langmuir* **2019,** *35* (37), 12130-12138.
279. Watanabe, S.; Yoshida, K.; Shinkawa, K.; Kumagawa, D.; Seguchi, H., Thioglucose-stabilized gold nanoparticles as a novel platform for colorimetric bioassay based on nanoparticle aggregation. *Colloids Surf B Biointerfaces* **2010,** *81* (2), 570-7.
280. Spampinato, V.; Parracino, M. A.; La Spina, R.; Rossi, F.; Ceccone, G., Surface Analysis of Gold Nanoparticles Functionalized with Thiol-Modified Glucose SAMs for Biosensor Applications. *Front Chem* **2016,** *4*, 8.
281. Geng, F.; Song, K.; Xing, J. Z.; Yuan, C.; Yan, S.; Yang, Q.; Chen, J.; Kong, B., Thio-glucose bound gold nanoparticles enhance radio-cytotoxic targeting of ovarian cancer. *Nanotechnology* **2011,** *22* (28), 285101.
282. Hu, C.; Niestroj, M.; Yuan, D.; Chang, S.; Chen, J., Treating cancer stem cells and cancer metastasis using glucose-coated gold nanoparticles. *Int J Nanomedicine* **2015,** *10*, 2065-77.
283. Suvarna, S.; Das, U.; Kc, S.; Mishra, S.; Sudarshan, M.; Saha, K. D.; Dey, S.; Chakraborty, A.; Narayana, Y., Synthesis of a novel glucose capped gold nanoparticle as a better theranostic candidate. *PLoS One* **2017,** *12* (6), e0178202.
284. Tomaszewska, E. e. a., Systematic Studies of Gold Nanoparticles Functionalised with Thioglucose and its Cytotoxic Effect. *Chemistry Select* **2021**.

285. Cruz, L. J.; Tacken, P. J.; Rueda, F.; Domingo, J. C.; Albericio, F.; Figdor, C. G., Targeting nanoparticles to dendritic cells for immunotherapy. *Methods Enzymol* **2012,** *509*, 143-63.
286. Jia, J.; Zhang, Y.; Xin, Y.; Jiang, C.; Yan, B.; Zhai, S., Interactions Between Nanoparticles and Dendritic Cells: From the Perspective of Cancer Immunotherapy. *Front Oncol* **2018,** *8*, 404.
287. Surendran, S. P.; Moon, M. J.; Park, R.; Jeong, Y. Y., Bioactive Nanoparticles for Cancer Immunotherapy. *Int J Mol Sci* **2018,** *19* (12).
288. Zhang, J.; Luo, X.; Wu, Y. P.; Wu, F.; Li, Y. F.; He, R. R.; Liu, M., Rod in Tube: A Novel Nanoplatform for Highly Effective Chemo-Photothermal Combination Therapy toward Breast Cancer. *ACS Appl Mater Interfaces* **2019,** *11* (4), 3690-3703.
289. Zhang, D.; Qin, X.; Wu, T.; Qiao, Q.; Song, Q.; Zhang, Z., Extracellular vesicles based self-grown gold nanopopcorn for combinatorial chemo-photothermal therapy. *Biomaterials* **2019,** *197*, 220-228.
290. Ding, Y.; Jiang, Z.; Saha, K.; Kim, C. S.; Kim, S. T.; Landis, R. F.; Rotello, V. M., Gold nanoparticles for nucleic acid delivery. *Mol Ther* **2014,** *22* (6), 1075-1083.
291. Sharon Madhuri, N. I., Sharon Maheshwar Platinum nanocomposites and its applications: A review. *Advances in materials Research* **2017**.
292. Chen, A.; Holt-Hindle, P., Platinum-based nanostructured materials: synthesis, properties, and applications. *Chem Rev* **2010,** *110* (6), 3767-804.
293. FDA Backgrounder on Platinum in Silicone Breast Implants. https://www.fda.gov/medical-devices/breast-implants/fda-backgrounder-platinum-silicone-breast-implants.
294. Horie, M.; Kato, H.; Endoh, S.; Fujita, K.; Nishio, K.; Komaba, L. K.; Fukui, H.; Nakamura, A.; Miyauchi, A.; Nakazato, T.; Kinugasa, S.; Yoshida, Y.; Hagihara, Y.; Morimoto, Y.; Iwahashi, H., Evaluation of cellular influences of platinum nanoparticles by stable medium dispersion. *Metallomics* **2011,** *3* (11), 1244-52.
295. Brown, A. L.; Kai, M. P.; DuRoss, A. N.; Sahay, G.; Sun, C., Biodistribution and Toxicity of Micellar Platinum Nanoparticles in Mice via Intravenous Administration. *Nanomaterials (Basel)* **2018,** *8* (6).
296. Gopal, J.; Hasan, N.; Manikandan, M.; Wu, H. F., Bacterial toxicity/compatibility of platinum nanospheres, nanocuboids and nanoflowers. *Sci Rep* **2013,** *3*, 1260.
297. Gopal, J.; Muthu, M.; Paul, D.; Kim, D. H.; Chun, S., Bactericidal activity of green tea extracts: the importance of catechin containing nano particles. *Sci Rep* **2016,** *6*, 19710.
298. Tanaka, S.; Miyazaki, J.; Tiwari, D. K.; Jin, T.; Inouye, Y., Fluorescent platinum nanoclusters: synthesis, purification, characterization, and application to bioimaging. *Angew Chem Int Ed Engl* **2011,** *50* (2), 431-5.
299. Yuan, X.; Luo, Z.; Zhang, Q.; Zhang, X.; Zheng, Y.; Lee, J. Y.; Xie, J., Synthesis of highly fluorescent metal (Ag, Au, Pt, and Cu) nanoclusters by electrostatically induced reversible phase transfer. *ACS Nano* **2011,** *5* (11), 8800-8.
300. Ju, Y.; Kim, J., Dendrimer-encapsulated Pt nanoparticles with peroxidase-mimetic activity as biocatalytic labels for sensitive colorimetric analyses. *Chem Commun (Camb)* **2015,** *51* (72), 13752-5.
301. Pedone, D.; Moglianetti, M.; De Luca, E.; Bardi, G.; Pompa, P. P., Platinum nanoparticles in nanobiomedicine. *Chem Soc Rev* **2017,** *46* (16), 4951-4975.
302. Porcel, E.; Liehn, S.; Remita, H.; Usami, N.; Kobayashi, K.; Furusawa, Y.; Le Sech, C.; Lacombe, S., Platinum nanoparticles: a promising material for future cancer therapy? *Nanotechnology* **2010,** *21* (8), 85103.
303. Yue, Y., Wagner, S., Medina-Kauwe, L., Cui, X., Zhang, G., Shiao, S., Sandler, H., Fraass, B., WE-FG-BRA-11: Theranostic Platinum Nanoparticle for Radiation Sensitization in Breast Cancer Radiotherapy. *Medical Physics* **2016**.
304. Kanav Midha, G. S., Manju Nagpal, Sandeep Arora, Potential Application of Silver Nanoparticles in Medicine. *Nanoscience & Nanotechnology-Asi* **2015**.

305. Siddiqi, K. S.; Husen, A.; Rao, R. A. K., A review on biosynthesis of silver nanoparticles and their biocidal properties. *J Nanobiotechnology* **2018,** *16* (1), 14.
306. Karthik, C. S.; Manukumar, H. M.; Sandeep, S.; Sudarshan, B. L.; Nagashree, S.; Mallesha, L.; Rakesh, K. P.; Sanjay, K. R.; Mallu, P.; Qin, H. L., Development of piperazine-1-carbothioamide chitosan silver nanoparticles (P1C-Tit*CAgNPs) as a promising anti-inflammatory candidate: a molecular docking validation. *Medchemcomm* **2018,** *9* (4), 713-724.
307. Mukti Sharma, S. Y., Man Srivastava, Narayanan Ganesh, Shalini Srivastava, Promising anti-inflammatory bio-efficacy of saponin loaded silver nanoparticles prepared from the plant Madhuca longifolia. **2018**.
308. Tang, S.; Zheng, J., Antibacterial Activity of Silver Nanoparticles: Structural Effects. *Adv Healthc Mater* **2018,** *7* (13), e1701503.
309. Burdusel, A. C.; Gherasim, O.; Grumezescu, A. M.; Mogoanta, L.; Ficai, A.; Andronescu, E., Biomedical Applications of Silver Nanoparticles: An Up-to-Date Overview. *Nanomaterials (Basel)* **2018,** *8* (9).
310. Rai, M.; Ingle, A. P.; Paralikar, P.; Gupta, I.; Medici, S.; Santos, C. A., Recent advances in use of silver nanoparticles as antimalarial agents. *Int J Pharm* **2017,** *526* (1-2), 254-270.
311. Benyettou, F.; Rezgui, R.; Ravaux, F.; Jaber, T.; Blumer, K.; Jouiad, M.; Motte, L.; Olsen, J. C.; Platas-Iglesias, C.; Magzoub, M.; Trabolsi, A., Synthesis of silver nanoparticles for the dual delivery of doxorubicin and alendronate to cancer cells. *J Mater Chem B* **2015,** *3* (36), 7237-7245.
312. Muhammad, Z.; Raza, A.; Ghafoor, S.; Naeem, A.; Naz, S. S.; Riaz, S.; Ahmed, W.; Rana, N. F., PEG capped methotrexate silver nanoparticles for efficient anticancer activity and biocompatibility. *Eur J Pharm Sci* **2016,** *91*, 251-5.
313. Petrov, P. D., Yoncheva, K., Gancheva, V., Konstantinov, S., Trzebicka, B., Multifunctional block copolymer nanocarriers for co-delivery of silver nanoparticles and curcumin: Synthesis and enhanced efficacy against tumor cells. *European Polymer Journal* **2016,** *81*.
314. Brown, P. K.; Qureshi, A. T.; Moll, A. N.; Hayes, D. J.; Monroe, W. T., Silver nanoscale antisense drug delivery system for photoactivated gene silencing. *ACS Nano* **2013,** *7* (4), 2948-59.
315. Ding, Q.; Liu, D.; Guo, D.; Yang, F.; Pang, X.; Che, R.; Zhou, N.; Xie, J.; Sun, J.; Huang, Z.; Gu, N., Shape-controlled fabrication of magnetite silver hybrid nanoparticles with high performance magnetic hyperthermia. *Biomaterials* **2017,** *124*, 35-46.
316. Poudel, B. K.; Soe, Z. C.; Ruttala, H. B.; Gupta, B.; Ramasamy, T.; Thapa, R. K.; Gautam, M.; Ou, W.; Nguyen, H. T.; Jeong, J. H.; Jin, S. G.; Choi, H. G.; Yong, C. S.; Kim, J. O., In situ fabrication of mesoporous silica-coated silver-gold hollow nanoshell for remotely controllable chemo-photothermal therapy via phase-change molecule as gatekeepers. *Int J Pharm* **2018,** *548* (1), 92-103.
317. Vedelago, J.; Mattea, F.; Valente, M., Integration of Fricke gel dosimetry with Ag nanoparticles for experimental dose enhancement determination in theranostics. *Appl Radiat Isot* **2018,** *141*, 182-186.
318. Noronha, V. T.; Paula, A. J.; Duran, G.; Galembeck, A.; Cogo-Muller, K.; Franz-Montan, M.; Duran, N., Silver nanoparticles in dentistry. *Dent Mater* **2017,** *33* (10), 1110-1126.
319. Manikandan, V.; Velmurugan, P.; Park, J. H.; Chang, W. S.; Park, Y. J.; Jayanthi, P.; Cho, M.; Oh, B. T., Green synthesis of silver oxide nanoparticles and its antibacterial activity against dental pathogens. *3 Biotech* **2017,** *7* (1), 72.
320. Chambers, C.; Stewart, S. B.; Su, B.; Jenkinson, H. F.; Sandy, J. R.; Ireland, A. J., Silver doped titanium dioxide nanoparticles as antimicrobial additives to dental polymers. *Dent Mater* **2017,** *33* (3), e115-e123.
321. Marek Konop, T. D., Aleksandra Misicka, Lidia Rudnicka, Certain Aspects of Silver and Silver Nanoparticles in Wound Care: A Minireview. *Journal of Nanomaterials* **2016**.
322. Hendiger, E. B.; Padzik, M.; Zochowska, A.; Baltaza, W.; Oledzka, G.; Zyskowska, D.; Bluszcz, J.; Jarzynka, S.; Chomicz, L.; Grodzik, M.; Hendiger, J.; Pinero, J. E.; Grobelny, J.; Ranoszek-Soliwoda, K.; Lorenzo-Morales, J., Tannic acid-modified silver nanoparticles enhance the

anti-Acanthamoeba activity of three multipurpose contact lens solutions without increasing their cytotoxicity. *Parasit Vectors* **2020,** *13* (1), 624.
323. Orlowski, P.; Kowalczyk, A.; Tomaszewska, E.; Ranoszek-Soliwoda, K.; Wegrzyn, A.; Grzesiak, J.; Celichowski, G.; Grobelny, J.; Eriksson, K.; Krzyzowska, M., Antiviral Activity of Tannic Acid Modified Silver Nanoparticles: Potential to Activate Immune Response in Herpes Genitalis. *Viruses* **2018,** *10* (10).
324. Orlowski, P.; Zmigrodzka, M.; Tomaszewska, E.; Ranoszek-Soliwoda, K.; Czupryn, M.; Antos-Bielska, M.; Szemraj, J.; Celichowski, G.; Grobelny, J.; Krzyzowska, M., Tannic acid-modified silver nanoparticles for wound healing: the importance of size. *Int J Nanomedicine* **2018,** *13*, 991-1007.
325. Orlowski, P.; Zmigrodzka, M.; Tomaszewska, E.; Ranoszek-Soliwoda, K.; Pajak, B.; Slonska, A.; Cymerys, J.; Celichowski, G.; Grobelny, J.; Krzyzowska, M., Polyphenol-Conjugated Bimetallic Au@AgNPs for Improved Wound Healing. *Int J Nanomedicine* **2020,** *15*, 4969-4990.
326. Paladini, F.; Pollini, M., Antimicrobial Silver Nanoparticles for Wound Healing Application: Progress and Future Trends. *Materials (Basel)* **2019,** *12* (16).
327. Jedrzejczyk, D.; Gendaszewska-Darmach, E.; Pawlowska, R.; Chworos, A., Designing synthetic RNA for delivery by nanoparticles. *J Phys Condens Matter* **2017,** *29* (12), 123001.
328. Mirkin, C. A.; Letsinger, R. L.; Mucic, R. C.; Storhoff, J. J., A DNA-based method for rationally assembling nanoparticles into macroscopic materials. *Nature* **1996,** *382* (6592), 607-9.
329. Cutler, J. I.; Auyeung, E.; Mirkin, C. A., Spherical nucleic acids. *J Am Chem Soc* **2012,** *134* (3), 1376-91.
330. Barnaby, S. N.; Perelman, G. A.; Kohlstedt, K. L.; Chinen, A. B.; Schatz, G. C.; Mirkin, C. A., Design Considerations for RNA Spherical Nucleic Acids (SNAs). *Bioconjug Chem* **2016,** *27* (9), 2124-31.
331. Kapadia, C. H.; Melamed, J. R.; Day, E. S., Spherical Nucleic Acid Nanoparticles: Therapeutic Potential. *BioDrugs* **2018,** *32* (4), 297-309.
332. Giljohann, D. A.; Seferos, D. S.; Prigodich, A. E.; Patel, P. C.; Mirkin, C. A., Gene regulation with polyvalent siRNA-nanoparticle conjugates. *J Am Chem Soc* **2009,** *131* (6), 2072-3.
333. Patel, P. C.; Hao, L.; Yeung, W. S.; Mirkin, C. A., Duplex end breathing determines serum stability and intracellular potency of siRNA-Au NPs. *Mol Pharm* **2011,** *8* (4), 1285-91.
334. Zheng, D.; Giljohann, D. A.; Chen, D. L.; Massich, M. D.; Wang, X. Q.; Iordanov, H.; Mirkin, C. A.; Paller, A. S., Topical delivery of siRNA-based spherical nucleic acid nanoparticle conjugates for gene regulation. *Proc Natl Acad Sci U S A* **2012,** *109* (30), 11975-80.
335. Jensen, S. A.; Day, E. S.; Ko, C. H.; Hurley, L. A.; Luciano, J. P.; Kouri, F. M.; Merkel, T. J.; Luthi, A. J.; Patel, P. C.; Cutler, J. I.; Daniel, W. L.; Scott, A. W.; Rotz, M. W.; Meade, T. J.; Giljohann, D. A.; Mirkin, C. A.; Stegh, A. H., Spherical nucleic acid nanoparticle conjugates as an RNAi-based therapy for glioblastoma. *Sci Transl Med* **2013,** *5* (209), 209ra152.
336. Kim, H. J.; Takemoto, H.; Yi, Y.; Zheng, M.; Maeda, Y.; Chaya, H.; Hayashi, K.; Mi, P.; Pittella, F.; Christie, R. J.; Toh, K.; Matsumoto, Y.; Nishiyama, N.; Miyata, K.; Kataoka, K., Precise engineering of siRNA delivery vehicles to tumors using polyion complexes and gold nanoparticles. *ACS Nano* **2014,** *8* (9), 8979-91.
337. Barnaby, S. N.; Lee, A.; Mirkin, C. A., Probing the inherent stability of siRNA immobilized on nanoparticle constructs. *Proc Natl Acad Sci U S A* **2014,** *111* (27), 9739-44.
338. Kranz, L. M.; Diken, M.; Haas, H.; Kreiter, S.; Loquai, C.; Reuter, K. C.; Meng, M.; Fritz, D.; Vascotto, F.; Hefesha, H.; Grunwitz, C.; Vormehr, M.; Husemann, Y.; Selmi, A.; Kuhn, A. N.; Buck, J.; Derhovanessian, E.; Rae, R.; Attig, S.; Diekmann, J.; Jabulowsky, R. A.; Heesch, S.; Hassel, J.; Langguth, P.; Grabbe, S.; Huber, C.; Tureci, O.; Sahin, U., Systemic RNA delivery to dendritic cells exploits antiviral defence for cancer immunotherapy. *Nature* **2016,** *534* (7607), 396-401.
339. Elbakry, A.; Zaky, A.; Liebl, R.; Rachel, R.; Goepferich, A.; Breunig, M., Layer-by-layer assembled gold nanoparticles for siRNA delivery. *Nano Lett* **2009,** *9* (5), 2059-64.

340. Kim, S. T.; Chompoosor, A.; Yeh, Y. C.; Agasti, S. S.; Solfiell, D. J.; Rotello, V. M., Dendronized gold nanoparticles for siRNA delivery. *Small* **2012,** *8* (21), 3253-6.
341. Conde, J.; Rosa, J.; de la Fuente, J. M.; Baptista, P. V., Gold-nanobeacons for simultaneous gene specific silencing and intracellular tracking of the silencing events. *Biomaterials* **2013,** *34* (10), 2516-23.
342. Shaat, H.; Mostafa, A.; Moustafa, M.; Gamal-Eldeen, A.; Emam, A.; El-Hussieny, E.; Elhefnawi, M., Modified gold nanoparticles for intracellular delivery of anti-liver cancer siRNA. *Int J Pharm* **2016,** *504* (1-2), 125-33.
343. Guo, J.; O'Driscoll, C. M.; Holmes, J. D.; Rahme, K., Bioconjugated gold nanoparticles enhance cellular uptake: A proof of concept study for siRNA delivery in prostate cancer cells. *Int J Pharm* **2016,** *509* (1-2), 16-27.
344. Hou, W.; Wei, P.; Kong, L.; Guo, R.; Wang, S.; Shi, X., Partially PEGylated dendrimer-entrapped gold nanoparticles: a promising nanoplatform for highly efficient DNA and siRNA delivery. *J Mater Chem B* **2016,** *4* (17), 2933-2943.
345. Graczyk, A.; Pawlowska, R.; Jedrzejczyk, D.; Chworos, A., Gold Nanoparticles in Conjunction with Nucleic Acids as a Modern Molecular System for Cellular Delivery. *Molecules* **2020,** *25* (1).
346. Radovic-Moreno, A. F.; Chernyak, N.; Mader, C. C.; Nallagatla, S.; Kang, R. S.; Hao, L.; Walker, D. A.; Halo, T. L.; Merkel, T. J.; Rische, C. H.; Anantatmula, S.; Burkhart, M.; Mirkin, C. A.; Gryaznov, S. M., Immunomodulatory spherical nucleic acids. *Proc Natl Acad Sci U S A* **2015,** *112* (13), 3892-7.
347. Majer, O.; Liu, B.; Barton, G. M., Nucleic acid-sensing TLRs: trafficking and regulation. *Curr Opin Immunol* **2017,** *44*, 26-33.
348. Zhuo, Z.; Yu, Y.; Wang, M.; Li, J.; Zhang, Z.; Liu, J.; Wu, X.; Lu, A.; Zhang, G.; Zhang, B., Recent Advances in SELEX Technology and Aptamer Applications in Biomedicine. *Int J Mol Sci* **2017,** *18* (10).
349. Lupold, S. E.; Hicke, B. J.; Lin, Y.; Coffey, D. S., Identification and characterization of nuclease-stabilized RNA molecules that bind human prostate cancer cells via the prostate-specific membrane antigen. *Cancer Res* **2002,** *62* (14), 4029-33.
350. Javier, D. J.; Nitin, N.; Levy, M.; Ellington, A.; Richards-Kortum, R., Aptamer-targeted gold nanoparticles as molecular-specific contrast agents for reflectance imaging. *Bioconjug Chem* **2008,** *19* (6), 1309-12.
351. Kim, D.; Jeong, Y. Y.; Jon, S., A drug-loaded aptamer-gold nanoparticle bioconjugate for combined CT imaging and therapy of prostate cancer. *ACS Nano* **2010,** *4* (7), 3689-96.
352. Ling, K.; Jiang, H.; Zhang, L.; Li, Y.; Yang, L.; Qiu, C.; Li, F. R., A self-assembling RNA aptamer-based nanoparticle sensor for fluorometric detection of Neomycin B in milk. *Anal Bioanal Chem* **2016,** *408* (13), 3593-600.
353. Garst, A. D.; Edwards, A. L.; Batey, R. T., Riboswitches: structures and mechanisms. *Cold Spring Harb Perspect Biol* **2011,** *3* (6).
354. Seetharaman, S.; Zivarts, M.; Sudarsan, N.; Breaker, R. R., Immobilized RNA switches for the analysis of complex chemical and biological mixtures. *Nat Biotechnol* **2001,** *19* (4), 336-41.
355. Hao, L.; Patel, P. C.; Alhasan, A. H.; Giljohann, D. A.; Mirkin, C. A., Nucleic acid-gold nanoparticle conjugates as mimics of microRNA. *Small* **2011,** *7* (22), 3158-62.
356. Lee, J. S.; Green, J. J.; Love, K. T.; Sunshine, J.; Langer, R.; Anderson, D. G., Gold, poly(beta-amino ester) nanoparticles for small interfering RNA delivery. *Nano Lett* **2009,** *9* (6), 2402-6.
357. Yi, Y.; Kim, H. J.; Mi, P.; Zheng, M.; Takemoto, H.; Toh, K.; Kim, B. S.; Hayashi, K.; Naito, M.; Matsumoto, Y.; Miyata, K.; Kataoka, K., Targeted systemic delivery of siRNA to cervical cancer model using cyclic RGD-installed unimer polyion complex-assembled gold nanoparticles. *J Control Release* **2016,** *244* (Pt B), 247-256.
358. Allhenn, D.; Boushehri, M. A.; Lamprecht, A., Drug delivery strategies for the treatment of malignant gliomas. *Int J Pharm* **2012,** *436* (1-2), 299-310.

359. Kong, L.; Qiu, J.; Sun, W.; Yang, J.; Shen, M.; Wang, L.; Shi, X., Multifunctional PEI-entrapped gold nanoparticles enable efficient delivery of therapeutic siRNA into glioblastoma cells. *Biomater Sci* **2017,** *5* (2), 258-266.
360. Gugliotti, L. A.; Feldheim, D. L.; Eaton, B. E., RNA-mediated control of metal nanoparticle shape. *J Am Chem Soc* **2005,** *127* (50), 17814-8.
361. Koyfman, A. Y.; Braun, G.; Magonov, S.; Chworos, A.; Reich, N. O.; Jaeger, L., Controlled spacing of cationic gold nanoparticles by nanocrown RNA. *J Am Chem Soc* **2005,** *127* (34), 11886-11887.
362. Chen, Y.; Liu, Q.; Guo, D., Emerging coronaviruses: Genome structure, replication, and pathogenesis. *J Med Virol* **2020,** *92* (4), 418-423.
363. Brenner, S.; Jacob, F.; Meselson, M., An unstable intermediate carrying information from genes to ribosomes for protein synthesis. *Nature* **1961,** *190*, 576-581.
364. Gros, F.; Hiatt, H.; Gilbert, W.; Kurland, C. G.; Risebrough, R. W.; Watson, J. D., Unstable ribonucleic acid revealed by pulse labelling of Escherichia coli. *Nature* **1961,** *190*, 581-5.
365. Adams, D.; Gonzalez-Duarte, A.; O'Riordan, W. D.; Yang, C. C.; Ueda, M.; Kristen, A. V.; Tournev, I.; Schmidt, H. H.; Coelho, T.; Berk, J. L.; Lin, K. P.; Vita, G.; Attarian, S.; Plante-Bordeneuve, V.; Mezei, M. M.; Campistol, J. M.; Buades, J.; Brannagan, T. H., 3rd; Kim, B. J.; Oh, J.; Parman, Y.; Sekijima, Y.; Hawkins, P. N.; Solomon, S. D.; Polydefkis, M.; Dyck, P. J.; Gandhi, P. J.; Goyal, S.; Chen, J.; Strahs, A. L.; Nochur, S. V.; Sweetser, M. T.; Garg, P. P.; Vaishnaw, A. K.; Gollob, J. A.; Suhr, O. B., Patisiran, an RNAi Therapeutic, for Hereditary Transthyretin Amyloidosis. *N Engl J Med* **2018,** *379* (1), 11-21.
366. Pardi, N.; Hogan, M. J.; Porter, F. W.; Weissman, D., mRNA vaccines - a new era in vaccinology. *Nat Rev Drug Discov* **2018,** *17* (4), 261-279.
367. Chaudhary, N.; Weissman, D.; Whitehead, K. A., mRNA vaccines for infectious diseases: principles, delivery and clinical translation. *Nat Rev Drug Discov* **2021,** *20* (11), 817-838.
368. Zhang, C.; Maruggi, G.; Shan, H.; Li, J., Advances in mRNA Vaccines for Infectious Diseases. *Front Immunol* **2019,** *10*, 594.
369. Linares-Fernandez, S.; Lacroix, C.; Exposito, J. Y.; Verrier, B., Tailoring mRNA Vaccine to Balance Innate/Adaptive Immune Response. *Trends Mol Med* **2020,** *26* (3), 311-323.
370. de Alwis, R.; Gan, E. S.; Chen, S.; Leong, Y. S.; Tan, H. C.; Zhang, S. L.; Yau, C.; Low, J. G. H.; Kalimuddin, S.; Matsuda, D.; Allen, E. C.; Hartman, P.; Park, K. J.; Alayyoubi, M.; Bhaskaran, H.; Dukanovic, A.; Bao, Y.; Clemente, B.; Vega, J.; Roberts, S.; Gonzalez, J. A.; Sablad, M.; Yelin, R.; Taylor, W.; Tachikawa, K.; Parker, S.; Karmali, P.; Davis, J.; Sullivan, B. M.; Sullivan, S. M.; Hughes, S. G.; Chivukula, P.; Ooi, E. E., A single dose of self-transcribing and replicating RNA-based SARS-CoV-2 vaccine produces protective adaptive immunity in mice. *Mol Ther* **2021,** *29* (6), 1970-1983.
371. Wu, C. J.; Huang, H. W.; Liu, C. Y.; Hong, C. F.; Chan, Y. L., Inhibition of SARS-CoV replication by siRNA. *Antiviral Res* **2005,** *65* (1), 45-8.
372. Lam, J. K.; Liang, W.; Chan, H. K., Pulmonary delivery of therapeutic siRNA. *Adv Drug Deliv Rev* **2012,** *64* (1), 1-15.
373. Idris, A.; Davis, A.; Supramaniam, A.; Acharya, D.; Kelly, G.; Tayyar, Y.; West, N.; Zhang, P.; McMillan, C. L. D.; Soemardy, C.; Ray, R.; O'Meally, D.; Scott, T. A.; McMillan, N. A. J.; Morris, K. V., A SARS-CoV-2 targeted siRNA-nanoparticle therapy for COVID-19. *bioRxiv* **2021**.
374. Nance, K. D.; Meier, J. L., Modifications in an Emergency: The Role of N1-Methylpseudouridine in COVID-19 Vaccines. *ACS Cent Sci* **2021,** *7* (5), 748-756.
375. Abbasi, J., COVID-19 and mRNA Vaccines-First Large Test for a New Approach. *JAMA* **2020,** *324* (12), 1125-1127.
376. Hawner, M.; Ducho, C., Cellular Targeting of Oligonucleotides by Conjugation with Small Molecules. *Molecules* **2020,** *25* (24).
377. Dugal-Tessier, J.; Thirumalairajan, S.; Jain, N., Antibody-Oligonucleotide Conjugates: A Twist to Antibody-Drug Conjugates. *J Clin Med* **2021,** *10* (4).

378. McClorey, G.; Banerjee, S., Cell-Penetrating Peptides to Enhance Delivery of Oligonucleotide-Based Therapeutics. *Biomedicines* **2018,** *6* (2).
379. Ryu, Y. C.; Kim, K. A.; Kim, B. C.; Wang, H. D.; Hwang, B. H., Novel fusion peptide-mediated siRNA delivery using self-assembled nanocomplex. *J Nanobiotechnology* **2021,** *19* (1), 44.
380. Sivakumar, P.; Kim, S.; Kang, H. C.; Shim, M. S., Targeted siRNA delivery using aptamer-siRNA chimeras and aptamer-conjugated nanoparticles. *Wiley Interdiscip Rev Nanomed Nanobiotechnol* **2019,** *11* (3), e1543.
381. Dinis Ano Bom, A. P.; da Costa Neves, P. C.; Bonacossa de Almeida, C. E.; Silva, D.; Missailidis, S., Aptamers as Delivery Agents of siRNA and Chimeric Formulations for the Treatment of Cancer. *Pharmaceutics* **2019,** *11* (12).
382. Graczyk, A.; Pawlowska, R.; Chworos, A., Gold Nanoparticles as Carriers for Functional RNA Nanostructures. *Bioconjug Chem* **2021,** *32* (8), 1667-1674.
383. Johnson, M. B.; Chandler, M.; Afonin, K. A., Nucleic acid nanoparticles (NANPs) as molecular tools to direct desirable and avoid undesirable immunological effects. *Adv Drug Deliv Rev* **2021,** *173*, 427-438.
384. Osborn, M. F.; Khvorova, A., Improving siRNA Delivery In Vivo Through Lipid Conjugation. *Nucleic Acid Ther* **2018,** *28* (3), 128-136.
385. Kubo, T.; Nishimura, Y.; Sato, Y.; Yanagihara, K.; Seyama, T., Sixteen Different Types of Lipid-Conjugated siRNAs Containing Saturated and Unsaturated Fatty Acids and Exhibiting Enhanced RNAi Potency. *ACS Chem Biol* **2021,** *16* (1), 150-164.
386. Springer, A. D.; Dowdy, S. F., GalNAc-siRNA Conjugates: Leading the Way for Delivery of RNAi Therapeutics. *Nucleic Acid Ther* **2018,** *28* (3), 109-118.
387. Swingle, K. L.; Hamilton, A. G.; Mitchell, M. J., Lipid Nanoparticle-Mediated Delivery of mRNA Therapeutics and Vaccines. *Trends Mol Med* **2021,** *27* (6), 616-617.
388. Hou, X.; Zaks, T.; Langer, R.; Dong, Y., Lipid nanoparticles for mRNA delivery. *Nat Rev Mater* **2021**, 1-17.
389. O'Brien, K.; Breyne, K.; Ughetto, S.; Laurent, L. C.; Breakefield, X. O., RNA delivery by extracellular vesicles in mammalian cells and its applications. *Nat Rev Mol Cell Biol* **2020,** *21* (10), 585-606.
390. Cully, M., Exosome-based candidates move into the clinic. *Nat Rev Drug Discov* **2021,** *20* (1), 6-7.
391. Dobrovolskaia, M. A.; Bathe, M., Opportunities and challenges for the clinical translation of structured DNA assemblies as gene therapeutic delivery and vaccine vectors. *Wiley Interdiscip Rev Nanomed Nanobiotechnol* **2021,** *13* (1), e1657.
392. Wang, Z.; Song, L.; Liu, Q.; Tian, R.; Shang, Y.; Liu, F.; Liu, S.; Zhao, S.; Han, Z.; Sun, J.; Jiang, Q.; Ding, B., A Tubular DNA Nanodevice as a siRNA/Chemo-Drug Co-delivery Vehicle for Combined Cancer Therapy. *Angew Chem Int Ed Engl* **2021,** *60* (5), 2594-2598.
393. Boo, S. H.; Kim, Y. K., The emerging role of RNA modifications in the regulation of mRNA stability. *Exp Mol Med* **2020,** *52* (3), 400-408.
394. Shi, H.; Chai, P.; Jia, R.; Fan, X., Novel insight into the regulatory roles of diverse RNA modifications: Re-defining the bridge between transcription and translation. *Mol Cancer* **2020,** *19* (1), 78.
395. Roberts, T. C.; Langer, R.; Wood, M. J. A., Advances in oligonucleotide drug delivery. *Nat Rev Drug Discov* **2020,** *19* (10), 673-694.
396. Cutler, J. I.; Zhang, K.; Zheng, D.; Auyeung, E.; Prigodich, A. E.; Mirkin, C. A., Polyvalent nucleic acid nanostructures. *J Am Chem Soc* **2011,** *133* (24), 9254-7.
397. Rong, M.; He, B.; McAllister, W. T.; Durbin, R. K., Promoter specificity determinants of T7 RNA polymerase. *Proc Natl Acad Sci U S A* **1998,** *95* (2), 515-9.
398. Khvorova, A.; Reynolds, A.; Jayasena, S. D., Functional siRNAs and miRNAs exhibit strand bias. *Cell* **2003,** *115* (2), 209-16.

399. Terry L Riss, R. A. M., Andrew L Niles, Sarah Duellman, Hélène A Benink, Tracy J Worzella, Lisa Minor, Cell Viability Assays. In *Assay Guidance Manual* 2016.
400. Sigma Aldrich. https://www.sigmaaldrich.com/PL/pl/product/aldrich/741957.
401. Gang, G. W.; Shin, J.; Kim, Y. H.; Ha, T. H.; Ogawa, T., Visualization of unstained homo/heterogeneous DNA nanostructures by low-voltage scanning transmission electron microscopy. *Sci Rep* **2020,** *10* (1), 4868.
402. Pratt, A. J.; MacRae, I. J., The RNA-induced silencing complex: a versatile gene-silencing machine. *J Biol Chem* **2009,** *284* (27), 17897-901.
403. Song, M. S.; Rossi, J. J., Molecular mechanisms of Dicer: endonuclease and enzymatic activity. *Biochem J* **2017,** *474* (10), 1603-1618.